

PDF hosted at the Radboud Repository of the Radboud University Nijmegen

The following full text is a publisher's version.

For additional information about this publication click this link.

<http://hdl.handle.net/2066/93622>

Please be advised that this information was generated on 2017-12-06 and may be subject to change.

Covert Visual Spatial Attention
a Robust Paradigm for Brain-Computer Interfacing

Copyright © 2012 Ali Bahramisharif, Nijmegen, the Netherlands
ISBN 978-94-6191-332-6



SIKS Dissertation Series No. 2012-20

The research reported in this thesis has been carried out under the auspices of SIKS, the Dutch Research School for Information and Knowledge Systems.



This research was supported by the BrainGain Smart Mix Programme of the Netherlands Ministry of Economic Affairs and the Netherlands Ministry of Education, Culture and Science.

Covert Visual Spatial Attention
a Robust Paradigm for Brain-Computer Interfacing

Proefschrift

ter verkrijging van de graad van doctor
aan de Radboud Universiteit Nijmegen
op gezag van de rector magnificus prof. mr. S.C.J.J. Kortmann,
volgens besluit van het college van decanen
in het openbaar te verdedigen op donderdag 5 juli 2012
om 13:30 uur precies
door

Ali Bahramisharif

geboren op 7 januari 1980
te Hamedan, Iran

Promotor:

Prof. dr. T.M. Heskes

Copromotoren:

Dr. M.A.J. van Gerven

Dr. O. Jensen

Manuscriptcommissie:

Prof. dr. P.W.M. Desain

Prof. dr. L.K. Hansen, Danmarks Tekniske Universitet, Kopenhagen

Prof. dr. K.R. Müller, Technische Universität Berlin, Berlijn

Acknowledgments

I would like to thank the people without whom it was not possible to have this thesis completed. I gratefully acknowledge the support of the BrainGain Smart Mix Programme of the Netherlands Ministry of Economic Affairs and the Netherlands Ministry of Education, Culture and Science.

I am truly indebted and thankful to my promotor Tom Heskes and my copromotores Marcel van Gerven and Ole Jensen for their kind support, advice, friendship and patience. I am thankful to Lars Kai Hansen and Klaus-Robert Müller for taking the time to read my thesis. I thank Tom Claassen and Stephen Whitmarsh who are helping me defend my thesis as my ‘Paranimfen’. I acknowledge Jan-Mathijs Schoffelen and Avgis Hadjipapas for the very useful discussions that I had with them. I thank my colleagues in the computer science department including Pavol Jancura, Saiden Abbas, Fabio Gori, Robbert Krebbers, Paul van den Hurk, Twan van Laarhoven, Wout Megchelenbrink, Max Hinne, Adriana Birlutiu, Perry Groot, Botond Cseke, Rasa Jurgelenaite, Evgeni Tsivtsivadze, Tjeerd Dijkstra, Elena Marchiori, Nicole Messink, and Simone Meeuwssen for everything that I learned from them and the time that we spent together. I specially thank Hein Vosmar for his useful tips and friendly advices. I thank Bert Kappen for everything that I learned from his machine learning course. I am thankful to my friends and colleagues at the Donders institute including Sander Berends, Jurrian van der Werf, Barbara Haendel, Esther Meeuwissen, Anne van Hoogmoed, Yuka Okazaki, Cristiano Micheli, Elena Shumskaya, and Ana Todorovic for the lovely discussions that we had.

I gladly extend my gratitude to Zoubin Ghahramani for giving me the

opportunity to work with him in Cambridge, Richard Turner for answering my questions and supporting me, and all other members in the machine learning group at Cambridge University including Frederik Eaton and Shakir Mohamed for the nice time in Cambridge. I thank Rik Henson for giving me the opportunity to present my work at MRC Cambridge and Nikolaus Kriegeskorte for the constructive comments on my work. I acknowledge Matthias Treder for his friendship and collaboration, and all other members in machine learning group at the Technical University Berlin including Benjamin Blankertz and Nico Schmidt for the nice time that I spent there. I thank Danny Plass-Oude Bos, Boris Reuderink, and all other members of the human media interaction group of the university of Twente for the nice collaboration that we had. I am thankful to Bahador Bahrami for the fruitful discussions that we had in London. I acknowledge all my previous supervisors from whom I learned how to think and what to do including Amir-Mansour Pezeshk, Mohammad-Hossein Alavi, Emad Fatemizadeh, and Ehsanolah Kabir.

I want to thank my friends all around the world that always have me in mind and support me when I need them including Hamed Hashemi, Rahim Delaviz, Babak Kaveh, Rouzbeh Amini, Siamak Taati, Alireza Kashef, Dario Poursarajian, Reza Mesbah, and Kaveh Vahdat. I especially thank my parents, Mohammad and Parvin, for their love, advice, encouragement, and support. Finally and foremost, I thank my wife Faranak who provides me with the home to rest and love to enjoy life.

Contents

1	Introduction	1
2	Covert Attention Allows For Continuous Control Of Brain-Computer Interfaces	5
2.1	Introduction	6
2.2	Materials and methods	8
2.2.1	Data collection	8
2.2.2	Preprocessing	10
2.2.3	Circular regression	10
2.2.4	Evaluation	11
2.3	Results	13
2.4	Discussion	17
3	Lateralized Responses During Covert Attention Are Modulated By Target Eccentricity	23
3.1	Introduction	24
3.2	Materials and Method	25
3.2.1	Data collection	25
3.2.2	Experimental design	26
3.2.3	Preprocessing	27
3.2.4	Classification	27
3.3	Results	28
3.4	Discussion	33

4	Decoding the direction of covert attention with EEG	35
4.1	Introduction	36
4.2	Materials and methods	38
4.2.1	Data collection	38
4.2.2	Preprocessing	41
4.2.3	Classification	41
4.3	Results	42
4.3.1	Behavioral results	42
4.3.2	Neurophysiological results	42
4.3.3	Classification	45
4.3.4	Left hemisphere versus right hemisphere contribution	50
4.3.5	Alpha rhythm based predictor of BCI performance .	52
4.3.6	Subject-independent learning	53
4.4	Discussion	55
5	Task-Specific Source Localization	59
5.1	Introduction	60
5.2	Source localization	61
5.2.1	Standard approach	61
5.2.2	Task-specific approach	62
5.2.3	Regularization parameters	65
5.3	Experiments	66
5.3.1	Simulated data	66
5.3.2	Empirical data	69
5.4	Discussion	70
5.A	Appendix A: Solving for W	73
5.B	Appendix B: Solving for S	75
5.C	Appendix C: Linear trick to estimate the power	76
6	The Dynamic Beamformer	77
6.1	Introduction	77
6.2	Method	78
6.2.1	Beamforming	78
6.2.2	Linear Gaussian model	79

6.2.3	Dynamic beamforming	80
6.2.4	Empirical data	80
6.2.5	Validation	81
6.3	Results	82
6.4	Conclusion	85
7	General Conclusion	87
	Bibliography	89

Chapter 1

Introduction

Normally we express the content of our mind by actions or speech. Current advances in brain monitoring devices such as electroencephalography (EEG), magnetoencephalography (MEG), functional magnetic resonance imaging (fMRI), or intracranial recordings allow us to think of new ways of communicating with other people directly through our brains. Recent findings have shown that we can control various devices by our ongoing brain activity through brain-computer interfaces (BCIs). Some of the applications are computer gaming [87, 86], communication devices for highly impaired patients [5], rehabilitation [84, 32], control of artificial limbs [67], and neuro-feedback [6].

To bypass muscle activity and directly use the brain for communication or control, we need to decode a mental state from brain activity. Different modalities have been used for brain-computer interfacing. Imaginary movement [134, 77, 20], steady-state visual evoked potentials (SSVEP) [61], spatial auditory [98], and tactile stimulation [24] are some of the successful BCI paradigms. Although depending on the application one may favor one paradigm over another, it is always beneficial to have more control signals in order to increase the reliability and information transfer rate of BCIs. Furthermore, it is important to work towards modalities which allow for a full two-dimensional continuous control since this affords applications such

as wheelchair or cursor control.

Covert visual spatial attention, which is called in short ‘covert attention’ in this thesis, is a well studied psychological process that has its unique brain signature. Humans can voluntarily deploy attention to locations in visual space without moving their eyes [88, 89]. While some modalities such as imaginary movement are natural for prosthetic control, they are less natural for settings in which a visually displayed object has to be controlled. We believe that, in this context, covert attention will provide a more natural control signal requiring less training.

Using EEG, covert attention has been shown to be characterized by changes in the alpha band (8-12 Hz) over the visual cortex [137]. It has been shown that on average when attention is directed to the left visual hemifield, alpha activity decreases in the right posterior hemisphere while simultaneously increasing in the left hemisphere and vice versa. Based on this result, in a preliminary MEG experiment by van Gerven et al. [118], we showed that it is possible to classify the direction of covert attention (left from right) on a single trial basis using alpha power extracted from the visual cortex. We further evaluated the possibility of having an online BCI setup, in which participants were asked to fixate at the center of the screen and to move the ‘background’ by directing their attention to the left or right. We showed that out of ten, two of the participants succeeded in moving the background in the desired direction in up to 83% of the given trials [12]. As a BCI gives the feeling of control if its performance is above 70% [66], the reported performance is very promising.

We know that the ability to covertly direct attention is not limited to only left and right. Many behavioral studies have shown the effects of different directions of visual attention [7, 16, 26, 138, 52]. The results hint at the possibility of going beyond left-right control in the context of covert attention-based BCIs. Furthermore, Rihs et al. set up an EEG experiment in which participants were asked to direct their attention to eight different directions [90]. Looking at the topographical alpha maps, they showed that there is a high correlation between the spatial distribution of alpha power between the neighboring directions, and the closer the directions, the higher the correlations. Are these changes robust enough to allow for decoding

different directions of covert attention on a single trial basis? To answer this question, we investigate the possibility of decoding all directions of covert attention using alpha extracted from the visual cortex in chapter 2. We develop an MEG study in which subjects are asked to fixate centrally and covertly track the direction of a moving target. The outcomes of this study are discussed at the end of the second chapter of this thesis. Subsequently, after studying the directions of covert attention, we explore the other free parameter that we have in two-dimensional space. In the third chapter, we investigate the effect of eccentricity on the modulations of brain activity by covert attention. We are also interested to see whether the results obtained for single trial classification of MEG data can be generalized to EEG. So, we study the possibility of decoding the direction of covert attention using EEG in chapter four. In that chapter, we also explore the possibility of using covert attention as a control signal for subject-independent BCI.

As we are interested in not only the application of covert attention for BCIs, but also in the neural sources underlying covert attention, we need to develop methods for source localization and apply them to our available covert attention data-set. As most source localization algorithms have not directly taken into account the modulation of source activations induced by certain experimental manipulations, we introduce a new source localization technique which incorporates the experimental design in the source localization procedure in the fifth chapter. We further incorporate source dynamics in the commonly used beamformer setup to explore the improvement over this standard source localization algorithm in chapter six. We end the thesis by a general conclusion and closing remarks.

Chapter 2

Covert Attention Allows For Continuous Control Of Brain-Computer Interfaces

1

While brain-computer interfaces (BCIs) can be used for controlling external devices, they also hold the promise of providing a new tool of studying the working brain. In this chapter we investigated whether modulations of brain activity by changes in covert attention can be used as a continuous control signal for BCI. Covert attention is the act of mentally focusing on a peripheral sensory stimulus without changing gaze direction. The ongoing brain activity was recorded using magnetoencephalography in subjects while they covertly attended to a moving cue while maintaining fixation. Based on posterior alpha power alone, the direction to which subjects were attending could be recovered using circular regression. Results show that the angle of attention could be predicted with a mean absolute deviation of 51 degrees in our best subject. Averaged over subjects, the mean devi-

¹This chapter is based on: Bahramisharif, A., van Gerven, M. A. J., Heskes, T., Jensen, O., ‘Covert attention allows for continuous control of brain-computer interfaces’, *European Journal of Neuroscience*, Vol. 31, pp 1501–1508, 2010

ation was approximately 70 degrees. In terms of information transfer rate, the optimal data length used for recovering the direction of attention was determined to be 1700 ms which resulted in a mean absolute deviation of 60 degrees for the best subject. The results were obtained without any subject-specific feature selection and did not require prior subject training. Our findings demonstrate that modulations of posterior alpha activity due to the direction of covert attention has potential as a control signal for continuous control in a BCI setting. Our approach will have several applications, including a brain-controlled computer mouse and improved methods for neuro-feedback that allow direct training of subjects' ability to modulate posterior alpha activity.

2.1 Introduction

There is a growing interest in the development of brain-computer interfaces (BCIs) and brain-machine interfaces (BMIs) [133, 84, 17, 132, 120, 79, 126]. In BMI/BCI applications, real-time brain activity is used to control various devices. One important application is the control of mechanical prostheses [104, 49, 127, 79]. BMI/BCI has also been proposed to be used for communication to aid severely paralyzed patients suffering, for instance, from amyotrophic lateral sclerosis (ALS) [18]. Possibilities with respect to neurological rehabilitation are currently under investigation [32]. Importantly BCI/BMI holds the promise of providing new tools which can be used to study the working human brain. Examples are neurofeedback [45, 92] and brain-state-dependent interventions [65, 114].

Impressive results on prosthetic control have been obtained using intracranial recordings in humans and monkeys [104, 49, 85, 79]. However, due to the invasive nature of intracranial recordings, there is a clear need to improve BMIs/BCIs using non-invasive techniques. Important progress has been made using EEG, MEG and fMRI [83, 17, 120]. With respect to EEG, convincing results have been obtained using evoked potentials and modulations in oscillatory activity [83, 28]. Often, imagined movement is applied to modulate the brain activity being used as a control signal [77].

It has been demonstrated that it is possible for subjects to achieve control in both one- and two-dimensions using motor imagery [134, 72]. While motor imagery has proven to work, it is obviously advantageous to have more control signals in order to increase the reliability and information transfer rate of BMI/BCI. In particular, it is important to work towards continuous control in two dimensions.

Cognitive research has demonstrated that posterior alpha activity (8–13 Hz) is strongly modulated in paradigms where fixation is kept centrally but attention is directed covertly [137]. When attention is directed to the left visual hemifield, alpha activity decreases in the right posterior hemisphere while increasing in the left hemisphere. The reverse pattern holds for covert attention directed to the right visual hemifield. Recently it was demonstrated that covert attention to the upper and lower hemifield modulates the vertical distribution of alpha activity [90].

The prospects of using covert attention and alpha modulation provide a new exciting possibility for a control signal to be used in BMI/BCI. Setups using covert attention would be convenient for controlling objects in the visual domain such as a computer mouse. Furthermore, it is well established that posterior alpha activity reflects the allocation of attentional resources. Thus, when subjects are learning to control their posterior alpha activity, it is likely to impact their ability to direct attention.

A few studies have applied multivariate classification approaches to demonstrate that the direction of covert attention can be coded on a single-trial basis from EEG and MEG data. Kelly et al. [61, 58, 60] have shown that left-right shifts in covert attention can be predicted at the single-trial level from alpha activity using EEG measurements. This has been confirmed in a subsequent MEG study [118]. Furthermore, inspired by the result of Rihs et al. [90], van Gerven et al. [121] have shown that four directions (up-down; left-right) of covert attention can be detected at the single-trial level with up to 69% accuracy (25% chance level).

The aim of this study was to investigate if an arbitrary direction of covert attention could be decoded from MEG data. If so, this will allow for continuous BMIs/BCIs control based on covert attention. To investigate this possibility we used MEG to record the ongoing brain activity from

eleven subjects. The task of the subjects was to covertly track the direction of a rotating cue while keeping fixation central. A circular regression algorithm was used to infer direction from posterior sensors.

2.2 Materials and methods

2.2.1 Data collection

Subjects

Eleven healthy volunteers were recruited for the experiment. The study was approved by the local ethics committee and written informed consent was obtained from the subjects.

MEG recordings

Brain activity was recorded by an MEG system with 275 axial gradiometers (VSM/ CTF systems, Port Coquitlam, Canada) while the subjects were in sitting position, data were sampled at 1200 Hz. Bipolar electrodes were attached to record the electrocardiogram (ECG) and electrooculogram (EOG) simultaneously with with MEG data. Three coils were placed at the nasion and in both ear canals to monitor head position.

The task

The task required subjects to fixate centrally at a cross while covertly attending to a target placed at a ‘wheel’ around the fixation cross. The wheel had one target and three differently colored distracters (Fig. 2.1). The visual angle between fixation cross and display was 7.5 degrees. The radius of the target and distracters was 0.33 degrees (visual angle). Subjects were sitting 50 cm away from the screen. The stimuli were constructed off-line using MATLAB (The MathWorks, Inc.) and stimulus presentation was controlled using Psychtoolbox3 [23]. All stimuli were presented via a mirror system on a back-projection screen using a calibrated LCD projector (60 Hz refresh rate).

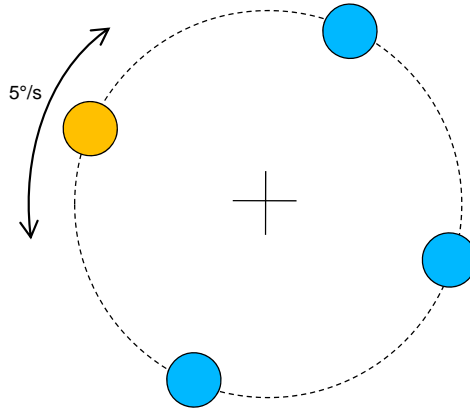


Figure 2.1: The display used in the task. Subjects were asked to covertly attend to the target dot, while fixating at the cross. The ‘wheel’ slowly rotated (5 degrees/s) while randomly changing directions.

An experiment consisted of six sessions each five minutes long. Within each session, the colors of both target and distracters changed eighteen times at random time points. The subjects were asked to count the number of times the color of the target changed, which served to keep the subjects alert. The distracters served two purposes. First, they balanced the visual display. Second, it has been proposed that the posterior alpha modulation serves to suppress visual distracters (e.g. [92]). Thus we expected the distracters to enhance the attention related modulation of alpha activity. Within a five minute session the rotation direction of the wheel was changed four times at random time points. To make the direction changes smooth, rotation speed increased or decreased exponentially from 0 to 5 degrees (polar angle) per second over a 1500 ms interval. Aside from direction changes, the rotation of the wheel was held constant at 5 degrees (polar angle) per second. The sessions were separated by three minutes rest periods. In the next session, the colors of both the distracters and the target were swapped in order to keep the design balanced.

2.2.2 Preprocessing

The data were down-sampled to 150 Hz after being lowpass filtered at 75 Hz. The planar gradient was approximated for each sensor using the signals calculated from a sensor and its neighboring sensors, effectively emulating a setup with planar gradiometers [14]. Following this approach, the strongest activity is measured directly above the sources [42].

Informed by the results of previous studies [61, 60, 58, 118, 121], we used the signals from 38 sensors over the left and right occipital regions (marked in Fig. 2.2). The analysis was focused on a frequency band centered at 10 Hz. The power was calculated using a 500 ms sliding Hanning window shifted every 30 ms. Due to the 500 ms window, the frequency smoothing was approximately 2 Hz, meaning that power over the 8–12 Hz alpha band was included.

Different trial lengths were obtained by averaging the power estimates over a number of consecutive time windows. For instance, since the time windows were shifted 30 ms, 160 consecutive time windows yielded an effective trial length of 5270 ms.

2.2.3 Circular regression

Since we are interested in predicting the angle of covert attention based on recorded brain activity, a circular regression algorithm was applied [35]. Circular regression is characterized by the fact that predictions for angles θ modulo 2π should be identical.

We approached the circular regression problem by estimating (‘training’) the regression coefficients for the recorded data with respect to the sine and cosine components of the target angle. This allowed us to later predict (‘test’) the sine and cosine components from a given time window and reconstruct the angle using an arctangent transform [69].

Let (θ, \mathbf{x}) be a pair where \mathbf{x} is the vector of estimated alpha activity for 38 occipital sensors measured with respect to the angle θ of the target. β_1 and β_2 are the regression coefficients for $\cos(\theta)$ and $\sin(\theta)$, respectively. The aim is to estimate β_1 and β_2 given the measured data (θ, \mathbf{X}) with

$\boldsymbol{\theta} = (\theta_1, \dots, \theta_n)^T$ and $\mathbf{X} = (\mathbf{x}_1, \dots, \mathbf{x}_n)^T$ where n is the number of time windows. The sum of the squared residuals are minimized by an ordinary least squares approach [33]:

$$\begin{aligned}\boldsymbol{\beta}_1 &= (\mathbf{X}^T \mathbf{X})^{-1} \mathbf{X}^T \cos(\boldsymbol{\theta}) \\ \boldsymbol{\beta}_2 &= (\mathbf{X}^T \mathbf{X})^{-1} \mathbf{X}^T \sin(\boldsymbol{\theta}).\end{aligned}$$

Finally, given the observed data \mathbf{x} the predicted angle ϕ is computed as $\phi = \text{atan2}(\mathbf{x}\boldsymbol{\beta}_2, \mathbf{x}\boldsymbol{\beta}_1)$, where atan2 stands for the four-quadrant inverse tangent.

2.2.4 Evaluation

We used data from five sessions for training the circular regressor and data from one session for testing. We repeated this training and testing over all six sessions using a six-fold cross-validation scheme. Since the sessions were separated by a rest period, there was no information regarding the test session in the training phase.

To evaluate the performance, we were interested in the absolute difference between true (θ , orientation of target) and predicted (ϕ , output of regression analysis) angles. Let $\boldsymbol{\psi} = \boldsymbol{\theta} - \boldsymbol{\phi}$ denotes the difference between the real and predicted angles. Note that $|\boldsymbol{\psi}|$ is always in the range of $[0, \pi]$. We compute the mean absolute deviation (error) $\overline{|\boldsymbol{\psi}|}$ as follows:

$$\overline{|\boldsymbol{\psi}|} = \text{atan2}(\langle \sin(|\boldsymbol{\psi}|) \rangle, \langle \cos(|\boldsymbol{\psi}|) \rangle) \quad (2.1)$$

where $\langle \cdot \rangle$ represents the averaging operator across trials.

In order to compute the standard deviation of the error for a given angle θ' , we use the following equation [35, 69]:

$$\text{SD}(\phi' - \theta') = \sqrt{-\ln(\langle \cos(\phi' - \theta') \rangle^2 + \langle \sin(\phi' - \theta') \rangle^2)}$$

where ϕ' denotes the subset of predicted angles $\boldsymbol{\phi}$ for which the real angle was θ' .

T-linear association is a measure of goodness of prediction for a circular regression problem. Assuming that n is the number of samples, T-linear association is calculated as follows [35]:

$$T = \frac{\sum_{j=1}^n \sum_{i=1}^j \sin(\theta_i - \theta_j) \sin(\phi_i - \phi_j)}{\sqrt{\sum_{j=1}^n \sum_{i=1}^j \sin^2(\theta_i - \theta_j) \sum_{j=1}^n \sum_{i=1}^j \sin^2(\phi_i - \phi_j)}} \quad (2.2)$$

The significance level was calculated using a one-sided t-test on a distribution over one million randomly generated T values. The randomly generated T values were obtained using the true angle θ and ‘prediction’ ϕ which was generated by adding a uniformly distributed angle between 0 and 2π to the angle θ .

Information transfer rate (ITR, bits per minute) is an important factor in BCI applications because it informs about the number of binary decisions which can be made per unit time and allows one to determine the optimal trial length. We calculated the ITR by dividing mutual information by trial length [99]. Mutual information between true (Θ) and predicted (Φ) responses is defined as follows [99]:

$$I(\Theta, \Phi) = H(\Theta) - H(\Theta | \Phi) \quad (2.3)$$

where H is the differential entropy. If we assume that the random variable X has a probability density function p , then the differential entropy is defined as follows:

$$H(X) = - \int p(x) \log p(x) dx \quad (2.4)$$

In order to compute the mutual information, we used the following approach. Let us assume that a random variable X is distributed according to the von Mises distribution

$$p(X = x) = \text{VM}(x; \mu, \kappa) = \frac{1}{2\pi I_0(\kappa)} e^{\kappa \cos(x-\mu)}$$

with mean μ , concentration parameter κ , and where I_0 is the modified Bessel function of order 0. The concentration parameter κ is the inverse

measure of dispersion, i.e., if κ is zero, the distribution is uniform and if κ is large, the distribution becomes concentrated around μ . In fact, as κ increases, the distribution approaches a normal distribution in X with mean μ and variance $\frac{1}{\kappa}$.

The differential entropy (base 2) for a von Mises distributed random variable X is given by

$$H(X) = \frac{1}{\ln 2} \left(-\kappa \frac{I_1(\kappa)}{I_0(\kappa)} + \ln(2\pi I_0(\kappa)) \right)$$

When calculating $H(\Theta)$, the concentration parameter κ of the von Mises distribution has to be 0 because true labels are uniformly distributed on the circle. Furthermore, assuming that the estimated angle is the true angle of attention which is subjected to additive von Mises noise, it follows that the conditional entropy $H(\Theta | \Phi)$ is equal to $H(\Psi)$ where $\Psi = \Theta - \Phi$. Again, if we assume the von Mises distribution for Ψ , the concentration parameter can be approximated using the following equations [35]:

$$\kappa = \begin{cases} 2r + r^3 + \frac{5}{6}r^5 & r < 0.53 \\ 1/(r^3 - 4r^2 + 3r) & r \geq 0.85 \\ -0.4 + 1.39r + 0.43/(1 - r) & \text{otherwise} \end{cases}$$

where $r = n\sqrt{\langle \cos(\psi) \rangle^2 + \langle \sin(\psi) \rangle^2}$ and n is the number of samples. This can then be applied to Eq. (2.3) in order to obtain the mutual information from which the information transfer rate (the bit-rate) is derived.

2.3 Results

First, for illustration we calculated the average power over subjects for the full recording period with respect to sixteen angular divisions (Fig. 2.2). The power averaged over all divisions (middle figure) was subtracted from the individual divisions. These results show that the spatial distribution of alpha power in posterior sensors reflects the angle of attention. This is consistent with previous findings [90, 121].

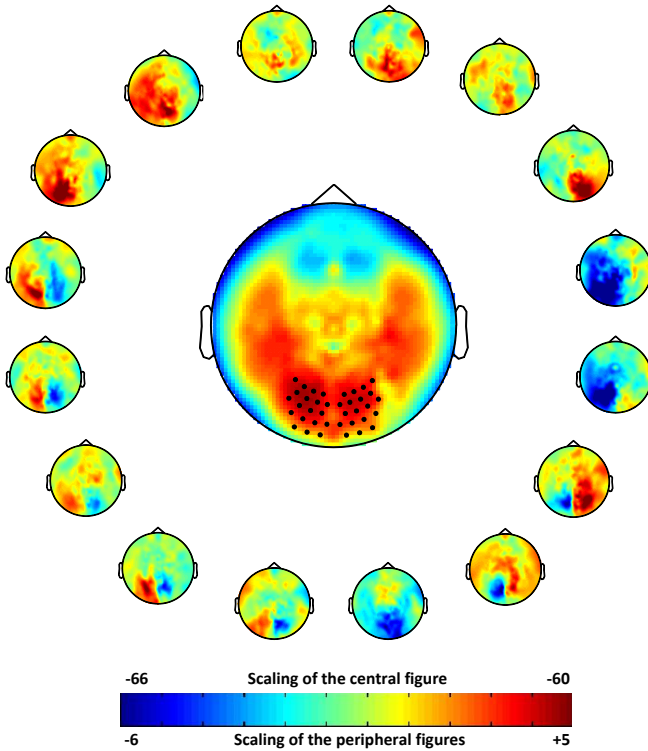


Figure 2.2: The distribution of alpha power with respect to 16 divisions. The arrangement of the figures reflects the direction of covert attention which is clearly correlated with the spatial topography. The central figure shows the alpha power averaged over all directions and the black dots show the selected sensors. Note that data is log-transformed prior to averaging.

We then set out to investigate to what extent single trial activity predicted the direction of covert attention. Figure 2.3a depicts an example where we estimated the angle of attention using the circular regression approach applied to the data of one subject. The individual trial lengths were in this case 1700 ms. Although the estimates (stars) showed deviations

around the mean (dots), the true angle of attention is predicted reasonably well. Figure 2.3b shows the mean and standard deviation of the predicted angle of attention for the same subject. A six-fold cross-validation scheme was used: the regressors were trained on data from 5 sessions and applied to predict the angle for the remaining session. The average standard deviation for this result was 80 degrees. Figure 2.3c shows the sine and cosine components predicted from the circular regressor.

Next, we applied the regression analysis to all subjects. Figure 2.4a shows how the mean absolute deviation (Eq. (2.1)) of the estimated angle varies over all trials and directions using occipital alpha. The analysis was done for time windows of increasing length. Chance level is 90 degrees (dashed line). Using occipital alpha, the absolute deviation decreased systematically with trial length. While the mean absolute deviation over subjects went down to approximately 70 degrees, the absolute deviation was as low as about 50 degrees in one subject. Since we wanted to establish that our results derive from brain activity and not eye movements, we repeated our analysis using horizontal and vertical EOG measurements recorded from four bipolar EEG electrodes (Fig. 2.4b). This demonstrated that activity derived from ocular artifacts does not carry information about the angle to which the subject covertly attends.

The information transfer rate was calculated using Eq. (2.3) in order to determine the optimal trial length in terms of the amount of information that can be transferred per unit time. Figure 2.5 shows that the average ITR is maximal for a trial length of about 1700 ms.

For the time window of 1700 ms, T-linear association values for occipital alpha and alpha computed using the EOG electrodes are calculated using Eq. (2.2) and shown in Table 2.1. This table shows that using occipital alpha, in seven out of eleven subjects we were able to estimate the attended angle beyond chance. This result correlates well with performance in terms of the mean absolute deviation. When considering the T-linear association for the EOG signals, the values were below chance which is in line with the findings in Fig. 2.4. These results substantiate the claim that ocular artifacts do not contribute to the estimate of the direction of covert attention.

Time 1700 ms	Signal of interest	
	Occipital alpha	EOG
Subject	T_B	T_E
11	-0.00	0.00
10	-0.00	-0.00
9	0.00	0.00
8	0.01	-0.01
7	0.01	0.00
6	0.01	-0.00
5	0.03	0.00
4	0.03	-0.00
3	0.04	-0.00
2	0.05	-0.00
1	0.09	-0.00

Table 2.1: T-linear association of the regression fits for occipital alpha and EOG data. Subjects are ranked according to performance in Fig. 2.4. A 1700 ms time-window was used. Significant values ($p < 0.01$, Bonferroni corrected) are shown in boldface.

In four subjects, we were not able to predict the angle of covert attention from the MEG data. Based on what has been shown in [121], we suspected a relationship between occipital alpha power and ability to predict the angle. To test this, we computed correlation (Spearman’s rank correlation) ρ between T values and average occipital alpha power over subjects [102]. This results in a correlation coefficient of $\rho = 0.67$ which shows that average alpha power is significantly ($p < 0.05$) correlated with the ability to predict covert attention from the neurophysiological data. In short, if the alpha power from a given subject is not sufficiently strong, the modulations in alpha activity are too small in order to be of use in the covert attention paradigm. We did not find any (linear) relation between the behavioral performance of the subjects on counting the number of color changes and the performance when predicting the angle of attention.

2.4 Discussion

In this chapter, our goal was to examine whether a covert attention paradigm could serve as the basis for continuous control in non-invasive BCIs. We have shown that, based on occipital alpha power alone, the direction to which a subject was attending could be estimated using a circular regression approach. The results obtained over all subjects (Fig. 2.4), show that the angle of attention could be predicted with a mean absolute deviation of 51 degrees in our best subject. Averaged over subjects, the mean deviation was approximately 70 degrees. The trial length ensuring optimal information transfer was 1700 ms. This is a reasonable time-window for realistic BCIs. For this time-window, the best subject's mean absolute deviation was 60 degrees and the mean over all subjects was 77 degrees. Finally, we showed that subjects with strong alpha power during the task also were the best performers.

We asked subjects to covertly track a slowly moving visual target on a circular array. The experimental setup used here is strictly speaking one-dimensional as only one parameter is varied - the polar angle. However, this is a step towards two-dimensional control. Imagine that a cursor (or the background) moves in the direction of attention. The second dimension would then be constituted by time. Another way to achieve full two-dimensional control would be to allow subjects to direct covert attention both in terms of polar angle and radial distance. Whether or not it is achievable to predict radial distance from the brain signals as well remains an open question.

The moving target was applied since it would correspond to a real life situation in which the desired direction of the control signal is continuously changed, e.g. two-dimensional cursor control. It also allowed us to sample many angles in a short period of time. It should be noted that the neuronal processes following cueing of a relevant spatial locations can be interpreted as a consequence of anticipatory attentional deployment [88, 137, 57]. This may imply that subjects in our experiment are using anticipatory processes to predict the movement of the target on the circle and this anticipation might be controlling the modulation in the alpha band. This does by no

means invalidate the use of our paradigm for BCI applications, even though it does change the interpretation of the alpha modulation in terms of its underlying neurophysiological substrate.

Another point of concern with regard to the current paradigm is whether the modulations in alpha activity are caused by exogenous modulations resulting from the moving cue with the different color rather than endogenous changes in attention. It should be mentioned that the color of the cue and distracters were counter-balanced over blocks. Furthermore, there is strong evidence that covert attention modulates posterior alpha activity in the absence of visual cues [137, 90, 121]. Thus, it is most likely that it is covert attention being the main cause of the modulation of the alpha activity applied for the decoding. However, the issue could be further investigated in future paradigms in which a momentarily cue indicates the target.

In the current design there was a tradeoff with respect to window length. For short time windows estimation accuracy would be low due to little data. For long time windows the cue would move substantially and thus result in estimation errors. Thus, an optimal design in a BCI setup would allow for enough data to be collected before it has consequences for the interface (e.g moving a cursor).

Inter-individual differences in alpha-band power during spatial attention tasks have been discussed in several studies [44, 76, 63, 91]. As a consequence of these differences, the performance of the regression analysis varied over subjects. We were able to reliably estimate the angle of covert attention in about half of the subjects. However, it remains to be tested if this can be improved by training. There were some preferred angles for individual subjects where we were able to do better predictions. However, those preferred angles were different from one subject to another and we could not infer any general patterns pertaining to all subjects.

Our analysis did demonstrate a strong correlation between absolute alpha power and the ability to make use of the alpha activity modulated by covert attention [121, 91]. Certainly, in a practical setting, this insight could be of use in order to pre-screen subjects. The stage is now set for testing how well covert attention can be used to control a BCI system in a closed-loop setting. First, we do expect the performance to increase as subjects

control a given setup by covert attention and receive visual feedback on how well they do. This will increase accuracy. Second, as the ability to control improves, it is also likely that the optimal time-window required for the estimation will reduce. Both of these factors will result in an increase in the information transfer rate. Had we constrained the predictions to only left-right directions performance would be likely to increase since an index of left versus right alpha power could be applied [118, 58, 57].

Using covert attention as a control signal for BCI will have several advantages. Often imaginary movements have been used to control BCI systems [134, 77, 72]. While this is natural for prosthetic control, it is less natural for settings in which a visually displayed object has to be controlled. We believe that, in this context, covert attention will provide for a more natural control signal requiring less training. One example is a cursor on a screen that moves in the direction to which the subject covertly attends, i.e., a brain controlled mouse. Such an achievement will have a large number of potential applications including control of BCI spellers and navigation in graphical user interfaces as well as wheel-chair control. An additional advantage of using spatial attention as an alternative to the imagined movement paradigms could be in the case of reduced motor cortex activity resulting from changes in cortical plasticity after injury or degenerative processes.

Several studies strongly suggest that posterior alpha activity reflects the active inhibition of regions not participating in a given task [137, 59, 90, 54, 113]. This active inhibition might be important for ensuring the allocation of computational resources to task-relevant areas in the engaged brain. It is quite conceivable that if alpha modulation by covert attention is being used as a control signal for BCI, extensive training by this principle also will increase a subject's ability to control their alpha activity. This might then impact performance in paradigms in which visual attention is tested behaviorally. Such studies hold the promise of providing new knowledge on the physiological substrate of resource allocation in the brain by changing a subject's ability to modulate alpha activity.

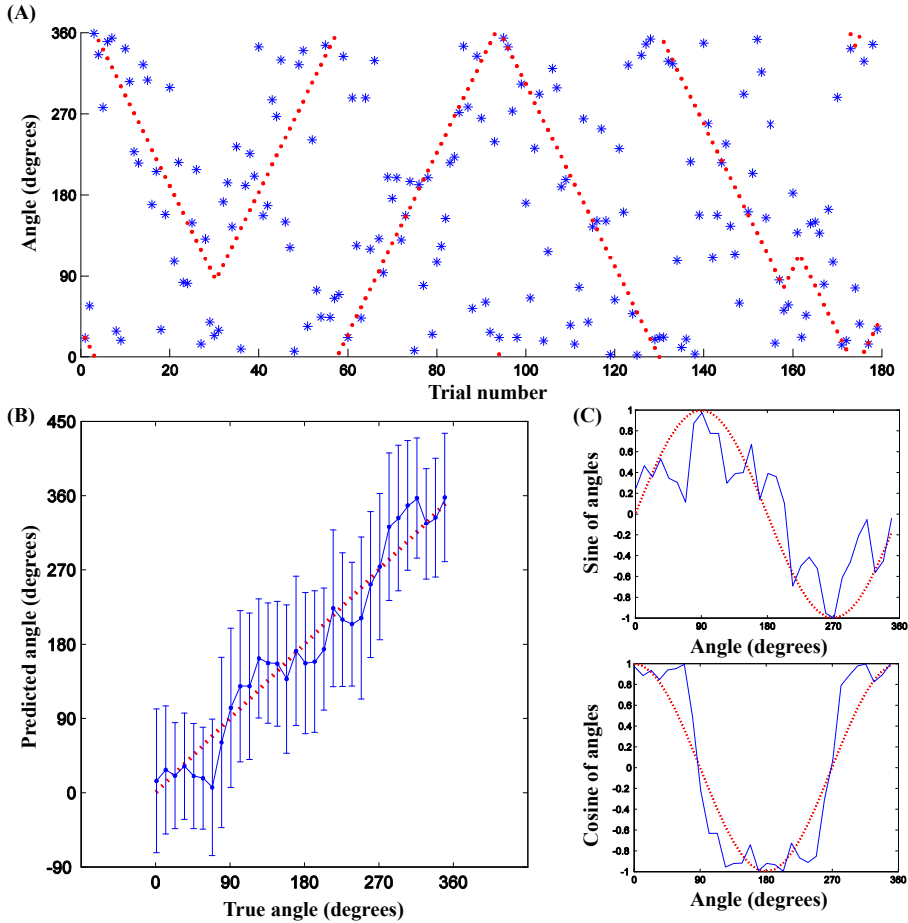


Figure 2.3: (A) Example from one subject showing the circular regression applied to 180 non-overlapping time-windows 1.7 s long. The dotted line is the actual angle of the target and the stars show the predicted angle. Note the change of direction around four random time points. (B) The regression results applied to the full data for the same subject. Error bars show the standard deviation. Mean absolute deviation was 61 degrees and average standard deviation was 80 degrees. (C) Sine and cosine components of the mean predicted angles.

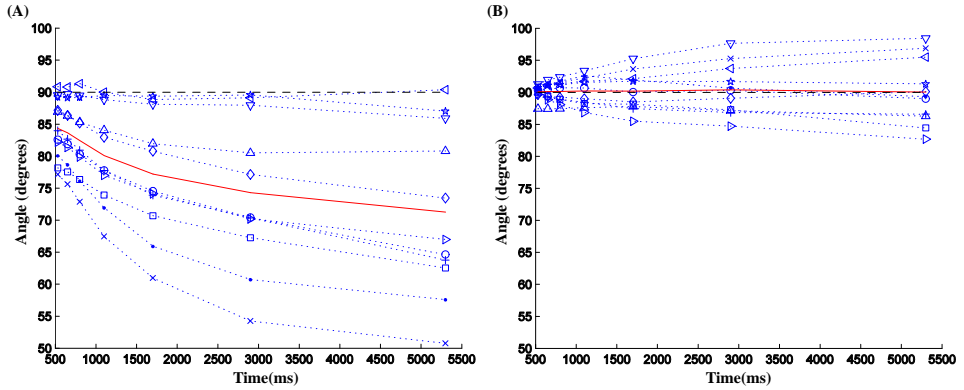


Figure 2.4: Mean absolute deviation using circular regression on (A) occipital alpha and (B) EOG. Solid line shows the average while dashed line shows the chance level.

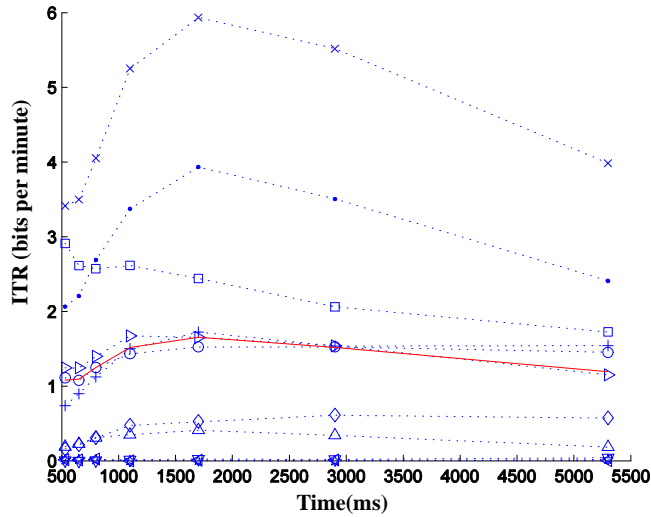


Figure 2.5: The information transfer rate (ITR) as a function of time for each subject. The solid line shows the grand-average indicating an optimal trial length of 1700 ms.

Chapter 3

Lateralized Responses During Covert Attention Are Modulated By Target Eccentricity

1

Various studies have demonstrated that covert attention to different locations in the visual field can be used as a control signal for brain computer interfacing. It is well known that when covert attention is directed to the left visual hemifield, posterior alpha activity decreases in the right hemisphere while simultaneously increasing in the left hemisphere and vice versa. However, it remains unknown if and how the classical lateralization pattern depends on the eccentricity of the locations to which one attends. In this chapter we study the effect of target eccentricity on the performance of a brain computer interface system that is driven by covert attention. Results show that the lateralization pattern becomes more pronounced as

¹This chapter is based on: Bahramisharif, A., Heskes, T., Jensen, O., van Gerven, M. A. J., ‘Lateralized responses during covert attention are modulated by target eccentricity’, *Journal of Neuroscience Letters*, Vol. 491, pp 35–39, 2011

target eccentricity increases and suggest that in the current design the minimum eccentricity for having an acceptable classification performance for two targets at equal distance from fixation in opposite hemifields is about six degrees of visual angle.

3.1 Introduction

Covert attention is the act of mentally focusing on a sensory stimulus without changing gaze direction [88]. Several studies have shown that when covert attention is directed to the left visual hemifield, posterior alpha activity decreases in the right hemisphere while simultaneously increasing in the left hemisphere and vice versa [137, 58, 90, 121]. Therefore, the ratio between left and right posterior alpha power, referred to as the alpha lateralization index (ALI), is strongly correlated with the direction of covert attention.

Kelly et al. [58] have introduced the use of the covert attention paradigm in a brain computer interface (BCI) setting using EEG. His results have been replicated in a subsequent MEG study by van Gerven et al. [118]. Furthermore, Rihs et al. [90] have shown the strong correlation between alpha power in posterior channels and covert attention to stimuli in eight different orientations. Inspired by these results, van Gerven et al. [121] have shown that, using the covert attention paradigm, four directions with a 90 degree angle between them can be detected at the single trial level with up to 70 percent accuracy. Finally, Bahramisharif et al. [11] have shown that continuous control is achievable by covertly attending to a target which describes a circular trajectory around the central fixation point.

These studies have shown that the lateralization pattern changes with the direction of the target to which one attends. While Kelly et al. [58] have located the center of the targets at 5 degrees of visual angle, Rihs et al. [90], van Gerven et al. [121, 118], and Bahramisharif et al. [11], have located them at 7.5 degrees of visual angle. This suggests, however, that the conventional covert attention paradigm, where two targets are placed on the midline in the left and right visual field at a fixed eccentricity, might

constitute a suboptimal design for driving a BCI in particular subjects. It remains an open question how the alpha lateralization pattern is modulated as a function of the eccentricity of the targets to which one should attend. Locations too close to central fixation might not induce the classical lateralization pattern observed in covert attention whereas locations too far away from central fixation might not lead to proper suppression of the distracter target in the contralateral visual field. Such interactions will directly affect the performance of a BCI system.

Multiple behavioral studies have shown the effect of eccentricity of covert attention on reaction times and spatial resolution in a variety of tasks, such as acuity, visual search, and texture segmentation [138, 26, 27]. It has been shown that directing attention to a given location allows us to better resolve the fine details of the visual scene at that location [138, 26, 27]. In this study, we examine the influence of target eccentricity on predictive performance in BCI systems. Specifically, we compute classification accuracy and ALI values as a function of eccentricity. Finally, we examine whether target eccentricity as such can be used as an additional degree of freedom in covert attention BCI paradigms.

3.2 Materials and Method

3.2.1 Data collection

Brain activity was measured during the task using an MEG system with 275 axial gradiometers (VSM/ CTF systems, Port Coquitlam, Canada) while the subjects were in sitting position. Data were sampled at 1200 Hz. Four EOG electrodes (2 horizontal and 2 vertical) were used to monitor eye movement. Eight healthy volunteers (six males and two females) were recruited for the experiment. Seven of the participants were naive and one of the participants was well-trained (subject 3). The well-trained subject practiced with this and similar experimental designs for more than 30 hours over the last year. The study was approved by the local ethics committee (CMO) and in agreement with the Declaration of Helsinki. Written informed consent was obtained from each of the subjects.

3.2.2 Experimental design

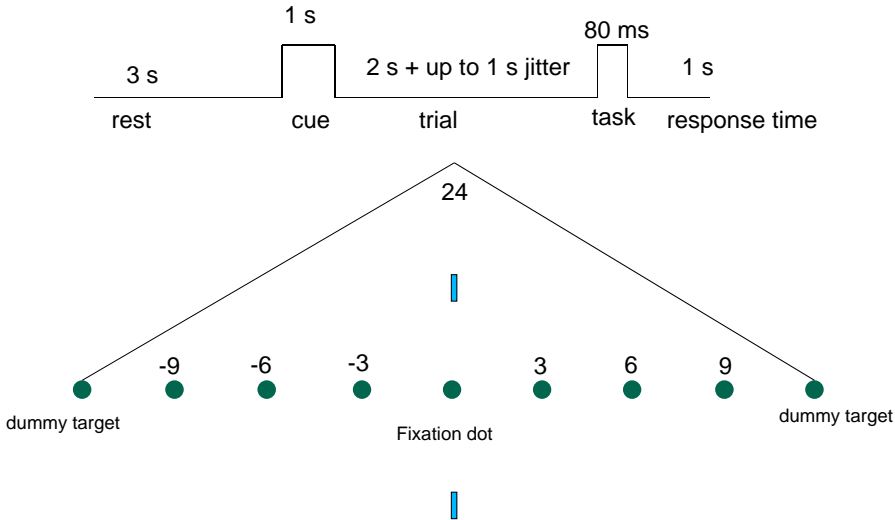


Figure 3.1: Experimental paradigm. Target dots were located in $[-9 -6 -3 +3 +6 +9]$ degrees of visual angle from the fixation dot.

There were nine equally spaced dots on the screen which was placed at a distance of 48 cm from the nasion (Fig. 3.1). The middle dot was marked with two small vertical lines and represented the fixation point. The diameter of each dot was one degree and the distances between the centers of the neighboring dots were three degrees of visual angle. I.e., the target dots were located at the following visual angles: $[-9 -6 -3 +3 +6 +9]$. The task was to fixate at the center of the screen and covertly attend to the location indicated by a cue (Fig. 3.1). The two far most right and left dots (visual angle of -12 and 12 degrees) were dummy targets and used to balance the design such that each target dot has two neighbors. The cue was given by showing a plus sign on the target dot and a minus sign on the five other possible targets for one second. During the cue, there was no minus sign on the fixation dot nor on the dummy targets. After at least two

seconds of attending to each target location, either an up or down arrow was shown on the target dot for 80 milliseconds. The task of the subject was to indicate whether an up or down arrow was presented by means of a button press with the right index or middle finger respectively. The response time was limited to one second. For each subject, each eccentricity was presented for fifty times, resulting in 300 trials for all six conditions.

3.2.3 Preprocessing

The planar gradient was approximated for each sensor using the signals calculated from a sensor and its neighboring sensors to obtain the strongest activity directly above the sources [42]. The first 500 ms of each trial were discarded since activity might be driven by the evoked response due to the cue. The power in the attention period was calculated using a 500 ms sliding Hanning window. Due to the 500 ms window we obtain a frequency smoothing of about 2 Hz, meaning that power over the 8–12 Hz alpha band was included. In this study, we only used the 10 Hz power components of 81 posterior channels (Fig. 3.2). Average alpha power over the 1500 ms attention period was centered to have mean zero and unit variance and used as input to the classifier. The alpha lateralization index was computed as the ratio between left and right posterior alpha power. It was used as an indirect measure of lateralization but not directly used for classification as [118] has shown that this leads to suboptimal classification performance.

3.2.4 Classification

L2 regularized logistic regression was used for classification. Logistic regression solves a classification problem by expressing the probability of class membership as [105, 139]:

$$p(c | \mathbf{x}, \boldsymbol{\theta}) \propto \exp(\boldsymbol{\theta}_c^T \mathbf{x})$$

where $\mathbf{x} = (x_1, \dots, x_M)$ is the set of features (including a bias term) and $\boldsymbol{\theta}_c$ is the parameter vector associated with class $c \in \{1, \dots, C\}$. A logistic

regression model is trained by minimizing the objective function:

$$E(\boldsymbol{\theta}) = L(\boldsymbol{\theta}) + R(\boldsymbol{\theta})$$

where $L(\boldsymbol{\theta}) = \sum_{n=1}^N \left(\log(\sum_{c=1}^C \exp(\boldsymbol{\theta}_c^T \mathbf{x}_n)) - \boldsymbol{\theta}_{c_n}^T \mathbf{x}_n \right)$ is the loss term which captures the fit of the model to the data and $R(\boldsymbol{\theta}) = \lambda \sum_{c=1}^C \boldsymbol{\theta}_c^T \boldsymbol{\theta}_c$ is the L2 regularizer which induces small parameter values [106]. A small fixed value of $\lambda = 1$ was used throughout all experiments in order to avoid collinearity issues.

Classification performance was calculated as the ratio between the number of correctly classified samples and the total number of samples. Significance levels for classification outcomes were computed using McNemar (approximate binomial) test comparing the classification outcomes with random outcomes ($p < 0.05$). For each subject, classification performance was averaged over ten subsets of data in a ten-fold cross-validation scheme.

3.3 Results

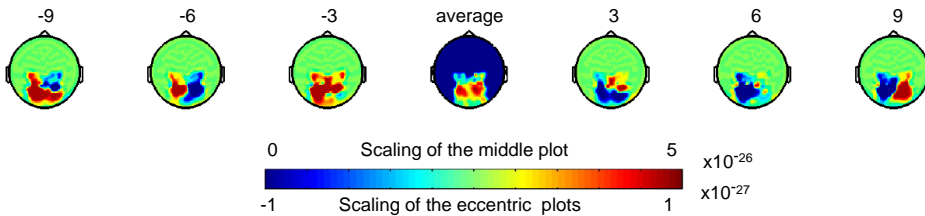


Figure 3.2: Relative differences of the average posterior alpha pattern for each eccentricity (from -9 to 9 degrees) with the average over all conditions. We plotted the 10 Hz power components of 81 posterior channels. The middle plot depicts the average over all conditions.

We first computed the change in posterior alpha power as a function of eccentricity averaged over all subjects. Figure 3.2 shows that there is a

clear alpha lateralization for the right and left directions and the pattern changes with the eccentricity of covert attention.

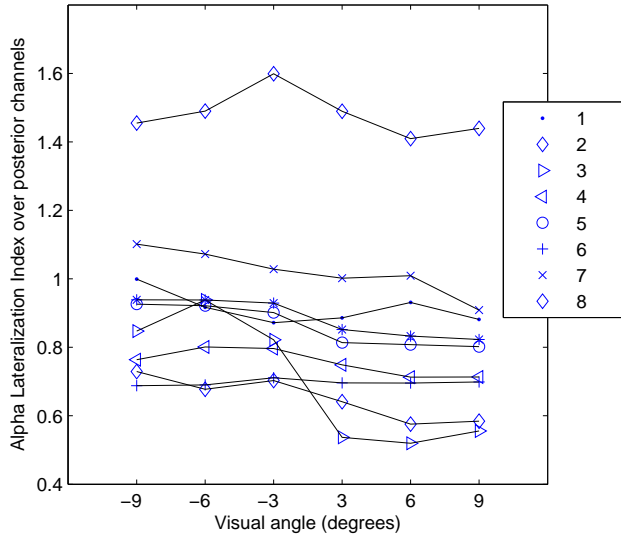


Figure 3.3: The alpha lateralization index versus eccentricity of the covert attention for all subjects. Average ALI over subjects is indicated by stars.

We then computed the ALI per subject for each eccentricity by dividing the average alpha power over left posterior channels by the average alpha power over the right ones (Fig. 3.3). Note that for most of the subjects, the ALI lies below one, meaning that the average posterior alpha power in the right hemisphere is stronger than in the left hemisphere. Furthermore, for each subject, we computed the Spearman rank correlation [102] between the ALIs and eccentricities. The average rank correlation over subjects was $\rho = -0.6$ ($p < 0.001$). When focusing on the eccentricities within one visual hemifield only, the average rank correlation would be $\rho = -0.25$ ($p < 0.1$). The obtained correlations imply that increasing eccentricity leads to a larger difference in the ALI with respect to baseline.

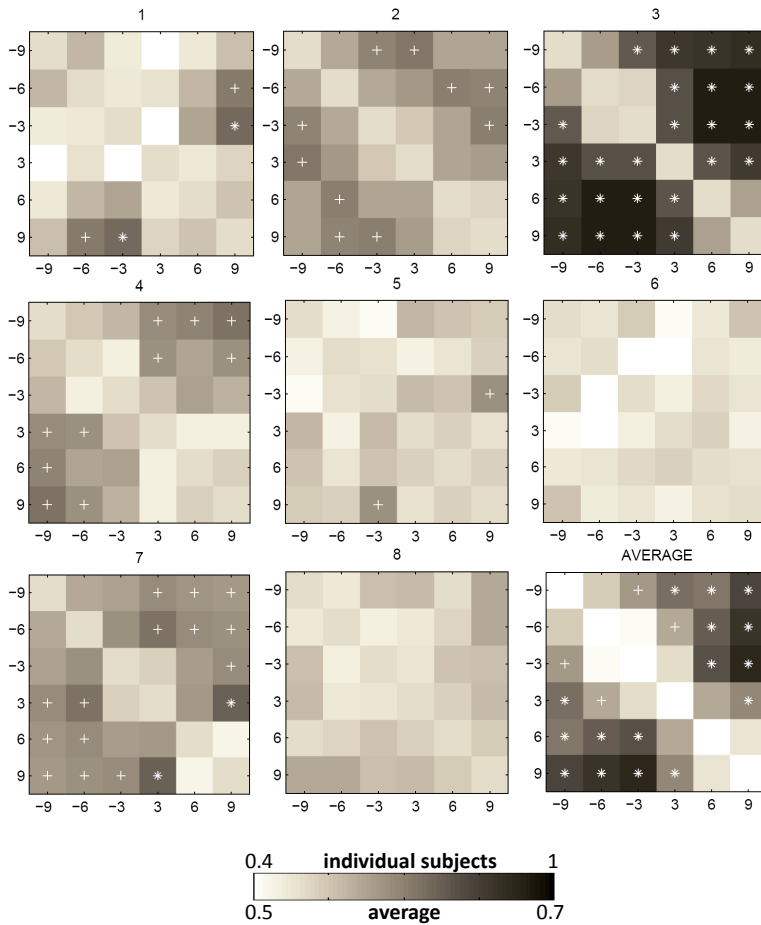


Figure 3.4: Pairwise classification performance versus eccentricity of covert attention for each subject and averaged over subjects. Significant discriminations are marked with a plus sign or a star (Bonferroni corrected). Random performance is 0.50.

We examined whether eccentricity could be used as an additional degree of freedom in a covert attention BCI. To this end, we trained regularized

logistic regression classifiers on all condition pairs in order to see which pairs of conditions are more classifiable than the others. Figure 3.4 shows the classification results for the pairwise comparisons of all six conditions averaged over all subjects as well as for the best subject (Subject 3). The significant pairs are indicated by means of a plus sign ($p < 0.05$) or a star (Bonferroni corrected for both the number of subjects and the number of pairs of conditions). The significance level for the average figure was obtained by first concatenating all trials over subjects and then comparing the results with assignments to a randomly selected class. For the average plot, the significance level was Bonferroni corrected for the number of pairs of conditions in order to control the family-wise error. It is evident that neighboring targets are often misclassified. Furthermore, it can be observed that for targets in the same visual hemifield, the performance is much lower than when they are from the different sides of the visual field. Still, for the best subject, classification of neighboring targets in the same visual hemifield can be achieved with classification performance that is above chance level.

In order to determine the optimal eccentricity for a left-right controlled covert attention BCI, we need to consult the opposite pairs in Fig. 3.4. From the average plot we see that classification of 3 versus -3 degrees of visual angle does not give significant results. However, classification of 6 or 9 degrees of visual angle with their contralateral counterparts does give significant classification performance ($p < 0.05$ Bonferroni corrected for the number of pairs of conditions).

We suspected a relationship between the classification performance and the differences of the ALIs for each pair of conditions. To check that, we computed correlation (Spearman's rank correlation) between the classification performances and the differences of the lateralization indexes over subjects [102]. This test resulted in a significant correlation of $\rho = 0.41$ ($p < 0.001$).

To check for confounds, we conducted the same analysis using the EOG electrodes. Our result showed that there is no direction-related information in the EOG data. We also checked for how well the subjects performed the task of producing the correct button response. The behavioral performance

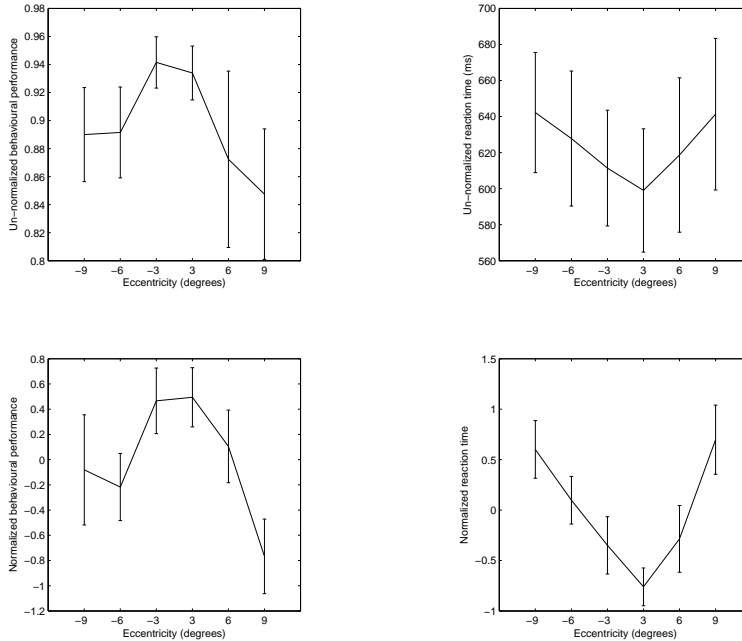


Figure 3.5: Average unnormalized (top-left) and normalized (bottom-left) reaction time together with the average unnormalized (top-right) and normalized (bottom-right) behavioral performance over all subjects for each eccentricity. The behavioral performance of the subject was defined as the ratio between the number of hits and the total number of hits and misses. The total number of hits and misses for each eccentricity for each subject was 50. The behavioral performances and reaction times were normalized by subtracting the mean and dividing by the standard deviation over all eccentricities within each subject. Error-bars indicate the standard error over eight subjects.

of the subject was defined as the ratio between the number of hits and the total number of hits and misses. Average behavioral performance decreases with target eccentricity and is inversely related to the average reaction

time, as shown in Fig. 3.5 and in line with previous findings [26, 27]. There was no correlation between the behavioral performances and the obtained classification performances.

3.4 Discussion

In this chapter we explored the influence of target eccentricity on the performance of a covert attention BCI. We found that the alpha lateralization index increases as a function of eccentricity, which is positively correlated with classification performance. The results suggest that in the current design, the minimum eccentricity for having an acceptable classification performance for classifying a target against its contralateral counter part is about six degrees of visual angle while performance does not change much as target eccentricity is further increased. Figure 3.5 shows that average normalized behavioral performance decreases with target eccentricity and is inversely related to the average reaction time. There was no correlation between the behavioral performances and the classification performances shown in Fig. 3.4.

Some of the subjects could not achieve proper BCI control, which is typical for most BCI experiments and referred to BCI illiteracy [125]. We found a significant correlation between the ALI differences and the classification performances, which implies that the ALI can be used to monitor subjects for BCI illiteracy. The well-trained subject showed by far the highest classification performances (>90% for left-right control) which indicates that subject training can lead to profound improvements. With regard to classification of targets in opposing hemifields, subject 2 did not follow the general trend in that he showed significant above chance performance for 6 degrees but not for 9 degrees of visual angle. Behavioral results for this subject nevertheless show the normal pattern of decreasing performance with increasing eccentricity.

Based on the classification performances for the six different eccentricity pairs, we conclude that target eccentricity cannot be used reliably as an additional degree of freedom in covert attention BCIs. The results do

indicate that peripheral targets can be distinguished from targets close to fixation. This may be useful with regard to the notion of a brain-controlled switch [70], where attending to fixation is used to activate or deactivate the BCI system.

Figure 3.2 shows that the lateralization pattern changes as a function of target eccentricity. Changes in the lateralization pattern are also observed when attention is directed towards targets at different angles relative to fixation [90, 121, 11] and may be due to the fact that visual attention to a spatial location is retinotopically organized [107], i.e., directing attention to a certain spatial location will cause stronger activations in different parts of visual cortex and therefore lead to different spatial topographies at the MEG sensor level. With respect to eccentricity, we find that the further one moves away from fixation, the larger the difference in alpha lateralization index with respect to fixation. Figure 3.3 shows that on average the difference in ALI when moving from an eccentricity of minus three to three degrees of visual angle is much larger than the difference when moving from three to six or nine degrees which could be the result of cortical magnification [93, 51]. Finally, the results also indicate that in six out of eight subjects the ALI has a bias in favor of the right hemisphere which could be related to asymmetries in cortical visual field representations [117, 16, 100].

Concluding, we have shown that target eccentricity strongly influences classification performance in covert attention BCIs. The observation that target eccentricity modulates the observed lateralization pattern in occipitoparietal cortex is also of importance and indicate that target eccentricity should be considered as an important confound when comparing studies of covert spatial attention.

Chapter 4

Decoding the direction of covert attention with EEG

1

Visual brain-computer interfaces (BCIs) often yield high performance only when targets are fixated with the eyes. Furthermore, many paradigms use intense visual stimulation, which can be irritating especially in long BCI sessions. However, BCIs can more directly tap the neural processes underlying visual attention. Covert shifts of visual attention induce changes in oscillatory alpha activity in posterior cortex, even in the absence of visual stimulation. The aim was to investigate whether different pairs of directions of attention shifts can be reliably differentiated based on the elec-

¹This chapter is based on:

- Treder, M. S., Bahramisharif, A., Schmidt, N. M., van Gerven, M. A. J., Blankertz, B., ‘Brain-Computer Interfacing using modulations of Alpha activity induced by covert shifts of attention’, *Journal of NeuroEngineering and Rehabilitation*, 8:24, 2011
- Wouters, H. J. P., van Gerven, M. A. J., Treder, M. S., Heskes, T., Bahramisharif, A., ‘Covert attention as a paradigm for subject-independent brain-computer interfacing’, *NIPS workshop on Machine Learning and Interpretation in Neuroimaging*, Sierra Nevada, Spain, 2011

troencephalogram. To this end, healthy participants ($N=8$) had to strictly fixate a central dot and covertly shift visual attention to one out of six cued directions. As expected, covert attention shifts induced a prolonged alpha synchronization over posterior electrode sites (PO and O electrodes). Spectral changes had specific topographies so that different pairs of directions could be differentiated. There was substantial variation across participants with respect to the direction pairs that could be reliably classified. Mean accuracy for the best-classifiable pair amounted to 74.6%. Furthermore, an alpha power index obtained during a relaxation measurement showed to be predictive of peak BCI performance ($\rho = .66$). Results confirm posterior alpha power modulations as a viable input modality for subject-independent BCI. The pair of directions yielding optimal performance varies across participants. Consequently, participants with low control for standard directions such as left-right might resort to other pairs of directions including top and bottom.

4.1 Introduction

A brain-computer interface (BCI) serves to decode user intention from brain signals, enabling a direct communication between brain and computer. Since the main target group of BCIs is patients with motor impairments, it is vital that the control of a BCI does not involve motor activity. However, this is not always the case. For instance, for the widely used Matrix speller (P300-speller), evidence accumulates that BCI control is efficient only when the target symbol is fixated with the eyes [108, 25].

Different routes have been taken to circumvent the problem of gaze dependence. For instance, one may fall back on other sensory modalities such as spatial auditory [98, 50] and tactile feedback [24]. Alternatively, one may rely on other paradigms such as motor imagery [40, 20]. However, motor imagery paradigms face the problem that a subset of participants does not obtain significant BCI control, a problem that is only partially solved [22, 125]. Also in the visual domain, there have been promising approaches to gaze-independent BCIs. For instance, recently, three visual

gaze-independent spellers have been introduced [108, 109]. In contrast to the Matrix speller, the selection process was broken down into two successive steps, and for the best speller, mean symbol selection accuracy amounted to about 97%. In another study, rapid serial visual presentation of symbols was used, with a mean symbol selection accuracy of up to 90% for selecting one symbol out of thirty [1].

Note, however, that these paradigms rely on visual stimulation. In particular, they exploit the fact that the event-related potential (ERP) associated with a visual stimulus can be modulated by attention. In the present study, we take a more fundamental approach. It has been shown that covert spatial attention shifts are accompanied by power changes in the alpha band (8–12 Hz) of the electroencephalogram (EEG) at posterior electrode sites [97]. Therefore, rather than measuring the effects of attention on the neural response to visual stimulation, we directly tap the neural process underlying covert attention shifts. This approach has several advantages over conventional paradigms based on ERPs. First, continuous visual stimulation, which can be tedious and irritating especially in long BCI sessions, is superfluous. Second, for some application domains such as spatial navigation, it seems more intuitive to shift attention to the desired location rather than to perform a task such as counting the occurrences of a flashing target. Third, a BCI based on changes in oscillatory alpha activity potentially allows for asynchronous control. That is, the user initiates a covert attention shift whenever he or she wants to issue a command, whereas in an ERP paradigm, the user has to adhere to the pace and timing of the visual stimulation sequence.

Kelly et al. suggested that the alpha paradigm may indeed be a feasible input modality for EEG-based BCIs [58]. Participants were instructed to deploy covert spatial attention to a target that was located either left or right of the fixation point. Offline classification showed that it is possible to discern attention shifts to either direction based on modulations of the posterior alpha rhythm. However, one of the caveats of this study was that the authors used targets flickering in different frequencies. Since the flickering might interact with the deployment of attention, it is unclear how these results transfer to a paradigm without continuous visual stimulation. Re-

cent studies using magnetoencephalography (MEG) mapped out multiple directions of attention shifts. It was shown that shifts to multiple spatial directions, including top and bottom, yield distinctive patterns of alpha modulation [90] that can be reliably classified [118, 121]. Follow-up studies investigated the role of stimulus eccentricity [10] and showed that arbitrary directions can be decoded [11]. However, it remained unclear whether the results from MEG transfer to EEG. After all, the former has a substantially higher spatial resolution which allows for a more accurate estimate of the topographical distribution of alpha power. Regarding practical application, however, an EEG-based solution is desirable due to its lower cost, portability, and the possibility to use it in a home environment.

The aim of the present study was to bring together these strands of research on visual alpha based BCIs. Expanding on the work by Kelly et al. [58], we investigated whether attention shifts to directions other than left-right would also induce distinctive patterns of alpha modulation.

4.2 Materials and methods

4.2.1 Data collection

Eight healthy volunteers (seven male, one female), aged 18–27 years, participated in this study. All participants had normal or corrected-to-normal vision. All participants gave written consent and the study was performed in accordance with the Declaration of Helsinki.

EEG

EEG was recorded from a Brain Products (Munich, Germany) 64 channel actiCAP, digitized at a sample rate of 1000 Hz, with impedances kept below 20 k Ω . We used electrodes Fp2, AF3,4, Fz, F1–10, FCz, FC1–6, T7,8, Cz, C1–6, TP7,8, CPz, CP1–6, Pz, P1–10, POz, PO3,4,7–10, Oz,1,2 and Iz,1,2, placed according to the international 10-10 system and referenced against a nose reference. Additionally, an EOG electrode labeled EOGvu was placed below the right eye. Vertical and horizontal bipolar EOG chan-

nels were created by referencing Fp2 against EOGvu, and F10 against F9, respectively. Stimuli were presented on a 24" TFT screen with a refresh rate of 60 Hz and a resolution of 1920×1200 px². The experiment was implemented in Python using the open-source BCI framework Pyff [124] with Pygame (<http://pygame.org>). Data analysis and classification were performed with MATLAB (The MathWorks, Natick, MA, USA) using custom functions and the Fieldtrip toolbox [80].

Task and Stimuli

Participants performed a cued visual attention task. The course of a trial is depicted in Fig. 4.1. First, a white central fixation dot surrounded by six white target discs was presented. The discs had a size of 3.27° of visual angle and they were presented at an eccentricity of 9° from the fixation dot. A cue appearing for 200 ms in the center of the screen indicated the target location. Participants had to shift attention to the cued disc while strictly fixating the central dot. Instead of arrows, we used an omnidirectional cue to reduce the danger of evoking event-related potentials specific to the direction of the cue. The cue was a hexagon with each of the six faces pointing to one of the target discs. Three of the faces were grey and the other three were colored blue, red, and green, respectively. One of these colors was used as target indicator, that is, the participant had to covertly direct and maintain attention to the disc to which this color was pointing. The use of one of the three colors as target color was counterbalanced across participants. After a variable duration (500–2000 ms) the target appeared for 200 ms in the disc as either a '+' or a 'x'. Participants indicated which symbol they had perceived by pressing with their thumb on one of two buttons lying in the palm of the right and left hands. Two different targets had been chosen to reduce readiness potentials for pressing a button, as suggested by [90]. After 200 ms, a star-shaped masker ('*') was presented at the target location for 200 ms in order to prevent an afterimage of the target and thereby increase task difficulty.

Each participant completed 600 trials in six blocks of 100 trials with two-minute breaks between blocks. Cues were valid in 80% of the trials.

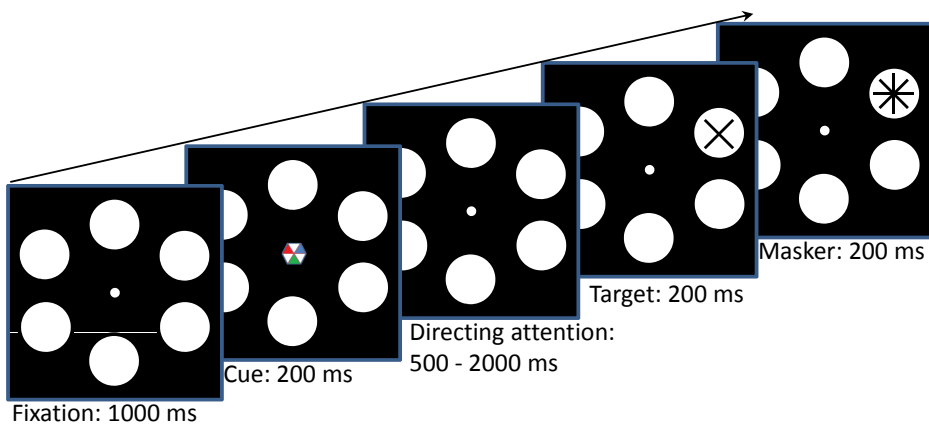


Figure 4.1: Covert attention task. After 1000 ms, a cue in form of a hexagon appeared. Participants had to attend to either the blue, red, or green face of the hexagon, and they had to covertly shift attention to the disc the face was pointing at. After a variable amount of time (500–2000 ms), a target ('+' or '×') appeared, followed by a masker ('*'). The participant indicated the perceived symbol by means of a button press with the right or left hand.

In the other 20% of the cases, the target appeared at a different random location. The target symbol was randomly chosen, with equal chances for ‘+’ and ‘×’. Target latency (i.e., the time between cue onset and target onset) was 2000 ms in 50% of the trials. To ensure that the participants shift their attention immediately after the appearance of the cue, 30% of the trials featured a short target latency of 500 ms. In the remaining trials, the target latency was randomized between 500 ms and 2000 ms in order to ensure that attention is sustained continuously until target appearance.

4.2.2 Preprocessing

For each electrode, a single spectral feature was extracted by estimating bandpower in the alpha range (8–12 Hz) for the 500–2000 ms interval using the Welch method [81]. In other words, the interval was split into 8 segments with 50% overlap between segments. Each segment was windowed using a Hamming window. Spectral power was estimated in each segment and then averaged across segments. During cross validation, for each subject, data was normalized to have zero mean and a standard deviation of one in the training set of the outer fold.

4.2.3 Classification

For each participant, and for each of the fifteen possible pairs of directions, we performed binary classification using L2-regularized logistic regression (LR) [139, 36] and a correlation based classifier (Cor) [48, 74] and computed classification accuracy under a ten-fold cross-validation scheme [64]. LR is explained in Sec. 3.2.4. The correlation based classifier (Cor) compares the Pearson correlation coefficient of a trial to a class template. The class templates are the average of all trials belonging to a class in the training set. A test sample is classified as the class which corresponds to the template with which the object has the highest correlation. In order to determine the optimal regularization parameter for LR, a grid search was performed and the smallest parameter value was chosen that gave highest accuracy as computed with five-fold cross-validation using just the training

data of the outer ten-fold cross-validation. Subsequently, the classifier was retrained using all training data in order to test the classifier on the test data. Significance levels were calculated by comparing classification outcomes with an assignment of all outcomes to the majority class using the binomial test [96].

4.3 Results

4.3.1 Behavioral results

Overall response accuracy was $86.62\% \pm 8.46\%$ SEM. The accuracies in the valid and invalid condition were compared using a paired-samples t-test and found to be not significantly different ($p = .199$). In contrast, the geometric means of the reaction times were significantly smaller in the valid condition than in the invalid one ($t = 4.49, p < .01$), indicating that the participants attended correctly the cued positions (valid: $719 \text{ ms} \pm 51 \text{ ms SEM}$; invalid: $881 \text{ ms} \pm 76 \text{ ms SEM}$).

We repeated the analysis on the subset of trials wherein the target latency was 2000 ms, since only this subset was used for neurophysiological analysis and classification (see next paragraph). For this subset, overall response accuracy amounted to $87.2\% \pm 8.6\%$. The accuracies in the valid and invalid condition were not significantly different ($p = .233$). The geometric means of the reaction times were significantly smaller in the valid condition than in the invalid one ($t = 3.92, p < .01$; valid: $742 \text{ ms} \pm 55 \text{ ms}$; invalid: $896 \text{ ms} \pm 84 \text{ ms}$).

4.3.2 Neurophysiological results

For neurophysiological analysis and classification, we used the subset of trials with a 2000 ms target latency. Trials with shorter target latencies were not considered since they were only intended to stimulate participants to shift their attention immediately after cue onset. In the former trials the whole 2000 ms contain the shift and maintenance of attention to the target without any external stimulus. The spatial resolution of the EEG data was

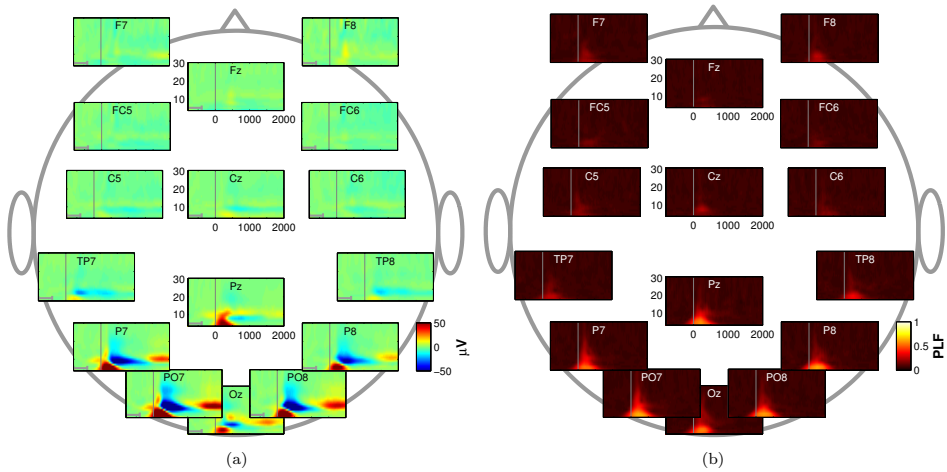


Figure 4.2: Grand average wavelet spectra. In each time-frequency plot, the interval of -800 to 2000 ms relative to cue onset (vertical line) is depicted on the x-axis. Morlet wavelet center frequencies, ranging from 4 to 30 Hz, are depicted on the y-axis. Color signifies wavelet amplitude in (a) and the phase-locking factor in (b). (a) At posterior electrode sites, three neurophysiological events can be observed, namely an early synchronization in the delta and theta bands, followed by a desynchronization and subsequent synchronization in the alpha band. (b) Phase-locking factor (PLF), specifying the amount of phase-locking to stimulus onset. Only the early synchronization in the delta and theta bands is phase-locked to stimulus onset. This supports the idea that the early component reflects the processing of the visual cue, while the alpha (de)synchronization is associated with the deployment of covert visual attention.

enhanced using a current source density estimate [56]. Figure 4.2 depicts grand-average wavelet spectra for a subset of scalp channels, averaged over all six directions and all participants. In Fig. 4.2a, wavelet coefficients were determined for single trials and then averaged over all trials and participants. Note that wavelets are acausal filters, that is, post-stimulus activity can leak into the pre-stimulus baseline. Therefore, baseline-correction was performed on the -800 to -419 ms interval, as indicated by the grey bar in each subplot. Choosing -419 as upper bound prevented post-cue activity from leaking into the baseline because it corresponds to half the width of the widest wavelet. The spectra show three distinct neurophysiological events preponderating at posterior electrode sites, with little event-related activity at other electrode sites. First, a synchronization in the delta and theta bands peaking at 200–300 ms. Second, a desynchronization in the alpha band peaking roughly at 500 ms. Third, a subsequent late synchronization alpha band evident from about 1500 ms. In Fig. 4.2b, the phase-locking factor (PLF) was calculated by first normalizing wavelet coefficients to unit magnitude, averaging over epochs and then determining the magnitude of the result [103]. Only the first of the events depicted in Fig. 4.2a displays phase-locking with stimulus onset, suggesting that the early delta and theta activity is caused by ERPs that reflect the visual processing of the cue. In line with the literature (e.g., [137, 97, 121]), we found that an alpha desynchronization and a subsequent synchronization indexes shifts of covert visual attention.

Alpha power over the occipital channels for different directions of attention averaged over all participants is shown in Fig.4.3. In this plot, there is a clear overall difference between different conditions. The obtained plot is consistent with the results shown in [11].

Moreover, the alpha lateralization index (ALI) is calculated as the ratio between the average alpha power over the left posterior channels and the average over the right ones. The average ALI over all subjects is shown in Fig. 4.4.

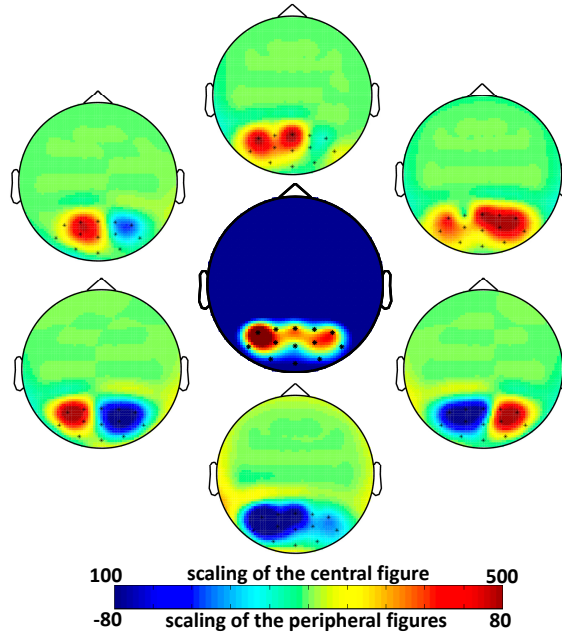


Figure 4.3: Occipital alpha activity for different directions of covert attention. The central panel shows the average alpha over all directions over all subjects. The peripheral panels show the relative differences with the average. The selected channels are marked with black stars.

4.3.3 Classification

Since alpha power peaks over occipital electrodes sites (see Fig. 4.9a), the subset of electrodes comprising PO3,4,7–10, and Oz,1,2, was selected as input to the classifier. We focused only on alpha synchronization, because the preceding alpha desynchronization did not show distinctive patterns for the different directions.

Average classification performances of all pairs of directions over all subjects for Cor and LR were $60.6\% \pm 0.7\%$ and $61.9\% \pm 0.7\%$, respectively. Figure 4.5 shows that there was a correlation of 0.78 ($p < .001$) between

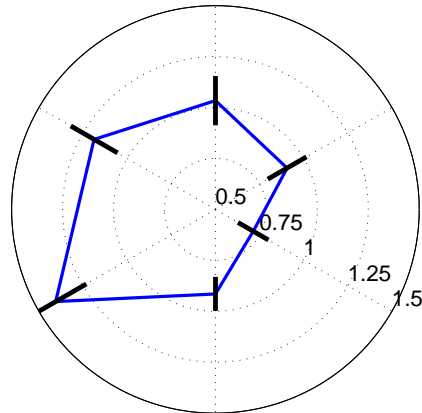


Figure 4.4: Average alpha lateralization index (ALI) for each direction of covert attention. Bars indicate the standard error of the mean ALI. Down-left (DL) and down-right (DR) have the highest and the lowest values, respectively.

the two sets of classification performances. As there was no significant difference between the results of the two classifiers and performance of LR was a bit higher, we show the results based on using LR.

Mean accuracy for the best pair of directions was $74.6\% \pm 2.3\%$. Figure 4.6 depicts the classification accuracy for each participant and for each pair of directions based on using LR. Colored pie pieces represent directions that were significant under a significance threshold of 0.05. Moreover, for three participants (*iac*, *mk*, and *iaa*) results were highly significant ($p < .001$). The figure reveals large individual differences. In particular, the pair of directions yielding the best classification performance varies substantially across participants. In most cases, some combination of left and right directions yields the best classification performance.

In line with earlier work [10], we suspected a relationship between the classification performances and the differences of the alpha lateralization indexes (ALIs). We found a correlation of 0.69 and 0.79 ($p < 0.001$) between the ALI differences and the classification results of LR and Cor, respectively.

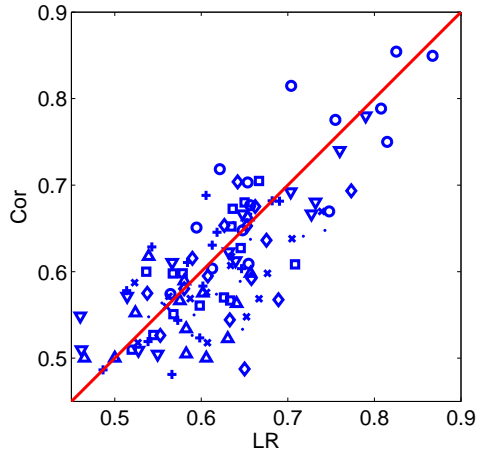


Figure 4.5: Classification accuracies of Cor versus LR.

To check for confounds, we applied a logistic regression classifier on the time series obtained with two bipolar EOG channels. Highly significant classification performance ($p < .001$) was obtained for only one direction in one participant. Under a significance threshold of 0.05, EOG data alone was not sufficient to obtain significant classification outcomes for three participants. For participants *mk*, *iae*, and *iac*, only one pair of directions was classifiable. For participant *gao*, this was the case for two pairs of directions (top-right versus top-left and bottom-right versus bottom-left). For participant *nh*, five pairs of directions could be classified. Note that the latter participant yielded the worst classification results on the EEG data (see Fig. 4.6), which suggests a dissociation of the processes underlying EOG activity and posterior alpha activity. In line with this, the scatter plot shown in Fig. 4.7 makes clear that there is no significant correlation ($\rho = .029$, $p = .75$) between the classification outcomes obtained using either EEG or EOG measurements.

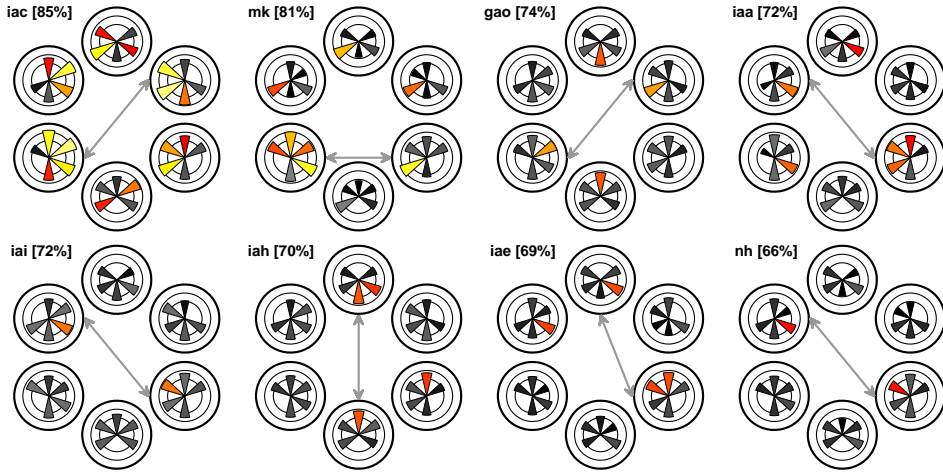


Figure 4.6: Binary classification results for each of the eight participants and for each pair of directions using L2-regularized logistic regression. Peak accuracy for the best-classifiable pair of directions is given in brackets after the participant code; this pair is also indicated by a double arrow. Classification scores are depicted for all binary pairings of directions. For each participant, the data consists of six polar plots placed at spatial locations analogous to the locations used in the experiment. Each polar plot contains five pie slices depicting classification accuracies between the location of the plot and each of the five other possible directions. Classification accuracies that are significantly different ($p < .05$) from chance level (50%) are given as yellow-red pie slices, non-significant accuracies are shaded grey. Both the length of a pie piece and its color indicate classification accuracy (lighter color for higher accuracy, darker color for lower accuracy). For instance, for participant *iai*, only the top-left and the bottom-right directions could be differentiated from each other significantly.

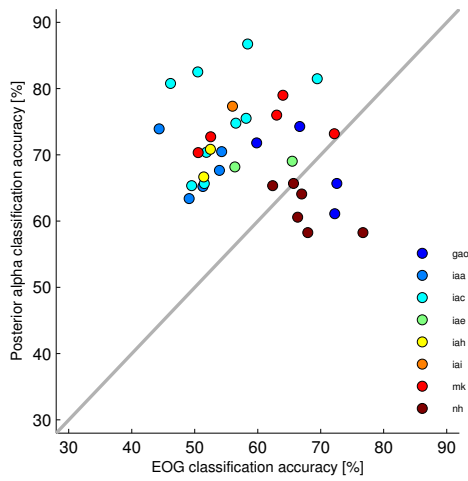


Figure 4.7: Classification accuracies using EOG versus EEG. For each participant, only those direction pairs are depicted which yielded significant classification results based on EEG and/or EOG. Notably, high accuracy for EEG-based classification usually comes with low accuracy for EOG-based classification, and vice versa. This suggests a dissociation between EEG- and EOG-based classification.

4.3.4 Left hemisphere versus right hemisphere contribution

There is evidence that the left and the right hemisphere do not contribute equally to shifts of visual attention [73]. In particular, the left hemisphere mainly supports shifts of attention in the contralateral (right) hemifield, while the right hemisphere is involved in attention shifts in both hemifields. To investigate whether this asymmetry applies to the present data as well, we pooled over both left and both right directions and estimated alpha power in the classification interval (500–2000 ms) for both directions. Subsequently, we calculated the signed square of the point-biserial correlation coefficient $sgn r^2$ (see, e.g., [21]), contrasting shifts to right directions with shifts to left directions. The results are depicted in Fig. 4.8a. In line with the literature, alpha power is higher at left hemisphere electrode sites when attention is directed to the right than when attention is directed to the left. For right hemisphere electrode sites, alpha power does not differ significantly for shifts to right and shifts to left directions.

As a consequence, one would expect an asymmetric impact of electrode position on BCI performance, with left hemisphere electrodes contributing more to classification success than right hemisphere electrodes. As Fig. 4.8b suggests, this is indeed the case. For most participants, classification on left hemisphere electrodes yields better scores than classification on right hemisphere electrodes. Nevertheless, taking into account both hemispheres usually improves performance, suggesting that right hemisphere electrodes add independent information. To compare these three conditions quantitatively, we performed a 1-way analysis of variance (ANOVA) on the peak performances in the three conditions. We found a significant effect of the electrode subset (left, right, or both hemispheres) on BCI performance ($F = 6.11$, $p < .01$). Tukey-Kramer post-hoc tests revealed that classification using both hemispheres gives better accuracy than classification using left hemisphere only. The other contrasts were not significant.

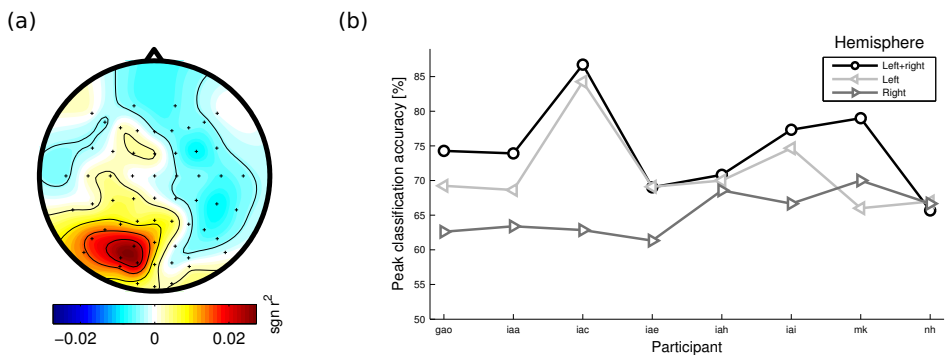


Figure 4.8: Contribution of left and right hemispheres to classification success. (a) Point-biserial correlation coefficient contrasting spectral power for shifts to right versus left directions. The $sgn r^2$ is peaking over the left hemisphere only. No differential effect is observed over the right hemisphere. (b) Peak classification accuracy when only left hemisphere electrodes, only right hemisphere electrodes, or both sets are used for classification. For illustrative purposes, data points belonging to the same electrode montage have been connected by lines. The graph suggests that left hemisphere electrodes yield a higher performance than right hemisphere electrodes.

4.3.5 Alpha rhythm based predictor of BCI performance

Due to the proliferation of BCI research in the last decade, there exists now a wide palette of BCI systems. However, there is no *a priori* criterion for assigning a particular BCI system or a particular input modality (such as event-related potentials or sensorimotor rhythm) to a new BCI user, despite the fact that there is high variability across users regarding the efficiency of particular BCI paradigms. As a result, BCI users might use a system that does not yield optimal performance. This problem is aggravated by the fact that a non-negligible proportion of participants fails to exhibit significant BCI control. For paradigms based on the modulation of the sensorimotor rhythm (SMR), this proportion amounts to 15–30% of the subject population [22].

Consequently, there is growing need for efficient screening procedures that allow for the estimation of prospective BCI performance. To be useful, screenings should be obtained within few minutes using a simple paradigm, in order to prevent a tedious and, upon failure, frustrating calibration procedure. For instance, Blankertz et al. showed that the *mu* rhythm generated in motor cortex is predictive of BCI performance in a motor imagery paradigm [22]. The predictor was obtained from a 2 minutes measurement during which participants were instructed to relax with eyes open. It showed a correlation of $\rho = .53$ with BCI performance.

In a similar fashion, our aim was to use posterior alpha power from the resting EEG as a predictor of BCI performance. To this end, we investigated the relaxation data recorded prior to each experiment. We considered the epochs wherein participants relaxed with eyes closed. After current source density filtering [56], the spectral peak in the 8–12 Hz alpha range was extracted for each electrode.

Figure 4.9a shows that alpha energy dominates at parieto-occipital electrode sites. Consequently, we considered pooled alpha power of symmetric electrode pairs at parieto-occipital sites as a predictor. For electrode pair PO3–PO4, a correlation of $\rho = .66$ ($p = .07$) was found, see Fig. 4.9b. For electrode pair PO7–PO8, correlation drops ($\rho = .54$; $p = .17$), despite the higher absolute power. We suppose that this might stem from the fact that

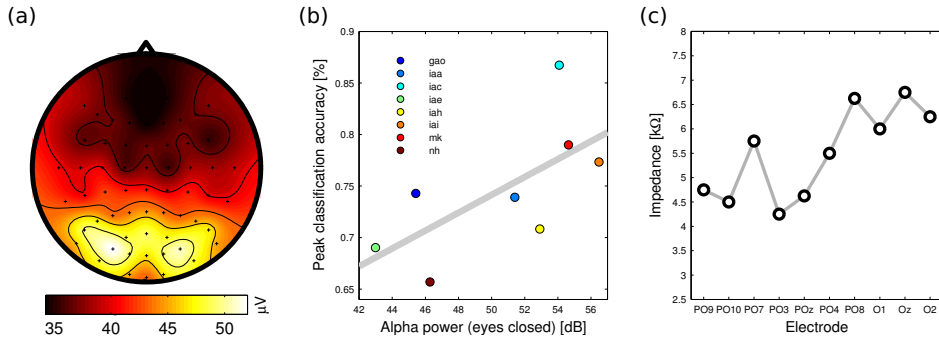


Figure 4.9: Prediction of BCI performance based on the alpha rhythm. (a) Spatial distribution of alpha energy during relaxation with eyes closed. Alpha amplitude is highest over the electrode subset that was used for classification (i.e., PO3,4,7–10, and Oz,1,2), with absolute peaks at electrodes PO7 and PO8. (b) Correlation between alpha power at electrode pair PO3–PO4 and peak classification accuracy ($\rho = .66$). The grey line gives a linear fit. (c) Mean impedances across participants show lower impedance for PO3–PO4 than for PO7–PO8. This possibly explains why the former pair is more predictive of BCI performance than the latter.

mean impedance was lower for PO3–PO4 than for PO7–PO8, yielding a cleaner EEG signal (Fig. 4.9c).

4.3.6 Subject-independent learning

For subject-independent learning the goal is to decode the direction of attention of a subject without any previous class information about that particular subject. For that, all trials except the ones belonging to the test subject are pooled in a single training set and used to build a classifier. This model is then used to classify data of the test subject. Evaluation was done using a leave-one-subject-out (LOSO) strategy. Pooling is shown with postscripts ‘P’ in the rest of this chapter.

The average classification performance of Cor_P and LR_P were $58.2\% \pm$

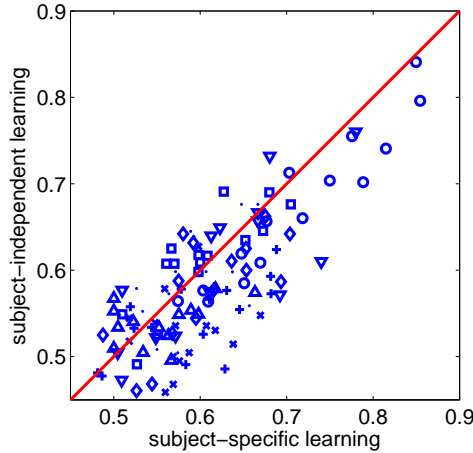


Figure 4.10: Classification performance of Cor_P versus Cor. Different symbols stand for different subjects. For all subjects, all pairs of directions are included.

0.7% and $56.9\% \pm 0.7\%$, respectively. Although for subject-specific learning, LR was performing a bit better than Cor, for subject-independent learning, Cor_P was performing a bit better than LR_P, so here we show the result of using Cor_P. As Cor is a very simple classifier without any parameter to be tuned, it is expected to perform well in the context of subject-independent learning.

Classification performance of Cor_P versus Cor is shown in Fig. 4.10. There is a correlation of 0.78 ($p < 0.001$) between the two sets of performances. This result implies that the performance of our BCI system highly depends on the subjects and how they perform the task and not whether the BCI system is trained using data of the same subject or not. Figure 4.11 shows the average classification performance of all pairs of directions over all subjects for Cor and Cor_P. It is shown in Fig. 4.10 that using Cor, on average, 7 pairs of directions out of 15 can be classified significantly ($p < 0.01$). This number reduces to 5 for Cor_P. If we only count the highly significant ones (Bonferroni corrected), we can only classify 4 pairs

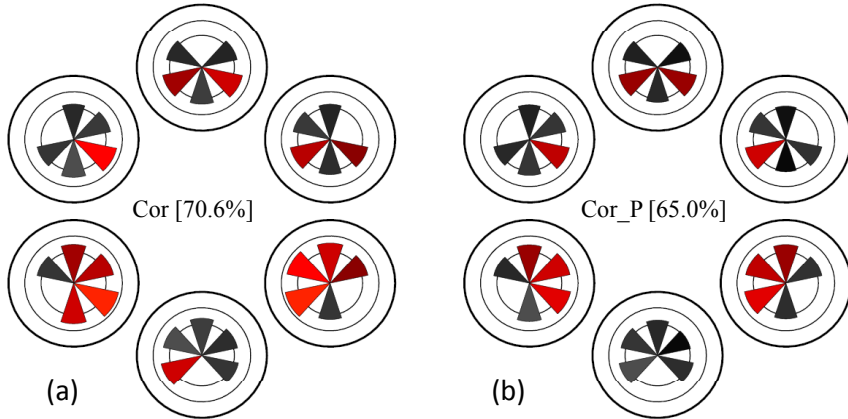


Figure 4.11: Average classification performance of all pairs of directions for (a) Cor and (b) Cor_P. Polar plots placed at spatial locations analogous to the locations used in the experiment. Each polar plot contains five pie slices depicting classification accuracies between the location of the plot and each of the five other possible directions. Significant accuracies ($p < 0.01$) are color coded in red. The brighter the color, the higher the accuracy. Peak accuracies are given in brackets. The increasing circle radii indicate 50%, 75%, and 100% classification performance.

of directions in both cases. That is, referring to each direction with the first letter of the direction (such as ‘D’ for down), the highly significantly classifiable pairs of directions are DR versus DL, DR versus UL, and U versus DR for both Cor and Cor_P, and D versus DL only for Cor and UR versus DL only for Cor_P.

4.4 Discussion

Shifts of covert visual attention induce changes in alpha power over posterior electrode sites. Initial analysis revealed that an early desynchronization was of little discriminative value regarding the direction of attention

shifts. We believe that this early desynchronization may be related to the preparation of covert attention shifts. A subsequent synchronization, however, yielded distinctive topographic patterns for the different directions and served as a basis for classification.

Using regularized logistic regression, significant binary classification performance was obtained for each participant, with a mean accuracy of 73.65% for the best pair of directions. A classification accuracy of 70% was proposed as performance threshold above which BCI performance can be considered as robust [66]. In the present study, six participants had a peak performance above 70%, and two participants had a performance that was slightly lower (66% and 69%). Interestingly, this figure is close to the accuracy obtained in earlier MEG studies, in spite of the significantly higher spatial resolution of MEG as compared to EEG [121, 118, 11]. This suggests that changes in alpha power following covert attention shifts are rather broadly distributed in visual cortex and, hence, can be mapped with sufficient precision using EEG.

Mean classification accuracy obtained in the present study is similar to the accuracy obtained by Kelly et al. [58]. However, there are significant methodological differences. First, Kelly et al. used visual stimulation in form of two flickering stimuli. It is unclear how the flickering affects the ease of deploying attention to the visual periphery. Second, just as we did, Kelly et al. used cross-validation to estimate classification performance. However, epochs were partly overlapping. In other words, the training set (used to train the classifier) partly contained information about the test set (used to verify the classifier), which might have led to an overestimation of classification accuracy.

Significant results were obtained for subject-independent learning. Accuracies shown in Fig. 4.11 demonstrate that on average, down-left versus down-right gives the highest classification performance using both Cor and Cor.P. As there is a highly significant correlation between the ALI differences and the classification accuracies, this result is consistent with Fig.4.4. It is also shown in Fig. 4.3 that for these two directions, the brain pattern changes in both left and right side of the occipital hemispheres compared to the average.

Averaged over all participants and directions, switching from Cor to Cor_P results in the decrease of $2.39 \pm 0.7\%$ in classification accuracy. Nevertheless, the high correlation between the two performances shown in Fig. 4.10 suggests that although the overall performance of subject-independent learning is lower than the subject-specific approach, almost the same pairs of directions can be classified significantly in a leave-one-subject-out setting. Furthermore, Fig. 4.10 shows that we can get a high accuracy of 0.84 for a well-performing participant, even if we do not train the classifier with the participant's own data. We expect to further improve performance by utilizing more sophisticated methods for the analysis of multi-subject data [95, 38].

The pair of directions yielding the highest classification performance varies considerably across participants (see grey double arrows in Fig. 4.6). For all but one participant, locations at opposite sides of the fixation point yield optimal performance. Furthermore, for seven participants, highest performance is achieved with a combination of left and right directions. Mostly, this combination also has a vertical offset (i.e., top-left combined with bottom-right, or bottom-left with top-right). For the other participant (*iah*), peak performance is achieved when attention is shifted in the vertical direction. This indicates that left versus right is not necessarily the optimal pair of directions. Therefore, participants with low control for these directions may resort to other pairs of directions including top and bottom.

Furthermore, we found an asymmetry regarding the contribution of electrode sites to classification success. In particular, left hemisphere electrodes contributed more to classification success than right hemisphere electrodes. This is in line with evidence that the left hemisphere supports mainly attention shifts to the right hemifield, while the right hemisphere is involved in attention shifts to both the right and the left hemifields [73].

In sum, the present study suggests that modulations of alpha power associated with covert attention shifts form a viable input modality for EEG-based BCIs. Furthermore, an alpha index obtained during a short relaxation measurement can predict prospective BCI performance. Analogous to the motor imagery paradigm, where different types of imagery

(e.g., movement of left hand, right hand, and foot) are tested preliminary and the best pair is chosen, eligible participants might then be screened for different directions of covert attention shifts. In order to maximize performance, the BCI would be tuned to the pair of directions that provides the best classification accuracy.

Chapter 5

Task-Specific Source Localization

¹ A key problem in brain research is to identify and reconstruct active neuronal sources from extracranially collected electrophysiological data. This problem of projecting signals measured in sensor space back to source space is often tackled by inverting a biophysically realistic forward model together with the use of particular prior assumptions for the sources. To date, however, most source localization algorithms have not directly taken into account the modulation of source activations induced by certain experimental manipulations. In this chapter, we introduce a new source localization technique which incorporates the experimental design in the source localization procedure. We show that this improves source reconstruction for simulated data as well as for an empirical data-set collected using a covert attention BCI paradigm.

¹This chapter is based on: Bahramisharif, A., van Gerven, M. A. J., Schoffelen, J. M., Heskes, T., ‘Task-specific source localization’, submitted

5.1 Introduction

Brain computer interfaces (BCIs) not only hold the promise as a tool for aiding the disabled and for augmenting human performance, but they also provide us with the ability to study the brain at work. A recent review paper has shown the utility of and the need for BCIs in the context of brain research [53]. One of the challenging topics in brain research is to identify and reconstruct active neuronal sources from electrophysiological data. Measures of brain activity obtained from EEG or MEG are known to have excellent temporal resolution but poor spatial resolution. In order to identify the location of neuronal generators which are responsible for the signals measured at the scalp, a lot of research has been devoted to solving this source localization problem [31, 43, 123, 30, 39]. This problem is typically addressed by inverting a biophysically realistic forward model which is constructed using an anatomical MRI. As normally the number of possible sources is much higher than the number of sensors, this inverse problem has many solutions, and it is required to use additional assumptions concerning the sources. One common approach is to assume the individual sources to be temporally uncorrelated, allowing for a reconstruction of each source independent of the other sources, referred to as beamforming [122]. Assumptions on the sparseness or smoothness of the sources have also been introduced [111, 101, 29, 46]. Such constraints are incorporated in recent Bayesian approaches to source localization using appropriate priors [71, 130, 119, 136].

Source localization studies are often conducted in a setting where different experimental conditions are compared with one another. In that case, the default approach is to construct a source estimate by comparing differences between the source estimates for two conditions. However, this approach is unsuitable in case the experimental design is characterized by multiple conditions or when the condition of interest is continuous-valued instead of discrete.

To cope with these problems, Trujillo-Barreto et al. [110] have introduced a Bayesian framework which combines contributions of both the experimental design and observed sensor readings. Here, in contrast, we use

an alternative approach which directly generalizes standard source localization algorithms. In our approach the sources are constructed such that they not only explain the sensor-level observations but also predict the experimental conditions as accurately as possible. We show that these requirements can be satisfied by solving a bi-convex problem using an iterative coordinate-descent scheme. This solution critically depends on the insight that, given fixed regression parameters that predict the experimental condition, we end up with a quadratic programming problem with linear equality constraints. The benefits of our approach are illustrated on simulated and empirical MEG data.

As empirical data we used a data-set which has previously been used in a covert attention BCI paradigm. The ability to identify the neural generators involved in such a paradigm should ultimately increase our understanding of what functional mechanisms give rise to good BCI performance.

5.2 Source localization

Let m , n , and t denote the number of sources, sensors, and samples, respectively. The goal of source localization is to estimate active sources $S \in \mathbb{R}^{m \times t}$ from sensor readings $X \in \mathbb{R}^{n \times t}$. In the source localization problem, sources are assumed to project linearly to the sensors via a leadfield matrix $L \in \mathbb{R}^{n \times m}$. In other words, $X = LS$, where L and X are given and S is to be estimated.

5.2.1 Standard approach

If we assume that the solution to the source localization problem can be written as a linear mapping from sensors to sources, the problem of source localization reduces to estimating the linear projection matrix $W \in \mathbb{R}^{n \times m}$ that projects the sensors to the sources. In other words, $S = W^T X$. Equivalently, W should be an inverse of the leadfield matrix L . As L is not square, this inverse problem has many solutions for $m > n$.

Let us first consider the case $m < n$ (more sensors than sources). The leadfield matrix L then corresponds to an expansion and W to a projection.

That is, $S = W^T X = W^T L S$, which implies that $W^T L = I_m$ where I_m denotes the $m \times m$ identity matrix. A standard approach is to minimize the variance of the sources and find the W which minimizes $\frac{1}{2} \text{Tr} S S^T = \frac{1}{2} \text{Tr} W^T \Sigma W$ subject to $W^T L = I_m$, where $\Sigma \equiv X X^T$ is the data covariance matrix and Tr is the trace operator. The solution is shown to be [123]:

$$\hat{W}_{m < n} = \Sigma^{-1} L (L^T \Sigma^{-1} L)^{-1} . \quad (5.1)$$

We now consider the case $m > n$ (more sources than sensors). In this case, W^T expands X to S and L projects back to X . That is, $X = L S = L W^T X$, which implies $L W^T = I_n$. So here we have to consider the constraint $L W^T = I_n$ instead. The solution is given by

$$\hat{W}_{m > n} = (L L^T)^{-1} L \quad (5.2)$$

and is known as the pseudo-inverse of the leadfield matrix [75, 31, 43]. In this chapter we refer to it as $S_p \equiv \hat{W}_{m > n}^T X$. A more common approach to source localization in the $m > n$ setting is to assume that all the sources are independent from each other. This approach is widely used in the neuroscience community and is known as beamforming [123]. Given this assumption, we can solve the inverse problem for each source location individually. In other words, for each source S_i , Eq. 5.1 can be used to give

$$\hat{W}_i = \Sigma^{-1} L_i (L_i^T \Sigma^{-1} L_i)^{-1} \quad (5.3)$$

where L_i is the leadfield matrix of the i -th location. The individual source estimates are then given by $S_i = \hat{W}_i^T X$. We refer to the beamformer solution as the ‘standard’ beamformer.

5.2.2 Task-specific approach

Source localization is almost never performed in isolation but rather in the context of some experimental design $Y \in \mathbb{R}^{r \times t}$, where r is the number of outputs and t the number of samples. These outputs can be experimental conditions but they can also be nuisance factors such as heart rate or

head movement. Our goal is to make use of the information embodied by the experimental design in order to obtain improved source estimates. A straightforward way of achieving this is to assume that the reconstructed sources should be predictive of (rows of) Y . That is, at the source level, we wish to minimize the sum-squared error

$$C(\Theta, S) \equiv \frac{1}{2} \text{Tr} (\Theta^T S - Y) (\Theta^T S - Y)^T$$

with $\Theta \in \mathbb{R}^{m \times r}$. The solution to the source localization problem changes depending on whether or not S can also be estimated as a linear projection of X . If we assume that S can be estimated as a linear projection of X , we can write $S = W^T X$ and we need to find a proper W based on our assumptions. However, if we assume that it is not necessarily optimal to project S to X linearly, we need to directly solve the equations for S . In the following we discuss both options and show how the experimental design can be integrated in the source estimation procedure.

Solving for W : a linear solution

Making use of $S = W^T X$, we want to find W and Θ that minimize

$$C(\Theta, W) = \frac{1}{2} \text{Tr} \Theta^T W^T \Sigma W \Theta - \text{Tr} \Theta^T W^T B + \frac{1}{2} \text{Tr} Y Y^T$$

with $B \equiv X Y^T$, under the constraint $W^T L = I_m$ if $m < n$ and $W L^T = I_n$ if $m > n$. Obviously, we can add additional regularization terms, both for Θ and W . Here, in order to enforce sparsity on the regression parameters, we choose an ℓ_1 regularization term for Θ [105]. To minimize the variance of the sources we add the usual term $\frac{1}{2} \text{Tr} S S^T$. Ignoring constant terms, the regularized cost function becomes:

$$C_{\alpha, \lambda}(\Theta, W) \equiv \alpha \left(\frac{1}{2} \text{Tr} \Theta^T W^T \Sigma W \Theta - \text{Tr} \Theta^T W^T B \right) + \frac{1}{2} \text{Tr} W^T \Sigma W + \lambda \|\Theta\|_1$$

where $\|\cdot\|_1$ stands for norm one and α and λ are regularization parameters. This problem is bi-convex, i.e., given W it is convex in Θ and given Θ it is convex in W . This observation suggests an iterative coordinate-descent scheme, in which we consecutively minimize Θ and W under the appropriate constraints and with the appropriate regularization terms. Solving for Θ given W boils down to a standard regularized regression problem [36]. Let us now consider solving for W , which boils down to the minimization of

$$R(W) \equiv \frac{\alpha}{2} \text{Tr} \Theta^T W^T \Sigma W \Theta - \alpha \text{Tr} \Theta^T W^T B + \frac{1}{2} \text{Tr} W^T \Sigma W$$

under the constraint $W^T L = I_m$ or $W L^T = I_n$ for fixed Θ .

An important contribution of this chapter is the realization that this minimization problem can be formulated as a quadratic programming problem with linear equality constraints. As shown in Appendix 5.A, Theorem A1 and A2, making use of the definitions $A \equiv I_m + \alpha \Theta \Theta^T$, $\tilde{A} \equiv I_r + \alpha \Theta^T \Theta$, $Q \equiv \alpha \Sigma^{-1} X Y^T \tilde{A}^{-1} \Theta^T$ and $\tilde{W}_{m>n} \equiv (L A^{-1} L^T)^{-1} L A^{-1}$, we obtain the closed form solutions:

$$W_{m<n} = Q + \hat{W}_{m<n} (I_m - L^T Q) \quad (5.4)$$

$$W_{m>n} = Q + (I_n - Q L^T) \tilde{W}_{m>n} \quad (5.5)$$

for $m < n$ and $m > n$, respectively. Note further that A^{-1} can be computed efficiently from $A^{-1} = I_m - \alpha \Theta \tilde{A}^{-1} \Theta^T$ using the matrix inversion lemma [135].

Source estimates $W_{m<n}^T X$ or $W_{m>n}^T X$ can be computed from these equations. We are particularly interested in the regime where we have more sources than sensors. We use $S_1 \equiv W_{m>n}^T X$ to refer to the *linear* solution to task-specific source localization. We can also assume independence between sources, and enforce each source to explain all the sensor readings and be predictive for the experimental condition. We can then compute $W_{m<n}$ for individual sources in the setting where we have more sources than sensors. This gives the task-specific extension to the beamformer, denoted by S_b .

Solving for S : a nonlinear solution

It is not necessarily optimal to write S as a linear projection of X . In fact, we could restrict ourselves to the constraint $X = LS$. This equation does not have an exact solution for $m < n$, as then we would have more equations than unknowns. Therefore, we only consider the case $m > n$. To incorporate the experimental design, similar to solving for W , we need to minimize

$$R(S) = \frac{\alpha}{2} \text{Tr } \Theta^T S S^T \Theta - \alpha \text{Tr } \Theta^T S Y^T + \frac{1}{2} \text{Tr } S S^T$$

for S and Θ under the constraint $LS = X$. As shown in Appendix 5.B, Theorem B1, using the same notation as introduced before, this leads to the following *non-linear* solution to task-specific source localization when we have more sources than sensors:

$$S_n \equiv \alpha (I_m - \tilde{W}_{m>n}^T L) A^{-1} \Theta Y + \tilde{W}_{m>n}^T X. \quad (5.6)$$

Note that if we set $\alpha = 0$, we obtain the linear solution mentioned in Eq. 5.2.

5.2.3 Regularization parameters

As large values for α would result in higher separability for conditions with respect to the experimental design and small values would result in lower variance in the sources, the important question remains how to choose α . As can be seen in the definition of $A = \alpha \Theta \Theta^T + I_m$, large α results in the first term being dominant and vice versa for small α . To reach a compromise between the first and the second term, we choose α such that the sum of the eigenvalues for each of the terms is the same. That is, given Θ we choose

$$\alpha = \frac{m}{\text{Tr } \Theta^T \Theta}. \quad (5.7)$$

Note that the optimal Θ depends on λ and S , which are both yet unknown. We therefore first compute S_p and then use cross-validation to

determine the optimal λ when regressing Y against S_p . We use the implementation of [36] to solve this regression problem. We use the estimate of Θ based on this optimal λ to compute α from Eq. 5.7.

For the task-specific beamformer, we start with the standard beamforming solution. We opt for having a general λ and α for all sources ($S_i, i = 1 \dots m$). Using a cross-validation procedure, we find the value of λ that minimizes the average sum-squared error obtained when regressing Y against each S_i . Given this λ we compute an α_i for each individual source S_i and then average these to obtain a single α for all sources.

5.3 Experiments

We evaluated our method using simulated and empirical data. For the simulation, we projected randomly generated sources S onto the sensors X using a leadfield L whose entries were drawn from a uniform distribution on the unit interval. Sources were projected onto the experimental design Y using another randomly generated matrix. For the empirical validation we used data of two subjects reported in [11].

5.3.1 Simulated data

Simulated data were generated in order to compare the performances of the task-specific source estimates with standard source estimates. Since in practice we are dealing with a number of sources that is much higher than the number of sensors ($m \gg n$), we only focused on that scenario.

In the first simulation, we were interested in analyzing how the quality of the source estimates changes as a function of the number of outputs r (rows of Y) when comparing the linear and nonlinear solutions S_l and S_n . Note that the standard solutions do not depend on this number and are thus equivalent to the solutions obtained for $r = 0$. We used eight sensors and 100 sources and varied the number of outputs from 0 to 90. Source activations were drawn from a standard normal distribution. Sensor amplitudes were generated by multiplying the leadfield matrix with the source activations and adding Gaussian noise with mean zero and variance

10^{-2} . In this simulation, we focused on quantifying how source estimates change as a function of the number of outputs. Therefore, we assumed that the regression model Θ , which was used to generate the outputs, was known. That is, when estimating task-specific sources, we fixed Θ and only computed the closed form solutions as described in Eqs. 5.5 and 5.6.

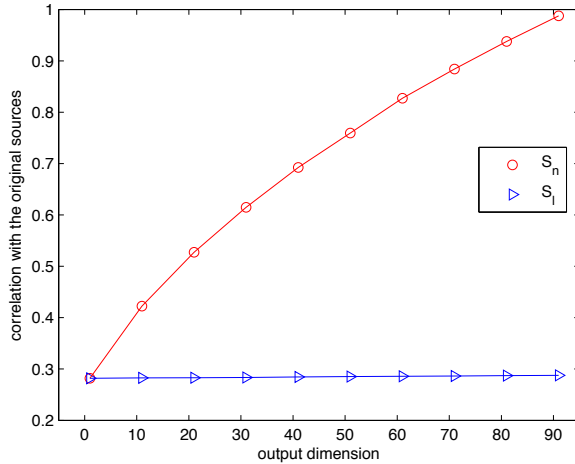


Figure 5.1: Impact of output dimension on the source reconstructions for the proposed linear and non-linear approaches for source localization.

Figure 5.1 shows how increasing the output dimension affects the source reconstruction using the linear or non-linear solution. It is evident that S_n outperforms S_l for increasing output dimension. The estimates for S_l only improve slightly, indicating that the assumption that S can be written as a linear projection of X is untenable.

In the second simulation, we focused on comparing the pseudo-inverse solution with the nonlinear solution S_n and the beamformer solution S_b . We assumed that there was only one source with strong amplitude among 100 sources which carried task-specific information. This source flipped from an amplitude of 2 to -2 (relative to baseline) after 1000 samples. Other sources

unrelated to the task were assumed to have zero amplitude. Amplitudes for ten sensors were generated by multiplying the leadfield matrix with the source activations and adding Gaussian noise with mean zero and variance one. An output was generated by multiplying the task-specific source with a constant. Contrary to the previous simulation, we solved for Θ as well, which required the application of the iterative coordinate-descent scheme advocated in this chapter. Hence, Θ was estimated by repeatedly solving a sparse regression problem.

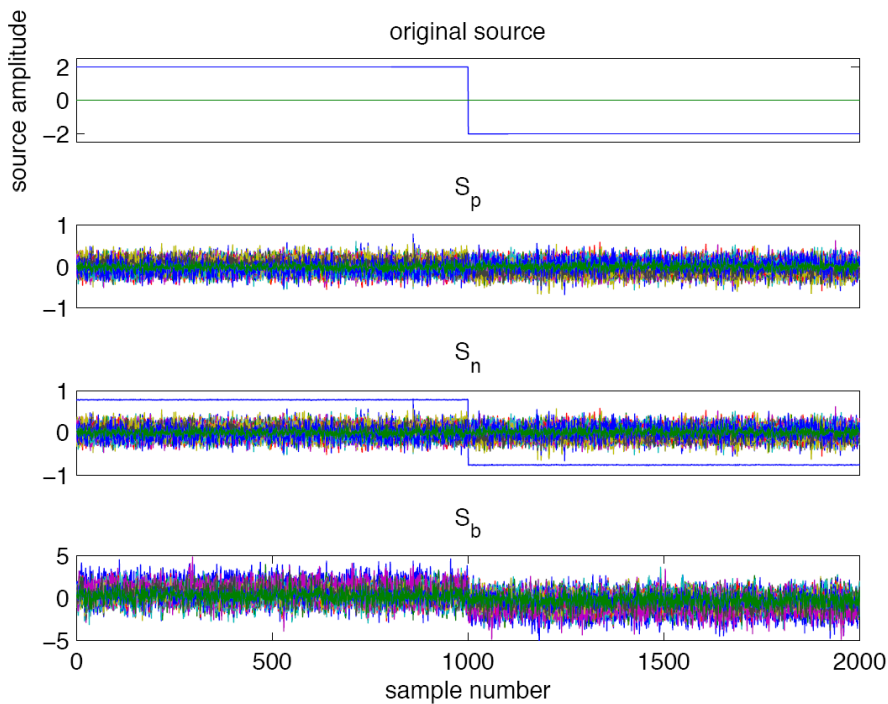


Figure 5.2: The original sources and their reconstruction using methods S_p , S_n , and S_b . There was hardly any difference between the results of the task-specific beamformer and the standard beamformer.

The results for the second simulation are shown in Fig. 5.2. It is clear

that both the pseudo-inverse solution S_p as well as the (task-specific) beamformer solution S_b fail to properly detect the relevant source while the task-specific solution S_n identifies the source correctly.

5.3.2 Empirical data

For the empirical data, we used data for two subjects that have previously been used in [11]. The subject’s task was to maintain central fixation while covertly attending to a target which followed a circular trajectory. The output Y was given by the sine and cosine of the angles between the target and the positive x -axis over time. To construct the leadfield matrix, we used a structural MRI and the head model developed in [78]. Then we discretized the brain volume into a grid with $1 \times 1 \times 1 \text{ cm}^3$ resolution. For each grid point the leadfield was calculated. Preprocessing and leadfield generation was done using FieldTrip [80].

As shown in [11], task-specific information for this data shows up as modulations of occipital alpha power (8–12 Hz) in the frequency domain and not in the amplitude of individual time points. Since estimating the power is a non-linear operation, we need to replace it with a linear preprocessing procedure in order to apply our source localization algorithm. To cope with this problem, we need a reference signal to align sensor readings and extract their power using a linear operation. We used the linear trick explained in Appendix 5.C to estimate the power.

Figure 5.3 shows the average absolute alpha source reconstructions over all directions using S_b , S_p and S_n . Clearly, both S_b and S_p fail to identify the occipital sources whereas S_n correctly identifies occipital sources that are known to be involved when subjects are covertly attending to a peripheral target [15]. Figure 5.3 also shows that the beamformer suffers from a bias towards deep sources [2, 128]. The default way to deal with this problem is to examine the difference between two conditions, thereby removing the contribution of the depth bias. In order to do so, we need to discretize our continuous condition of interest. As an illustration, we chose to focus on four directions on interest: ‘left’ when $\cos(Y) < 0$, ‘right’ when $\cos(Y) > 0$, ‘up’ when $\sin(Y) > 0$, and ‘down’ when $\sin(Y) < 0$. Figure 5.4

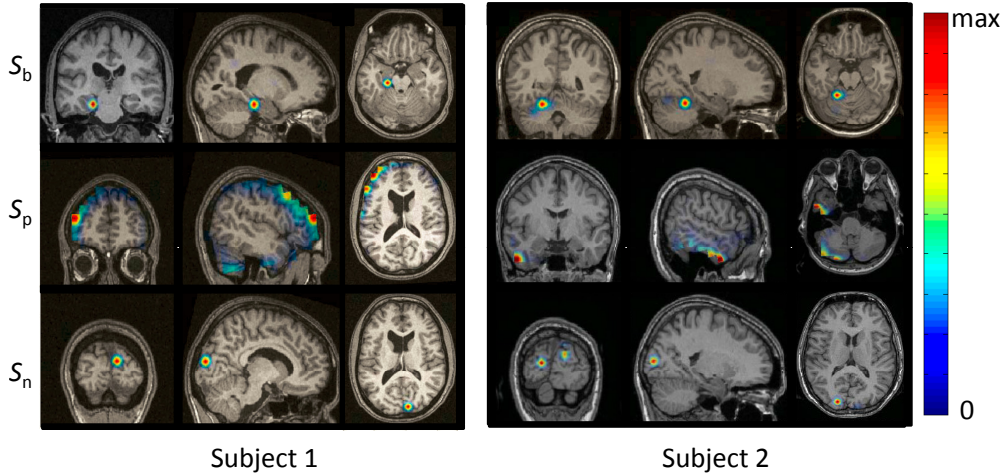


Figure 5.3: Source estimates using the task-specific beamformer S_b , the pseudo-inverse solution S_p , and the non-linear method S_n for two subjects. There was hardly any difference between the results of the task-specific beamformer and the standard beamformer.

shows the normalized differences of the standard beamformer results for left versus right and up versus down. As expected, there is an overall occipital activity, which is very coarse compared to the results obtained for S_n in Fig. 5.3.

5.4 Discussion

In this chapter we proposed a new method for source localization which makes use of task-specific information. We showed that by starting from the standard solutions to source localization, as shown in Eqs. 5.1 and 5.2, and by adding the constraint that the estimated sources should explain the design matrix, we arrive at the solutions for task-specific source localization. The task-specific source estimates are obtained by solving a bi-convex problem using an iterative coordinate-descent scheme. It depends on the

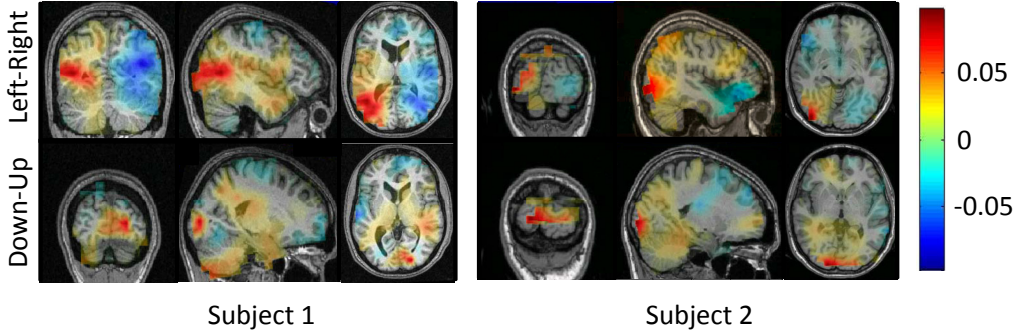


Figure 5.4: Normalized differences of the standard beamformer outputs. The angle is discretized into left,right, up, and down.

observation that, given fixed regression parameters that predict the experimental condition, we end up with a quadratic programming problem with linear equality constraints, which has a closed form solution.

For the proposed method, the underlying assumption is that the experimental design affects the sources and can help locating these sources by acting as additional virtual sensors. When there is no correlation between the experimental design and the sources, the method reduces to standard source localization.

Depending on whether sources can be described by a linear projection of sensors or not, we derived a linear (Eq. 5.5) and a non-linear (Eq. 5.6) solution, respectively. Simulation results showed that the non-linear variant of the proposed task-specific source localization method S_n outperformed the linear variant S_l . The non-linear method was also shown to outperform the (task-specific) beamformer results S_b as well as the pseudoinverse results S_p . This result implies that it is not optimal to assume that the solution to the source localization problem can always be written as a linear mapping from sensors to sources.

The second simulation showed that the task-specific beamformer S_b did not perform well. It seems to perform suboptimally in the presence of high-variance sensor noise. With regard to the empirical data, the task-specific

beamformer was found to perform similar to the standard beamformer. Since the experimental conditions cannot be properly explained from single source activity, the regression parameters vanish and the influence of the experimental conditions on the source reconstruction disappears. Furthermore, Fig. 5.3 shows that S_b suffers from a depth bias. In the case of having a discrete set of conditions, we can look at the differences of the beamformer results to get a rough estimate about the location of the sources as shown in Fig. 5.4. Note however that, next to the coarse estimation of the source locations, in our case, this required the discretization of a continuous condition of interest, which may not be desirable.

The results on empirical data confirmed the good performance of the non-linear method as the source locations that were hypothesized to be involved in the task were correctly identified by S_n . Interestingly, Subjects 1 and 2 had one occipital source in common for S_n . Additionally, Subject 2 showed another occipital source in the opposite hemisphere. Not surprisingly, the obtained solution depends on the (procedure for the) setting of the regularization parameter λ and, to a lesser extent, α . For example, we do find another active source in the left hemisphere of Subject 1 as well when we slightly increase λ . An arguably better strategy could be to consider a regularization path, along the lines of LARS [34], considering a range of λ 's that all lead to (close to) optimal prediction performance instead of taking a single value.

To incorporate task-specific information, we minimized the sum-squared error of the task predictions. Other error functions or maximum likelihood approaches, possibly in combination with other regularizers such as the elastic net [36], can be treated within the same framework, but will require more involved optimization procedures. These may then also be translated to a Bayesian approach, along the lines of [119].

The proposed method can be applied either in the time domain or in the frequency domain. Using the method in the time domain is straightforward but presupposes that outputs can be predicted from instantaneous source activations. Application of the methods in the frequency domain allows one to make use of induced responses restricted to particular frequency bands but needs additional preprocessing steps based on a proper reference signal

as shown in the analysis of the empirical data. Evidently, the choice of the reference signal itself will affect which sources will be identified.

From the result of the first simulation, it is evident that the task-specific source localizer starts to outperform the standard methods when there are multiple independent outputs. In a way, these outputs can be interpreted as additional virtual sensors for which the leadfield matrix is unknown. In practice, the task-specific source localizer S_n is expected to show the most benefit for experimental designs in which multiple stimulus properties are varied independently throughout the course of an experiment.

Finally, identification of the neural generators involved in BCI paradigms can result in improved BCI performance. For instance, identification of the relevant sources reduces BCI calibration time [3] and may facilitate multi-task learning approaches [4]. Follow-up studies could further explore the merits of task-specific source localization in such contexts.

5.A Appendix A: Solving for W

Theorem A1

For fixed Θ , minimization of

$$R(W) = \frac{1}{2} \text{Tr } W^T \Sigma W A - \text{Tr } W^T C$$

with $C \equiv \alpha B \Theta^T$ under the constraint $W^T L = I_m$, results in the solution shown in Eq. 5.4.

Proof

Build the Lagrangian:

$$\mathcal{L}(W, \Lambda) = \frac{1}{2} \text{Tr } W^T \Sigma W A - \text{Tr } W^T C - \text{Tr} (W^T L - I_m) \Lambda^T .$$

Setting the derivative for W^T to zero and solving for W gives

$$W = \Sigma^{-1} (C + L \Lambda^T) A^{-1} .$$

Plugging this back into the constraint $L^T W = I_m$ and solving for Λ^T yields

$$\Lambda^T = (L^T \Sigma^{-1} L)^{-1} (A - L^T \Sigma^{-1} C) ,$$

and thus

$$W = \Sigma^{-1} L (L^T \Sigma^{-1} L)^{-1} + \alpha \Sigma^{-1} \left[I_n - L (L^T \Sigma^{-1} L)^{-1} L^T \Sigma^{-1} \right] X Y^T \Theta^T A^{-1}$$

where we plugged in the definition of C . Using the Woodbury identity [135], we further have

$$A^{-1} = (I_m + \alpha \Theta \Theta^T)^{-1} = I_m - \alpha \Theta (I_r + \alpha \Theta^T \Theta)^{-1} \Theta^T ,$$

and thus

$$A^{-1} \Theta = \Theta (I_r + \alpha \Theta^T \Theta)^{-1} .$$

Substitution then leads to

$$W_{m < n} = \hat{W}_{m < n} + (I_n - \hat{W}_{m < n} L^T) Q = Q + \hat{W}_{m < n} (I_m - L^T Q) . \quad \square$$

Theorem A2

For fixed Θ , minimization of

$$R(W) = \frac{1}{2} \text{Tr} W^T \Sigma W A - \text{Tr} W^T C$$

with $C \equiv \alpha B \Theta^T$ under the constraint $L W^T = I_n$, results in the solution shown in Eq. 5.5.

Proof

Here we get the Lagrangian

$$\mathcal{L}(W) = \frac{1}{2} \text{Tr} \Sigma W A W^T - \text{Tr} C W^T - \text{Tr} \Lambda^T (L W^T - I_n) .$$

Setting the derivative for W^T to zero and solving for W now gives

$$W = \Sigma^{-1} (C + \Lambda^T L) A^{-1} .$$

Plugging this back into the constraint $WL^T = I_n$ and solving for Λ^T yields

$$\Lambda^T = (\Sigma - CA^{-1}L^T) (LA^{-1}L^T)^{-1},$$

and thus

$$W = (LA^{-1}L^T)^{-1} LA^{-1} + \Sigma^{-1}CA^{-1} \left[I_m - L^T (LA^{-1}L^T)^{-1} LA^{-1} \right]$$

which leads to

$$W_{m>n} = \tilde{W}_{m>n} + Q(I_m - L^T \tilde{W}_{m>n}) = Q + (I_n - QL^T) \tilde{W}_{m>n}. \quad \square$$

5.B Appendix B: Solving for S

Theorem B1

For fixed Θ , minimization of

$$R(S) = \frac{1}{2} \text{Tr } S^T AS - \text{Tr } D^T S$$

with $D \equiv \Theta Y$ under the constraint $LS = X$, results in the solution shown in Eq. 5.6.

Proof

Build the Lagrangian:

$$\mathcal{L}(S, \Lambda) = \frac{1}{2} \text{Tr } S^T AS - \text{Tr } D^T S + \text{Tr } \Lambda^T (LS - X)$$

Setting the derivative for S to zero and solving for S gives

$$S^T = (D^T - \Lambda^T L) A^{-1}$$

or equivalently:

$$S = A^{-1} (D - L^T \Lambda)$$

Plugging this back into the constraint $X = LS$ and solving for Λ yields

$$\Lambda = (LA^{-1}L^T)^{-1} (LA^{-1}D - X)$$

which leads to

$$S_n \equiv \alpha [I_m - \tilde{W}_{m>n}^T L] A^{-1} \Theta Y + \tilde{W}_{m>n}^T X. \quad \square$$

5.C Appendix C: Linear trick to estimate the power

Imagine that we have a reference signal which has the same frequency and the same phase as the signal that we want to decode. We take the Fourier transform of the data, which is a linear operation, only focusing on the desired frequency, and subtract the phase of the reference signal. Then, the real part of the Fourier transform would represent the amplitude of the signal which, averaged over a time window, results in an estimate of the power of the signal over that frequency. Note that the reference signal is extracted from the sensor readings and is not necessarily related to the location of the sources. This method is widely used in telecommunication for amplitude demodulation [81]. There is no non-linearity involved in these steps, which means we can just apply it to our data before using it as input to the source localization algorithm. As the reference signal we choose the average signal over eight channels which showed the highest average alpha power. For the Fourier transform, we used a 500 ms time window.

Chapter 6

The Dynamic Beamformer

¹ Beamforming is one of the most commonly used methods for estimating the active neural sources from the MEG or EEG sensor readings. The basic assumption in beamforming is that the sources are uncorrelated, which allows for estimating each source independent of the others. In this chapter, we incorporate the independence assumption of the standard beamformer in a linear dynamical system, thereby introducing the dynamic beamformer. Using empirical data, we show that the dynamic beamformer outperforms the standard beamformer in predicting the condition of interest which strongly suggests that it also outperforms the standard method in localizing the active neural generators.

6.1 Introduction

As the number of possible neural sources is much higher than the number of MEG or EEG sensor readings, the inverse problem of estimating source amplitudes from sensor readings has many solutions. A common approach to tackle this problem is to assume that all sources are independent from

¹This chapter is based on: Bahramisharif, A., van Gerven, M. A. J., Schoffelen, J. M., Ghahramani, Z., Heskes, T., ‘The dynamic beamformer’, NIPS workshop on Machine Learning and Interpretation in Neuroimaging, Sierra Nevada, Spain, 2011

each other. This approach is widely used in the neuroscience community and is known as beamforming [31, 43, 30, 39].

Since the source amplitude is likely to change smoothly over time, we expect to improve the source localization by taking the temporal dynamics into account. Smoothness constraints have been combined with source localization in a Bayesian framework [82, 71, 129]. Furthermore, source localization with a multivariate autoregressive source model has been presented in [47], where the sources are assumed to be independent and identically distributed in time and the components are subject to non-Gaussian distributions. The Kalman filter and particle filter have also been introduced in the context of EEG and MEG source localization based on dipole-fitting approaches [8, 9]. The model introduced in [8, 9] relies on the integration of many dynamic dipolar neural models. In this chapter, in contrast to the previous methods, we start from the standard beamforming solution and we show that we can incorporate the independence assumption of the standard beamformer in a linear dynamical system. We demonstrate that by using the leadfield matrix as the observation model and setting the covariance of the observation noise proportional to the covariance of the observation, we arrive at the dynamic beamformer.

6.2 Method

6.2.1 Beamforming

Let m , n , and T denote the number of sources, sensors, and samples, respectively. The goal of source localization is to estimate active sources $S \in \mathbb{R}^{m \times T}$ from sensor readings $X \in \mathbb{R}^{n \times T}$. In the source localization problem, sources are assumed to project linearly to the sensors via a leadfield matrix $L \in \mathbb{R}^{n \times m}$. In other words, $X = LS$, where L and X are given and S is to be estimated. If we further assume that the solution to the source localization problem can be written as a linear mapping from sensors to sources, the problem of source localization reduces to estimating the linear projection matrix $W \in \mathbb{R}^{n \times m}$ that projects the sensors to the sources; in other words: $S = W'X$.

Beamforming derives from the assumption that the sources are uncorrelated. Defining $\mathbf{s}_i \equiv S_{i,\cdot}$, $\boldsymbol{\ell}_i \equiv L_{i,\cdot}$, and $\mathbf{w}_i \equiv W_{i,\cdot}$, for each source $\mathbf{s}_i \equiv (s_{i,1}, \dots, s_{i,T})$, we can write: $\mathbf{s}_i = \mathbf{w}_i' X = \mathbf{w}_i' \boldsymbol{\ell}_i \mathbf{s}_i$, which implies that $\mathbf{w}_i' \boldsymbol{\ell}_i = 1$ for all $i \in 1, \dots, m$. A standard approach is to minimize the variance of the sources and find the \mathbf{w}_i which minimizes $\mathbf{s}_i \mathbf{s}_i' = \mathbf{w}_i' \Sigma \mathbf{w}_i$ subject to $\mathbf{w}_i' \boldsymbol{\ell}_i = 1$, where $\Sigma \equiv X X'$. The solution is shown to be [123]:

$$\mathbf{s}_i = (\boldsymbol{\ell}_i' \Sigma^{-1} \boldsymbol{\ell}_i)^{-1} \boldsymbol{\ell}_i' \Sigma^{-1} X \tag{6.1}$$

for all $i \in 1, \dots, m$.

6.2.2 Linear Gaussian model

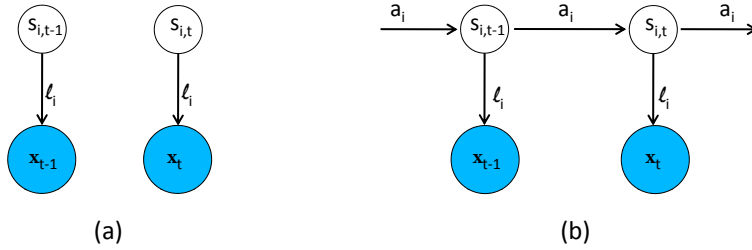


Figure 6.1: (a) Graphical representation of a linear Gaussian model. (b) Graphical representation of the dynamic beamformer.

The beamformer can be interpreted as a specific kind of linear probabilistic model. Assume that we have a linear Gaussian model, as shown in Fig. 6.1a, in which $\mathbf{x}_t \equiv X_{\cdot t}$ is the observation at time t where $1 \leq t \leq T$, and $\boldsymbol{\ell}_i$ is given. Sensor observations linearly depend on source activations through $\mathbf{x}_t = \boldsymbol{\ell}_i \mathbf{s}_{i,t} + \mathbf{u}_{i,t}$, where $\mathbf{u}_{i,t} \sim \mathcal{N}(0, R)$. Now we try to find \mathbf{s}_i which maximizes the likelihood of the parameters given the observations and R . Ignoring the constant terms, the negative log-likelihood can be written as $\frac{1}{2} (\mathbf{X} - \boldsymbol{\ell}_i \mathbf{s}_i)' R^{-1} (\mathbf{X} - \boldsymbol{\ell}_i \mathbf{s}_i)$, which is minimized by

$$\mathbf{s}_i = (\boldsymbol{\ell}_i' R^{-1} \boldsymbol{\ell}_i)^{-1} \boldsymbol{\ell}_i' R^{-1} X. \tag{6.2}$$

Comparing Eqs. 6.1 and 6.2, we see that with R proportional to Σ , the model depicted in Fig. 6.1a is equivalent to the standard beamformer. In other words, a linear Gaussian model is a beamformer if we assume that the covariance of the observation noise is proportional to the covariance of the observations and use the leadfield matrix as the observation model.

6.2.3 Dynamic beamforming

The correspondence between the beamformer and the linear Gaussian model suggests that a similar correspondence can be exploited using a linear dynamical system. We introduce the dynamic beamformer, which can be obtained by just using the leadfield matrix as the observation model of a linear dynamical system and setting the covariance of the observation noise to be proportional to the covariance of the observation. The graphical model of the dynamic beamformer is shown in Fig. 6.1b. For each source $\mathbf{s}_i \equiv (s_{i,1}, \dots, s_{i,T})$, dynamic beamforming can be mathematically expressed as

$$\mathbf{x}_t = \boldsymbol{\ell}_i s_{i,t} + \mathbf{u}_{i,t} \quad (6.3)$$

$$s_{i,t} = a_i s_{i,t-1} + v_{i,t} \quad (6.4)$$

where $\mathbf{u}_{i,t} \sim \mathcal{N}(0, \alpha_i \Sigma)$ and $v_{i,t} \sim \mathcal{N}(0, q_i)$ independently for $i \in 1, \dots, m$ and $1 \leq t \leq T$. Note that $s_{i,t}$, a_i , q_i , and α_i are scalar values. Note further that each \mathbf{s}_i should be predictive for the full observation X , so there is no i in the left side of Eq. 6.3. Following the equations reported in [94], we can find a_i , q_i , α_i , and \mathbf{s}_i by means of an expectation maximization algorithm. We use both filtering and smoothing (forward and backward) equations to have a better estimate of the sources.

6.2.4 Empirical data

We evaluated our method using MEG data of the best performing subject reported in [11]. The subject's task was to maintain central fixation while covertly attending to a target which followed a circular trajectory. The condition was given by the sine and cosine of the angles between the target

and the positive x -axis over time. To construct the leadfield matrix, we used a structural MRI and the head model developed in [78]. Then we discretized the brain volume into a grid with $1 \times 1 \times 1 \text{ cm}^3$ resolution. For each grid point the leadfield was calculated. Preprocessing and leadfield generation was done using FieldTrip [80].

The complexity of the dynamic beamformer increases with the number of time points. As shown in [11], task-specific information for this data shows up as modulations of occipital alpha power (8–12 Hz) in the frequency domain. Applying the dynamic beamformer on the frequency domain results in a much lower processing time. In this study we used the linear trick explained in Appendix 5.C to estimate the power in order not to violate the linearity of the beamformer. To include all variations of the alpha band in predicting the conditions, there was a 400 ms overlap between the consecutive trials.

6.2.5 Validation

Brain source localization is difficult to validate as mostly there is no certain knowledge about the exact location of the active sources. In this chapter, we validated our method by decoding the experimental design from the source estimates. We used 25 minutes of data for training and 5 minutes for testing our algorithm. To optimize parameters based on the training set, we used a two-fold cross-validation approach, i.e., the first half (12.5 minutes) for training and the second half for testing and vice versa. After optimizing parameters, we computed the performance on the test set. We used the correlation between the actual and predicted sine and cosine of the angle as the performance measure.

We validated our beamformer results using two different approaches: a stationary and a dynamic approach. The stationary validation approach uses two L2 regularized linear regressors to predict sine and cosine of the direction of attention from the alpha sources. Showing sine and cosine of the direction of attention with $\Theta \in \mathbb{R}^{2 \times T}$, we obtain the graphical representation of our linear regression model as shown in Fig. 6.2a.

From the experimental design reported in [11], we know that the di-

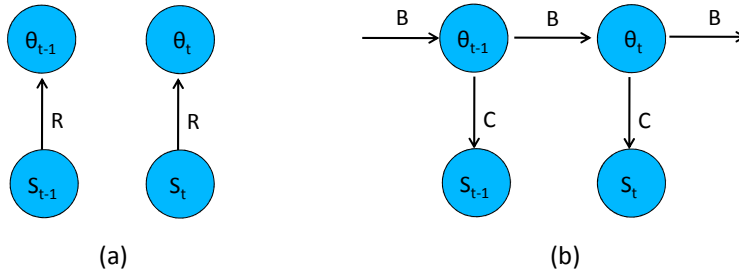


Figure 6.2: (a) Graphical representation of the linear regression model used to predict the direction of attention from the reconstructed sources. R stand for the regression coefficients. (b) Graphical representation of the linear dynamical system used to predict the direction of attention from the reconstructed sources. B and C stand for the state transition matrix and the observation model in the linear dynamical system, respectively.

rection of attention changes smoothly over time. That is, the predicted direction of attention not only depends on the alpha activity but is also highly related to the previous predicted direction. In our dynamic validation approach, we model this smoothness assumption again in a linear dynamical system framework. The graphical representation of this model is presented in Fig. 6.2b. Using data of the training set and again following the equations reported in [94], we can learn the parameters of this model and use it for predicting the conditions of the test set.

6.3 Results

We computed the absolute correlation of the sources reconstructed using both the beamformer and the dynamic beamformer with the experimental design which, in our case, is given by the sine and cosine of the direction of attention. As shown in Fig. 6.3a, occipital sources are more correlated with the experimental design in the dynamic beamformer reconstruction. These occipital sources are known to be involved when subjects are covertly at-

tending to a peripheral target [15]. Here, the higher correlation is expected, as the experimental design changes very smoothly and the dynamic beamformer enforces the smooth transition of the sources which results in a higher correlation.

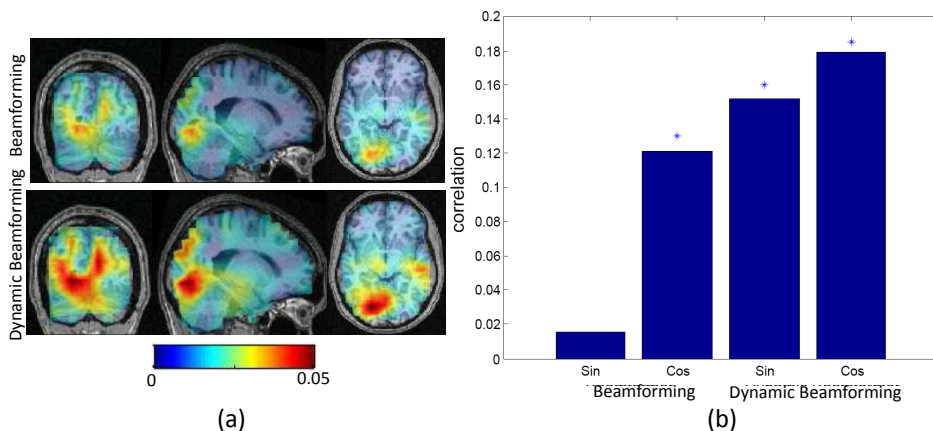


Figure 6.3: (a) Correlation of the sources reconstructed using both the beamformer and the dynamic beamformer with the experimental conditions. (b) Correlation between actual and predicted experimental design based on the sources reconstructed using either the beamformer or the dynamic beamformer. Significant correlations ($p < 0.001$) are marked with a ‘*’.

Following the stationary validation approach, we show the prediction results using two L2 regularized linear regressors. Figure 6.3b shows the correlation of the predictions for sine and cosine based on the sources reconstructed using the beamformer and the dynamic beamformer with the true values. As shown, the dynamic beamformer results in a better prediction of the conditions than the standard beamformer. Specifically, the dynamic beamformer is performing much better for the sine component of the angle than the standard version. As the sign of the cosine and sine represent left versus right and up versus down, respectively, Fig. 6.3b implies that it

is more difficult to discriminate up from down than left from right using the sources reconstructed with standard beamforming. Furthermore, if we look at the absolute regression coefficients obtained by either standard or dynamic beamforming shown in Fig. 6.4, we see that only the regression coefficients of the dynamic beamformer are consistent with the correlations shown in Fig. 6.3a. As the trained regressor on the sources reconstructed from standard beamforming focuses on the task-irrelevant brain regions, the poor performances of the beamforming part of Fig. 6.3b is expected.

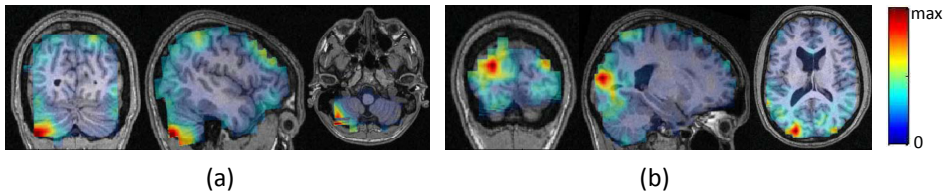


Figure 6.4: Average absolute value of the regression coefficients for predicting sine and cosine of the direction of attention using the sources obtained by (a) standard beamforming and (b) dynamic beamforming.

We further checked whether we could improve predictive performance by making use of a linear dynamical system on the dynamic beamformer results following the dynamic validation approach. Having the sources reconstructed from the dynamic beamformer, based on the training data, we sorted the sources according to their correlation with the experimental condition. We then checked whether we need all the sources to have a good prediction. Using a linear dynamical system on a subset of sources, from 1 to 500 sources, we show how the average absolute correlation between the predictions and the true directions changes in Fig. 6.5a. As the performance drops dramatically by adding more sources than 400, we did not go beyond analyzing 500 sources. It can be seen in Fig. 6.5a that the optimal number of sources to be used for predicting the direction of attention is about 300. Using a linear dynamical system on the 300 sources, the prediction result is shown in Fig. 6.5b. This result is equivalent to a correlation of 0.42 for sine and 0.58 for cosine compared to the results shown in Fig. 6.3b. In other

words, making use of a linear dynamical system on a subset of sources, the prediction of the experimental condition becomes about three times better than using two linear regressors. The predictions are consistent with the results shown in [53].

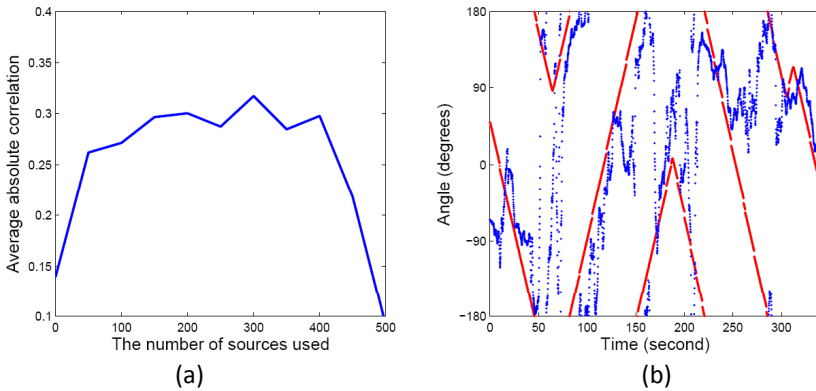


Figure 6.5: (a) Average absolute correlation between the experimental condition and the predictions using a linear dynamical system model. (b) The prediction on the test set using 300 sources. Red dots show the true angle and blue dots show the predictions.

6.4 Conclusion

In this chapter, we showed that we can incorporate the independence assumption of the standard beamformer in a linear dynamical system by using the leadfield matrix as the observation model and setting the covariance of the observation noise to be proportional to the covariance of the observation. This led to our formulation of the dynamic beamformer. We evaluated our method using an MEG data-set reported in [11]. We validated our method by decoding the experimental design from the sources extracted using both the standard beamformer and the dynamic beamformer. Our validation as shown in Fig. 6.3b, demonstrated that the dynamic beam-

former outperforms the standard beamformer in predicting the direction to which a subject was covertly attending. We further showed in Fig. 6.5 that we can improve the prediction of the attended direction from the sources by making use of a linear dynamical system. Our results strongly suggest that the dynamic beamformer outperforms the standard approach in estimating the active neural generators. Further Bayesian optimization approaches other than the maximum likelihood can be applied to improve the performance of the dynamic beamformer in future studies [19].

Chapter 7

General Conclusion

Covert attention is the act of mentally focusing on a target without changing gaze. Offline MEG and EEG-based experiments in this thesis, which were presented in the first four chapters, demonstrate that modulations in alpha activity with covert attention can be used as a robust control signal for BCI. The results offer the possibility of extending the current applications of covert attention from one-dimensional left-right control to full two-dimensional control over different directions and eccentricities. Such a two-dimensional BCI control has only been achieved in a few non-invasive BCI studies [134, 68]. Furthermore, the possibility of subject-independent decoding of the direction of attention as shown in chapter 4 shows how robust the modulation of alpha activity induced by covert attention across subjects is, which shows that there is a similar general structure in the mechanism that individuals covertly direct their attention. As attention is a fundamental brain mechanism, the notion that this is implemented similarly in different people may offer new insight into the nature of cognition [131].

The last two chapters of this thesis were dedicated to the source localization algorithms. The source localization approaches introduced in this thesis were applied on the covert visual attention data-set from chapter 2. However, the methods are general and can be applied in place of stan-

standard source localization algorithms. Future studies might show whether the methods are beneficial for other data-sets.

Although in this thesis we focused on modulations of alpha activity caused by manipulating covert visual attention, it might be interesting to look at modulations of oscillatory activity due to covert attention in other modalities as well. Shifting attention from the visual to the auditory modality, directing the auditory attention to sounds presented to the left or the right, or shifting attention from the left to the right hand provides modulations in alpha activity [37, 62, 13, 55, 116, 115, 41]. These findings can be further evaluated and used as a basis to introduce new alpha-based BCIs.

Mostly, BCIs have been used for communication and control, whereas they can also be used for cognitive enhancement. One can think of the covert-attention BCI as a way to train people to better direct their attention by giving proper neurofeedback. As there is some evidence on the applications of neurofeedback for improving performance of various cognitive tasks [6, 112], training attention might benefit people with attention disorders such as people who suffer from attention deficit hyperactivity disorders (ADHD). This training approach and its consequences on the performance of people in their daily life can be seen as a future direction of BCI research.

Bibliography

- [1] L. Acqualagnav, M.S. Treder, M. Schreuder, and B. Blankertz. A novel brain-computer interface based on the rapid serial visual presentation paradigm. In *Annual International Conference of the IEEE Engineering in Medicine and Biology Society (EMBC)*, pages 2686–2689, 2010.
- [2] S.P. Ahlfors, R.J. Ilmoniemi, and M.S. Hämäläinen. Estimates of visually evoked cortical currents. *Electroencephalogr Clin Neurophysiol*, 82(3):225–236, 1992.
- [3] M. Ahn, H. Cho, and S.C. Jun. Calibration time reduction through source imaging in brain computer interface (BCI). *HCI International 2011-Posters Extended Abstracts*, pages 269–273, 2011.
- [4] M. Alamgir, M. Grosse-Wentrup, and Y. Altun. Multitask learning for brain-computer interfaces. *J. Mach. Learn. Res.- Proceedings Track*, pages 17–24, 2010.
- [5] B.Z. Allison, E.W. Wolpaw, and J.R. Wolpaw. Brain-computer interface systems: progress and prospects. *Expert Rev. Med. Devic.*, 4(4):463–474, 2007.
- [6] E. Angelakis, S. Stathopoulou, J.L. Frymiare, D.L. Green, J.F. Lubar, and J. Kounios. EEG neurofeedback: a brief overview and an example of peak alpha frequency training for cognitive enhancement in the elderly. *Clin. Neuropsychol.*, 21(1):110–129, 2007.

- [7] S.M. Anstis. Letter: A chart demonstrating variations in acuity with retinal position. *Vision Res.*, 14(7):589–592, 1974.
- [8] J.M. Antelis and J. Minguez. Dynamic solution to the EEG source localization problem using Kalman filters and particle filters. In *Annual International Conference of the IEEE Engineering in Medicine and Biology Society (EMBC)*, pages 77–80, 2009.
- [9] J.M. Antelis and J. Minguez. DYNAMO: Dynamic multi-model source localization method for EEG and/or MEG. In *Annual International Conference of the IEEE Engineering in Medicine and Biology Society (EMBC)*, pages 5141–5144, 2010.
- [10] A. Bahramisharif, T. Heskes, O. Jensen, and M.A.J. van Gerven. Lateralized responses during covert attention are modulated by target eccentricity. *Neurosci. Lett.*, 491:35–39, 2011.
- [11] A. Bahramisharif, M.A.J. van Gerven, T. Heskes, and O. Jensen. Covert attention allows for continuous control of brain-computer interfaces. *Eur. J. Neurosci.*, 31(8):1501–1508, 2010.
- [12] A. Bahramisharif, M.A.J. van Gerven, Y. Okazaki, T. Heskes, and O. Jensen. Posterior alpha activity modulated by covert attention used as a control signal for BCI. In *Front Neurosci Conference Abstract: Biomag 2010-17th International Conference on Biomagnetism*, 2010.
- [13] S. Banerjee, A.C. Snyder, S. Molholm, and J.J. Foxe. Oscillatory alpha-band mechanisms and the deployment of spatial attention to anticipated auditory and visual target locations: Supramodal or sensory-specific control mechanisms? *J. Neurosci.*, 31(27):9923–9932, 2011.
- [14] M. Bastiaansen and T.R. Knosche. Tangential derivative mapping of axial MEG applied to event-related desynchronization research. *Clin. Neurophysiol.*, 111(7):1300–1305, 2000.

- [15] M.S. Beauchamp, L. Petit, T.M. Ellmore, J. Ingeholm, and J.V. Haxby. A parametric fMRI study of overt and covert shifts of visuospatial attention. *NeuroImage*, 14(2):310–321, 2001.
- [16] N. Berardi and A. Fiorentini. Visual field asymmetries in pattern discrimination: a sign of asymmetry in cortical visual field representation? *Vision Res.*, 31(10):1831–1836, 1991.
- [17] N. Birbaumer. Breaking the silence: brain–computer interfaces(BCI) for communication and motor control. *Psychophysiology*, 43(6):517–532, 2006.
- [18] N. Birbaumer, A.R. Murguialday, and L. Cohen. Brain–computer interface in paralysis. *Curr. Opin. Neurol.*, 21(6):634–638, 2008.
- [19] C.M. Bishop. *Pattern Recognition and Machine Learning*. Springer, 2006.
- [20] B. Blankertz, G. Dornhege, M. Krauledat, K.R. Müller, and G. Curio. The non-invasive Berlin brain-computer interface: fast acquisition of effective performance in untrained subjects. *NeuroImage*, 37(2):539–550, 2007.
- [21] B. Blankertz, S. Lemm, M. Treder, S. Haufe, and K.R. Müller. Single-trial analysis and classification of ERP components—A tutorial. *NeuroImage*, 56(2):814–825, 2011.
- [22] B. Blankertz, C. Sannelli, S. Halder, E.M. Hammer, A. Kübler, K.R. Müller, G. Curio, and T. Dickhaus. Neurophysiological predictor of SMR-based BCI performance. *NeuroImage*, 51(4):1303–1309, 2010.
- [23] D. H. Brainard. The psychophysics toolbox. *Spatial Vision*, 10:433–436, 1997.
- [24] A.M. Brouwer and J.B.F. van Erp. A tactile P300 brain-computer interface. *Front. Neurosc.*, 4, 2010.

- [25] P. Brunner, S. Joshi, S. Briskin, J.R. Wolpaw, H. Bischof, and G. Schalk. Does the ‘p300’ speller depend on eye gaze? *J. Neural Eng.*, 7:056013, 2010.
- [26] M. Carrasco and Y. Yeshurun. The contribution of covert attention to the set-size and eccentricity effects in visual search. *Journal of Experimental Psychology Human Perception and Performance*, 24:673–692, 1998.
- [27] M. Carrasco and Y. Yeshurun. Covert attention effects on spatial resolution. *Progress in Brain Research*, 176:65–86, 2009.
- [28] L. Citi, R. Poli, C. Cinel, and F. Sepulveda. P300-based BCI mouse with genetically-optimized analogue control. *IEEE T. Rehabil. Eng.*, 16(1):51–61, 2009.
- [29] S.F. Cotter, B.D. Rao, K. Engan, and K. Kreutz-Delgado. Sparse solutions to linear inverse problems with multiple measurement vectors. *IEEE T. Signal Proces.*, 53(7):2477–2488, 2005.
- [30] A.M. Dale, A.K. Liu, B.R. Fischl, R.L. Buckner, J.W. Belliveau, J.D. Lewine, and E. Halgren. Dynamic statistical parametric mapping: Combining fMRI and MEG for high-resolution imaging of cortical activity. *Neuron*, 26(1):55–67, 2000.
- [31] A.M. Dale and M.I. Sereno. Improved localization of cortical activity by combining EEG and MEG with MRI cortical surface reconstruction: a linear approach. *J. Cognitive Neurosci.*, 5(2):162–176, 1993.
- [32] J.J. Daly and J.R. Wolpaw. Brain–computer interfaces in neurological rehabilitation. *Lancet Neurol.*, 7(11):1032–1043, 2008.
- [33] N.R. Draper and H. Smith. *Applied Regression Analysis*. Wiley-Interscience, 3rd edition, 1998.
- [34] B. Efron, T. Hastie, I. Johnstone, and R. Tibshirani. Least angle regression. *Ann. Stat.*, 32(2):407–499, 2004.

- [35] N.I. Fisher. *Statistical Analysis of Circular Data*. Cambridge University Press, 1996.
- [36] J. Friedman, T. Hastie, and R. Tibshirani. Regularization paths for generalized linear models via coordinate descent. *J. Stat. Softw.*, 33(1):1–22, 2010.
- [37] K.M.G. Fu, J.J. Foxe, M.M. Murray, B.A. Higgins, D.C. Javitt, and C.E. Schroeder. Attention-dependent suppression of distracter visual input can be cross-modally cued as indexed by anticipatory parieto-occipital alpha-band oscillations. *Cognitive Brain Res.*, 12(1):145–152, 2001.
- [38] A. Gelman, J.B. Carlin, H.S. Stern, and D.B. Rubin. *Bayesian Data Analysis*. CRC press, 2004.
- [39] J. Gross, J. Kujala, M. Hämäläinen, L. Timmermann, A. Schnitzler, and R. Salmelin. Dynamic imaging of coherent sources: studying neural interactions in the human brain. *P. Natl. Acad. Sci. USA*, 98(2):694–699, 2001.
- [40] C. Guger, H. Ramoser, and G. Pfurtscheller. Real-time EEG analysis with subject-specific spatial patterns for a brain-computer interface (BCI). *IEEE T. Rehabil. Eng.*, 8(4):447–456, 2000.
- [41] S. Haegens, D. Osipova, R. Oostenveld, and O. Jensen. Somatosensory working memory performance in humans depends on both engagement and disengagement of regions in a distributed network. *Hum. Brain Mapp.*, 31(1):26–35, 2010.
- [42] M. Hämäläinen, R. Hari, R.J. Ilmoniemi, J. Knuutila, and O.V. Lounasmaa. Magnetoencephalography-theory, instrumentation, and applications to noninvasive studies of the working human brain. *Rev. Mod. Phys.*, 65(2):413–497, 1993.

- [43] M.S. Hämäläinen and R.J. Ilmoniemi. Interpreting magnetic fields of the brain: minimum norm estimates. *Med. Biol. Eng. Comput.*, 32(1):35–42, 1994.
- [44] S. Hanslmayr, A. Aslan, T. Staudigl, W. Klimesch, C.S. Herrmann, and K.H. Bäuml. Prestimulus oscillations predict visual perception performance between and within subjects. *NeuroImage*, 37(4):1465–1473, 2007.
- [45] S. Hanslmayr, P. Sauseng, M. Doppelmayr, M. Schabus, and W. Klimesch. Increasing individual upper alpha power by neuro-feedback improves cognitive performance in human subjects. *Appl. Psychophysiol. Biofeedback*, 30(1):1–10, 2005.
- [46] S. Haufe, V.V. Nikulin, A. Ziehe, K.R. Müller, and G. Nolte. Combining sparsity and rotational invariance in EEG/MEG source reconstruction. *NeuroImage*, 42(2):726–738, 2008.
- [47] S. Haufe, R. Tomioka, G. Nolte, K.R. Müller, and M. Kawanabe. Modeling sparse connectivity between underlying brain sources for EEG/MEG. *IEEE T. Bio-Med. Eng.*, 57(8):1954–1963, 2010.
- [48] J.V. Haxby, M.I. Gobbini, M.L. Furey, A. Ishai, J.L. Schouten, and P. Pietrini. Distributed and overlapping representations of faces and objects in ventral temporal cortex. *Science*, 293(5539):2425, 2001.
- [49] L.R. Hochberg, M.D. Serruya, G.M. Friehs, J.A. Mukand, M. Saleh, A.H. Caplan, A. Branner, D. Chen, R.D. Penn, and J.P. Donoghue. Neuronal ensemble control of prosthetic devices by a human with tetraplegia. *Nature*, 442:164–171, 2006.
- [50] J. Höhne, M. Schreuder, B. Blankertz, and M. Tangermann. Two-dimensional auditory p300 speller with predictive text system. In *Annual International Conference of the IEEE Engineering in Medicine and Biology Society (EMBC)*, pages 4185–4188, 2010.

- [51] J.C. Horton and W.F. Hoyt. The representation of the visual field in human striate cortex: a revision of the classic Holmes map. *Archives of Ophthalmology*, 109(6):816, 1991.
- [52] J. Intriligator and P. Cavanagh. The Spatial Resolution of Visual Attention. *Cognitive Psychol*, 43(3):171–216, 2001.
- [53] O. Jensen, A. Bahramisharif, R. Oostenveld, S. Klanke, A. Hadjipapas, Y.O. Okazaki, and M.A.J. van Gerven. Using brain–computer interfaces and brain-state dependent stimulation as tools in cognitive neuroscience. *Front. Psychol.*, 2(100), 2011.
- [54] D. Jokisch and O. Jensen. Modulation of gamma and alpha activity during a working memory task engaging the dorsal or ventral stream. *J. Neurosci.*, 27(12):3244–3251, 2007.
- [55] S.R. Jones, C.E. Kerr, Q. Wan, D.L. Pritchett, M. Hämäläinen, and C.I. Moore. Cued spatial attention drives functionally relevant modulation of the mu rhythm in primary somatosensory cortex. *J. Neurosci.*, 30(41):13760–13765, 2010.
- [56] J. Kayser and C.E. Tenke. Principal components analysis of Laplacian waveforms as a generic method for identifying ERP generator patterns: I. Evaluation with auditory oddball tasks. *Clin. Neurophysiol.*, 117(2):348–368, 2006.
- [57] S.P. Kelly, M. Gomez-Ramirez, and J.J. Foxe. The strength of anticipatory spatial biasing predicts target discrimination at attended locations: a high-density EEG study. *Eur. J. Neurosci.*, 30(11):2224–2234, 2009.
- [58] S.P. Kelly, E. Lalor, R.B. Reilly, and J.J. Foxe. Independent brain computer interface control using visual spatial attention-dependent modulations of parieto–occipital alpha. In *Conference Proceedings. 2nd International IEEE EMBS Conference on Neural Engineering*, pages 667–670, 2005.

- [59] S.P. Kelly, E. Lalor, R.B. Reilly, and J.J. Foxe. Increases in alpha oscillatory power reflect an active retinotopic mechanism for distracter suppression during sustained visuo-spatial attention. *J. Neurophysiol.*, 95:3844–3851, 2006.
- [60] S.P. Kelly, E.C. Lalor, C. Finucane, G. McDarby, and R.B. Reilly. Visual spatial attention control in an independent brain-computer interface. *IEEE T. Biomed. Eng.*, 52(9):1588–1596, 2005.
- [61] S.P. Kelly, E.C. Lalor, R.B. Reilly, and J.J. Foxe. Visual spatial attention tracking using high-density SSVEP data for independent brain-computer communication. *IEEE T. Neur. Sys. Reh.*, 13(2):172–178, 2005.
- [62] J.R. Kerlin, A.J. Shahin, and L.M. Miller. Attentional gain control of ongoing cortical speech representations in a ‘cocktail party’. *J. Neurosci.*, 30(2):620–628, 2010.
- [63] W. Klimesch, P. Sauseng, and S. Hanslmayr. EEG alpha oscillations: the inhibition-timing hypothesis. *Brain Res. Rev.*, 53(1):63–88, 2007.
- [64] R. Kohavi. A study of cross-validation and bootstrap for accuracy estimation and model selection. In *International joint Conference on artificial intelligence*, volume 14, pages 1137–1145, 1995.
- [65] S.Y. Kruglikov and S.J. Schiff. Interplay of electroencephalogram phase and auditory-evoked neural activity. *J. Neurosci.*, 23(31):10122–10127, 2003.
- [66] A. Kübler, N. Neumann, B. Wilhelm, T. Hinterberger, and N. Birbaumer. Predictability of brain-computer communication. *J. Psychophysiol.*, 18(2-3):121, 2004.
- [67] M.A. Lebedev and M.A.L. Nicolelis. Brain-machine interfaces: past, present and future. *Trends Neurosci.*, 29(9):536–546, 2006.

- [68] Y. Li, J. Long, T. Yu, Z. Yu, C. Wang, H. Zhang, and C. Guan. An EEG-based BCI system for 2-D cursor control by combining Mu/Beta rhythm and P300 potential. *IEEE T. Bio-Med. Eng.*, 57(10):2495–2505, 2010.
- [69] K.V. Mardia and P.E. Jupp. *Directional Statistics*. Wiley, 2nd edition, 1999.
- [70] S.G. Mason and G.E. Birch. A brain-controlled switch for asynchronous control applications. *IEEE T. Bio-Med. Eng.*, 47(10):1297–1307, 2000.
- [71] J. Mattout, C. Phillips, W.D. Penny, M.D. Rugg, and K.J. Friston. MEG source localization under multiple constraints: an extended Bayesian framework. *NeuroImage*, 30(3):753–767, 2006.
- [72] D.J. McFarland, D.J. Krusienski, W.A. Sarnacki, and J.R. Wolpaw. Emulation of computer mouse control with a noninvasive brain-computer interface. *J. Neural Eng.*, 5(2):101–110, 2008.
- [73] M.M. Mesulam. Spatial attention and neglect: parietal, frontal and cingulate contributions to the mental representation and attentional targeting of salient extrapersonal events. *Philos. T. Roy. Soc. B*, 354(1387):1325–1346, 1999.
- [74] M. Misaki, Y. Kim, P.A. Bandettini, and N. Kriegeskorte. Comparison of multivariate classifiers and response normalizations for pattern-information fMRI. *NeuroImage*, 53(1):103–118, 2010.
- [75] E.H. Moore. On the reciprocal of the general algebraic matrix. *Bull. Amer. Math. Soc.*, 26:394–395, 1920.
- [76] M. Näpflin, M. Wildi, and J. Sarnthein. Test–retest reliability of resting EEG spectra validates a statistical signature of persons. *Clin. Neurophysiol.*, 118(11):2519–2524, 2007.

- [77] C. Neuper, G.R. Müller-Putz, R. Scherer, and G. Pfurtscheller. Motor imagery and EEG-based control of spelling devices and neuroprostheses. *Prog. Brain Res.*, 159:393–409, 2006.
- [78] G. Nolte. The magnetic lead field theorem in the quasi-static approximation and its use for magnetoencephalography forward calculation in realistic volume conductors. *Phys. Med. Biol.*, 48:3637–3652, 2003.
- [79] J.E. O Doherty, M. Lebedev, T.L. Hanson, N. Fitzsimmons, and M.A. Nicolelis. A brain-machine interface instructed by direct intracortical microstimulation. *Front. Integr. Neurosci.*, 3(20), 2009.
- [80] R. Oostenveld, P. Fries, E. Maris, and J.M. Schoffelen. FieldTrip: open source software for advanced analysis of MEG, EEG, and invasive electrophysiological data. *Computat. Intell. Neurosc.*, 2011:1, 2011.
- [81] A.V. Oppenheim, A.S. Willsky, and S.H. Nawab. *Signals and Systems*. Pearson education, 1998.
- [82] W. Penny, S. Kiebel, and K. Friston. Variational Bayesian inference for fMRI time series. *NeuroImage*, 19(3):727–741, 2003.
- [83] G. Pfurtscheller, D. Flotzinger, and J. Kalcher. Brain-computer interface – a new communication device for handicapped people. *J. Microcomput. Appl.*, 16(3):293–299, 1993.
- [84] G. Pfurtscheller and C. Neuper. Future prospects of ERD/ERS in the context of brain-computer interface (BCI) developments. *Prog. Brain Res.*, 159:433–437, 2006.
- [85] T. Pistohl, T. Ball, A. Schulze-Bonhage, A. Aertsen, and C. Mehring. Prediction of arm movement trajectories from ECoG-recordings in humans. *J. Neurosci. Meth.*, 167(1):105–114, 2008.
- [86] D. Plass-Oude Bos, M. Duvinage, O. Oktay, J. Delgado Saa, H. Guerueler, A. Istanbulu, M. van Vliet, B. van de Laar, M. Poel,

- L. Roijendijk, L. Tonin, A. Bahramisharif, and B. Reuderink. Looking around with your brain in a virtual world. In *IEEE Symposium on Computational Intelligence, Cognitive Algorithms, Mind, and Brain (CCMB)*, pages 1–8, 2011.
- [87] D. Plass-Oude Bos, B. van de Laar, M. Duvinage, O. Oktay, J. Delgado Saa, M. van Vliet, M. Poel, L. Roijendijk, A. Bahramisharif, and B. Reuderink. Wild photoshoot: Applying overt and covert attention. *Neurosci. Lett.*, 500:e10, 2011.
- [88] M.I. Posner. Orienting of attention. *Q. J. Exp. Psychol.*, 32(1):3–25, 1980.
- [89] M.I. Posner and S.E. Petersen. The attention system of the human brain. *Annu. Rev. Neurosci.*, 13:25–42, 1990.
- [90] T.A. Rihs, C.M. Michel, and G. Thut. Mechanisms of selective inhibition in visual spatial attention are indexed by α -band EEG synchronization. *Eur. J. Neurosci.*, 25(2):603–610, 2007.
- [91] T.A. Rihs, C.M. Michel, and G. Thut. A bias for posterior α -band power suppression versus enhancement during shifting versus maintenance of spatial attention. *NeuroImage*, 44(1):190–199, 2009.
- [92] G. Rota, R. Sitaram, R. Veit, M. Erb, N. Weiskopf, G. Dogil, and N. Birbaumer. Self-regulation of regional cortical activity using real-time fMRI: the right inferior frontal gyrus and linguistic processing. *Hum. Brain Mapp.*, 30(5):1605–1614, 2009.
- [93] J. Rovamo and V. Virsu. An estimation and application of the human cortical magnification factor. *Experimental Brain Research*, 37(3):495–510, 1979.
- [94] S. Roweis and Z. Ghahramani. A unifying review of linear Gaussian models. *Neural Comput.*, 11(2):305–345, 1999.

- [95] I. Rustandi, M.A. Just, and T.M. Mitchell. Integrating multiple-study multiple-subject fMRI datasets using canonical correlation analysis. In *Proceedings of the MICCAI Workshop*, 2009.
- [96] S.L. Salzberg. On comparing classifiers: Pitfalls to avoid and a recommended approach. *Data Min. Knowl. Disc.*, 1(3):317–328, 1997.
- [97] P. Sauseng, W. Klimesch, W. Stadler, M. Schabus, M. Doppelmayr, S. Hanslmayr, W.R. Gruber, and N. Birbaumer. A shift of visual spatial attention is selectively associated with human EEG alpha activity. *Eur. J. Neurosci.*, 22(11):2917–2926, 2005.
- [98] M. Schreuder, B. Blankertz, and M. Tangermann. A new auditory multi-class brain-computer interface paradigm: spatial hearing as an informative cue. *PLoS One*, 5(4):e9813, 2010.
- [99] C.E. Shannon and W. Weaver. *Mathematical Theory of Communication*. University of Illinois Press, 1998.
- [100] G.L. Shulman, D.L.W. Pope, S.V. Astafiev, M.P. McAvoy, A.Z. Snyder, and M. Corbetta. Right hemisphere dominance during spatial selective attention and target detection occurs outside the dorsal frontoparietal network. *J. Neurosci.*, 30(10):3640–3651, 2010.
- [101] C. Silva, J.C. Maltez, E. Trindade, A. Arriaga, and E. Ducla-Soares. Evaluation of L1 and L2 minimum norm performances on EEG localizations. *Clin. Neurophysiol.*, 115(7):1657–1668, 2004.
- [102] C.E. Spearman. The proof and measurement of association between two things. *Am. J. Psychol.*, 15(1):72–101, 1904.
- [103] C. Tallon-Baudry, O. Bertrand, C. Delpuech, and J. Permier. Oscillatory gamma-band (30-70 Hz) activity induced by a visual search task in humans. *J. Neurosci.*, 17(2):722–734, 1997.
- [104] D.M. Taylor, S.I. Tillery, and A.B. Schwartz. Direct cortical control of 3D neuroprosthetic devices. *Science*, 296:1829–1832, 2002.

- [105] R. Tibshirani. Regression shrinkage and selection via the Lasso. *J. Roy. Stat. Soc. B.*, 58:267–288, 1996.
- [106] A.N. Tikhonov. On the stability of inverse problems. *Doklady Akademii Nauk SSSR*, 39(5):195–198, 1943.
- [107] R.B.H. Tootell, N. Hadjikhani, E.K. Hall, S. Marrett, W. Vanduffel, J.T. Vaughan, and A.M. Dale. The retinotopy of visual spatial attention. *Neuron*, 21(6):1409–1422, 1998.
- [108] M.S. Treder and B. Blankertz. (C) overt attention and visual speller design in an ERP-based brain-computer interface. *Behavioral and Brain Functions*, 6(1):28, 2010.
- [109] M.S. Treder, N.M. Schmidt, and B. Blankertz. Gaze-independent brain-computer interfaces based on covert attention and feature attention. *J. Neural Eng.*, 8:066003, 2011.
- [110] N.J. Trujillo-Barreto, E. Aubert-Vázquez, and W.D. Penny. Bayesian M/EEG source reconstruction with spatio-temporal priors. *NeuroImage*, 39(1):318–335, 2008.
- [111] K. Uutela, M. Hämäläinen, and E. Somersalo. Visualization of magnetoencephalographic data using minimum current estimates. *NeuroImage*, 10(2):173–180, 1999.
- [112] G.J.M. van Boxtel, A. Denissen, M. Jäger, D. Vernon, M.K.J. Dekker, V. Mihajlovic, and M.M. Sitskoorn. A novel self-guided approach to alpha activity training. *Int. J. Psychophysiol.*, doi:10.1016/j.ijpsycho.2011.11.004, 2011.
- [113] J. van der Werf, O. Jensen, P. Fries, and W.P. Medendorp. Gamma-band activity in human posterior parietal cortex encodes the motor goal during delayed prosaccades and antisaccades. *J. Neurosci.*, 28(34):8397–8405, 2008.

- [114] Y.D. van der Werf, E. Altena, M.M. Schoonheim, E.J. Sanz-Arigitá, J.C. Vis, W. De Rijke, and E.J. Van Someren. Sleep benefits subsequent hippocampal functioning. *Nat. Neurosci.*, 12(2):122–123, 2009.
- [115] F. van Ede, F. de Lange, O. Jensen, and E. Maris. Orienting attention to an upcoming tactile event involves a spatially and temporally specific modulation of sensorimotor alpha-and beta-band oscillations. *J. Neurosci.*, 31(6):2016–2024, 2011.
- [116] F. van Ede, O. Jensen, and E. Maris. Tactile expectation modulates pre-stimulus [beta]-band oscillations in human sensorimotor cortex. *NeuroImage*, 51(2):867–876, 2010.
- [117] D.C. Van Essen, W.T. Newsome, and J.H.R. Maunsell. The visual field representation in striate cortex of the macaque monkey: asymmetries, anisotropies, and individual variability. *Vision Res.*, 24(5):429–448, 1984.
- [118] M.A.J. van Gerven, A. Bahramisharif, T. Heskes, and O. Jensen. Selecting features for BCI control based on a covert spatial attention paradigm. *Neural Networks*, 22:1271–1277, 2009.
- [119] M.A.J. van Gerven, B. Cseke, R. Oostenveld, and T. Heskes. Bayesian source localization with the multivariate Laplace prior. *Advances in Neural Information Processing Systems*, 22:1901–1909, 2009.
- [120] M.A.J. van Gerven, J. Farquhar, R. Schaefer, R. Vlek, J. Geuze, A. Nijholt, N. Ramsey, P. Haselager, L. Vuurpijl, S. Gielen, and P. Desain. The brain–computer interface cycle. *J. Neural Eng.*, 6(4), 2009.
- [121] M.A.J. van Gerven and O. Jensen. Attention modulations of posterior alpha as a control signal for two-dimensional brain-computer interfaces. *J. Neurosci. Meth.*, 179(1):78–84, 2009.
- [122] B.D. Van Veen and K.M. Buckley. Beamforming: a versatile approach to spatial filtering. *IEEE ASSP Magazine*, 5(2):4–24, 1988.

- [123] B.D. Van Veen, W. van Drongelen, M. Yuchtman, and A. Suzuki. Localization of brain electrical activity via linearly constrained minimum variance spatial filtering. *IEEE T. Bio-Med. Eng.*, 44(9):867–880, 1997.
- [124] B. Venthur, S. Scholler, J. Williamson, S. Dähne, M.S. Treder, M.T. Kramarek, K.R. Müller, and B. Blankertz. Pyff-a pythonic framework for feedback applications and stimulus presentation in neuroscience. *Front. Neurosci.*, 4:179, 2010.
- [125] C. Vidaurre and B. Blankertz. Towards a cure for BCI illiteracy. *Brain Topogr.*, 23(2):194–198, 2010.
- [126] S. Waldert, T. Pistohl, C. Braun, T. Ball, A. Aertsen, and C. Mehring. A review on directional information in neural signals for brain-machine interfaces. *J. Physiology-Paris*, 103(3-5):244–254, 2009.
- [127] S. Waldert, H. Preissl, E. Demandt, C. Braun, N. Birbaumer, A. Aertsen, and C. Mehring. Hand movement direction decoded from MEG and EEG. *J. Neurosci.*, 28(4):1000–1008, 2008.
- [128] J.Z. Wang, S.J. Williamson, and L Kaufman. Magnetic source images determined by a lead-field analysis: the unique minimum-norm least-squares estimation. *IEEE T. Bio-Med. Eng.*, 39(7):665–675, 1992.
- [129] D. Wipf and S. Nagarajan. A unified Bayesian framework for MEG/EEG source imaging. *NeuroImage*, 44(3):947–966, 2009.
- [130] D. Wipf, R. Ramírez, J. Palmer, S. Makeig, and B. Rao. Analysis of empirical Bayesian methods for neuroelectromagnetic source localization. *Advances in Neural Information Processing Systems*, 19:1505, 2007.
- [131] L. Wittgenstein. *The Brown and Blue Books*. Blackwell Publishing, 1958.

- [132] J.R. Wolpaw. Brain-computer interfaces as new brain output pathways. *J. Physiol.*, 579:613–619, 2007.
- [133] J.R. Wolpaw, N. Birbaumer, D.J. McFarland, G. Pfurtscheller, and T.M. Vaughan. Brain-computer interfaces for communication and control. *Clin. Neurophysiol.*, 113(6):767–791, 2002.
- [134] J.R. Wolpaw and D.J. McFarland. Control of a two-dimensional movement signal by a noninvasive brain-computer interface in humans. In *P. Natl. Acad. Sci. USA*, volume 101, pages 17849–17854, 2004.
- [135] M.A. Woodbury. Inverting modified matrices. *Memorandum report*, 42:106, 1950.
- [136] M. Woolrich, L. Hunt, A. Groves, and G. Barnes. MEG beamforming using Bayesian PCA for adaptive data covariance matrix regularisation. *NeuroImage*, 57(4):1466–1479, 2011.
- [137] M.S. Worden, J.J. Foxe, N. Wang, and G.V. Simpson. Anticipatory biasing of visuospatial attention indexed by retinotopically specific alpha-band electroencephalography increases over occipital cortex. *J. Neurosci.*, 20(6), 2000.
- [138] Y. Yeshurun and M. Carrasco. Attention improves or impairs visual performance by enhancing spatial resolution. *Nature*, 396:72–75, 1998.
- [139] H. Zou and T. Hastie. Regularization and variable selection via the Elastic Net. *J. Roy. Stat. Soc. B.*, 67(2):301–320, 2005.

Samenvatting

Wanneer we uiting willen geven aan onze gedachten, maken we gebruik van onze spieren, om bijvoorbeeld te spreken, te schrijven, gebaren te maken, of te typen. Dankzij de huidige ontwikkelingen in het monitoren van hersenactiviteit kunnen we nu echter ook nieuwe manieren van communiceren onderzoeken door middel van direct gebruik van onze hersensignalen. Recente bevindingen hebben aangetoond dat we verschillende apparaten kunnen aansturen met onze hersenactiviteit in de zogenoemde brein-computer interfaces (BCIs). Verschillende modaliteiten zijn gebruikt voor BCI. Voorbeelden hiervan zijn het inbeelden van een beweging zonder deze te maken en het richten van aandacht op visuele stimuli van een specifieke frequentie of op auditieve of tactiele stimuli op specifieke locaties. Hoewel men, afhankelijk van de toepassing, de voorkeur kan hebben voor de ene experimentele opstelling boven de andere, is het altijd gunstig om meer controle signalen te hebben om de betrouwbaarheid en snelheid van BCIs te verhogen. Voorts is het waardevol om te streven naar modaliteiten die gemakkelijker een volledige tweedimensionale controle mogelijk maken, zodat deze toegepast kunnen worden in bijvoorbeeld rolstoel- of cursorbesturing.

Covert visuele spatiële aandacht, in dit proefschrift aangeduid met ‘covert attention’, is de mogelijkheid vrijwillig onze (visuele) aandacht te richten in de wereld om ons heen, zonder onze ogen daarbij te bewegen. Het is een uitvoerig bestudeerd psychologisch proces dat gepaard gaat met unieke patronen van hersenactiviteit. Dit proefschrift onderzoekt de mogelijkheid deze ‘covert attention’ te gebruiken als een BCI modaliteit. De eerste

vier hoofdstukken laten zien dat met behulp van magneto-encefalografie (MEG) en electro-encefalografie (EEG) signalen het mogelijk is om zowel de richting als de excentriciteit van de ‘covert attention’ te bepalen. In hoofdstuk 4 blijkt dat het ook mogelijk is om ‘covert attention’ als stuur signaal te gebruiken voor persoonsonafhankelijke BCI.

De laatste hoofdstukken van het proefschrift zijn gewijd aan de ontwikkeling van nieuwe methoden voor het lokaliseren van bronnen binnenin het brein op grond van EEG of MEG metingen op de schedel. Hoofdstuk 5 introduceert een nieuwe techniek voor bronlokalisatie die de additionele informatie, zoals de experimentele set-up, mee kan nemen. Hoofdstuk 6 verbetert de standaard ‘beamformer’ methode voor bronlokalisatie door expliciet de dynamiek van de bronnen te modelleren. De voorgestelde methoden resulteren in een consistente bepaling van de lokatie van de neurale bronnen die aan de grondslag liggen van ‘covert attention’. Toekomstige studies zullen het potentieel van deze algoritmen voor bronlokalisatie in andere contexten verder verkennen.

Summary

Normally we express the content of our mind by actions or speech. Current advances in brain monitoring devices allow us to think of new ways of communicating with other people directly through our brains. Recent findings have shown that we can control various devices by our ongoing brain activity through brain-computer interfaces (BCIs). Different modalities have been used for brain-computer interfacing. Imaginary movement, steady-state visual evoked potentials, spatial auditory, and tactile stimulation are some of the successful BCI paradigms. Although depending on the application one may favor one paradigm over another, it is always beneficial to have more control signals in order to increase the reliability and information transfer rate of BCIs. Furthermore, it is important to work towards modalities which more easily allow for a full two-dimensional continuous control since this affords applications such as wheelchair or cursor control.

Covert visual spatial attention, which is called in short ‘covert attention’ in this thesis, is a well studied psychological process that has its unique brain signature. Humans can voluntarily deploy attention to locations in visual space without moving their eyes. This thesis explores the possibility of using covert attention as a BCI modality. The first four chapters show that using magneto-encephalography (MEG) and electro-encephalography (EEG) signals, it is possible to decode the direction and eccentricity of covert attention. Chapter 4 shows that it is also possible to use covert attention as a control signal for subject-independent BCI.

The last chapters of the thesis are dedicated to developing novel methods for source localization and applying them to data sets related to covert

attention. Chapter 5 introduces a new source localization technique which incorporates the experimental design in the source localization procedure. Chapter 6 further incorporates source dynamics in the commonly used beamformer setup to explore the improvement over this standard source localization algorithm. The proposed methods resulted in a consistent estimation of the neural sources underlying covert attention. Future studies will reveal the potential of these algorithms for source localization in other contexts.

Curriculum Vitae

Ali Bahramisharif was born on January 7th, 1980 in Hamedan, Iran. From his childhood, he wanted to become an electrical engineer, to follow his father's steps. During his secondary school, he found his interest in mathematics specially in algebra and geometry and after three years of effort, he was ranked the first in the national mathematics olympiad in his hometown. In 1997, he got his high school diploma in mathematics and physics from the national organization for development of exceptional talents in his hometown, and after getting the rank of 126 among more than 250000 participants in the university national entrance exam (Konkour), he managed to enter Sharif University of Technology, the most prestigious engineering university of Iran. There, he studied electrical engineering and he got his bachelors degree in electrical and electronics engineering in 2002. Soon after that, he started his master studies in Tarbiat Modares University in the same field. Following the image-processing course by Prof. Kabir, his interest gradually shifted from electronics to image processing and machine learning. After finishing his master thesis in the field of image processing, he got interested in statistical pattern recognition and he had the chance to work with fMRI data with Dr Fatemizadeh. In April 2008, he moved to the Netherlands and started his PhD at the Radboud University Nijmegen to work on a project on brain-computer interfacing, and began his new life. The main results obtained in the four years of his PhD study can be found in this thesis. Since April 2012, he works as a post-doctoral researcher in groups of Dr Jensen and Dr Van Gerven to work on the analysis of intracranial electrocorticography in collaboration with Prof. Ramsey.

SIKS Dissertation Series

=====
2009
=====

- 2009-01 Rasa Jurgelenaite (RUN)
Symmetric Causal Independence Models
- 2009-02 Willem Robert van Hage (VU)
Evaluating Ontology-Alignment Techniques
- 2009-03 Hans Stol (UvT)
A Framework for Evidence-based Policy Making Using IT
- 2009-04 Josephine Nabukenya (RUN)
Improving the Quality of Organisational Policy Making using
Collaboration Engineering
- 2009-05 Sietse Overbeek (RUN)
Bridging Supply and Demand for Knowledge Intensive Tasks
Based on Knowledge, Cognition, and Quality
- 2009-06 Muhammad Subianto (UU)
Understanding Classification
- 2009-07 Ronald Poppe (UT)
Discriminative Vision-Based Recovery and Recognition of Human Motion
- 2009-08 Volker Nannen (VU)
Evolutionary Agent-Based Policy Analysis in Dynamic Environments
- 2009-09 Benjamin Kanagwa (RUN)
Design, Discovery and Construction of Service-oriented Systems
- 2009-10 Jan Wielemaker (UVA)
Logic programming for knowledge-intensive interactive applications
- 2009-11 Alexander Boer (UVA)
Legal Theory, Sources of Law & the Semantic Web
- 2009-12 Peter Massuthe (TUE, Humboldt-Universitaet zu Berlin)
Deriving Guidelines for Services
- 2009-13 Steven de Jong (UM)
Fairness in Multi-Agent Systems

- 2009-14 Maksym Korotkiy (VU)
From ontology-enabled services to service-enabled ontologies
(making ontologies work in e-science with ONTO-SOA)
- 2009-15 Rinke Hoekstra (UVA)
Ontology Representation - Design Patterns and Ontologies that Make Sense
- 2009-16 Fritz Reul (UvT)
New Architectures in Computer Chess
- 2009-17 Laurens van der Maaten (UvT)
Feature Extraction from Visual Data
- 2009-18 Fabian Groffen (CWI)
Armada, An Evolving Database System
- 2009-19 Valentin Robu (CWI)
Modeling Preferences, Strategic Reasoning and Collaboration
in Agent-Mediated Electronic Markets
- 2009-20 Bob van der Vecht (UU)
Adjustable Autonomy: Controlling Influences on Decision Making
- 2009-21 Stijn Vanderlooy (UM)
Ranking and Reliable Classification
- 2009-22 Pavel Serdyukov (UT)
Search For Expertise: Going beyond direct evidence
- 2009-23 Peter Hofgesang (VU)
Modelling Web Usage in a Changing Environment
- 2009-24 Annerieke Heuvelink (VUA)
Cognitive Models for Training Simulations
- 2009-25 Alex van Ballegooij (CWI)
"RAM: Array Database Management through Relational Mapping"
- 2009-26 Fernando Koch (UU)
An Agent-Based Model for the Development of Intelligent Mobile Services
- 2009-27 Christian Glahn (OU)
Contextual Support of social Engagement and Reflection on the Web
- 2009-28 Sander Evers (UT)
Sensor Data Management with Probabilistic Models

- 2009-29 Stanislav Pokraev (UT)
Model-Driven Semantic Integration of Service-Oriented Applications
- 2009-30 Marcin Zukowski (CWI)
Balancing vectorized query execution with bandwidth-optimized storage
- 2009-31 Sofiya Katrenko (UVA)
A Closer Look at Learning Relations from Text
- 2009-32 Rik Farenhorst (VU) and Remco de Boer (VU)
Architectural Knowledge Management: Supporting Architects and Auditors
- 2009-33 Khiet Truong (UT)
How Does Real Affect Affect Affect Recognition In Speech?
- 2009-34 Inge van de Weerd (UU)
Advancing in Software Product Management:
An Incremental Method Engineering Approach
- 2009-35 Wouter Koelewijn (UL)
Privacy en Politiegegevens; Over geautomatiseerde normatieve informatie-uitwisseling
- 2009-36 Marco Kalz (OUN)
Placement Support for Learners in Learning Networks
- 2009-37 Hendrik Drachsler (OUN)
Navigation Support for Learners in Informal Learning Networks
- 2009-38 Riina Vuorikari (OU)
Tags and self-organisation:
a metadata ecology for learning resources in a multilingual context
- 2009-39 Christian Stahl (TUE, Humboldt-Universitaet zu Berlin)
Service Substitution – A Behavioral Approach Based on Petri Nets
- 2009-40 Stephan Raaijmakers (UvT)
Multinomial Language Learning: Investigations into the Geometry of Language
- 2009-41 Igor Berezhnny (UvT)
Digital Analysis of Paintings
- 2009-42 Toine Bogers
Recommender Systems for Social Bookmarking
- 2009-43 Virginia Nunes Leal Franqueira (UT)
Finding Multi-step Attacks in Computer Networks
using Heuristic Search and Mobile Ambients

2009-44 Roberto Santana Tapia (UT)
Assessing Business-IT Alignment in Networked Organizations

2009-45 Jilles Vreeken (UU)
Making Pattern Mining Useful

2009-46 Loredana Afanasiev (UvA)
Querying XML: Benchmarks and Recursion

====

2010

====

2010-01 Matthijs van Leeuwen (UU)
Patterns that Matter

2010-02 Ingo Wassink (UT)
Work flows in Life Science

2010-03 Joost Geurts (CWI)
A Document Engineering Model and Processing Framework for Multimedia documents

2010-04 Olga Kulyk (UT)
Do You Know What I Know?
Situational Awareness of Co-located Teams in Multidisplay Environments

2010-05 Claudia Hauff (UT)
Predicting the Effectiveness of Queries and Retrieval Systems

2010-06 Sander Bakkes (UvT)
Rapid Adaptation of Video Game AI

2010-07 Wim Fikkert (UT)
Gesture interaction at a Distance

2010-08 Krzysztof Siewicz (UL)
Towards an Improved Regulatory Framework of Free Software.
Protecting user freedoms in a world of software communities and eGovernments

2010-09 Hugo Kielman (UL)
A Politiele gegevensverwerking en Privacy, Naar een effectieve waarborging

2010-10 Rebecca Ong (UL)
Mobile Communication and Protection of Children

- 2010-11 Adriaan Ter Mors (TUD)
The world according to MARP: Multi-Agent Route Planning
- 2010-12 Susan van den Braak (UU)
Sensemaking software for crime analysis
- 2010-13 Gianluigi Folino (RUN)
High Performance Data Mining using Bio-inspired techniques
- 2010-14 Sander van Splunter (VU)
Automated Web Service Reconfiguration
- 2010-15 Lianne Bodenstaff (UT)
Managing Dependency Relations in Inter-Organizational Models
- 2010-16 Sicco Verwer (TUD)
Efficient Identification of Timed Automata, theory and practice
- 2010-17 Spyros Kotoulas (VU)
Scalable Discovery of Networked Resources: Algorithms, Infrastructure, Applications
- 2010-18 Charlotte Gerritsen (VU)
Caught in the Act: Investigating Crime by Agent-Based Simulation
- 2010-19 Henriette Cramer (UvA)
People's Responses to Autonomous and Adaptive Systems
- 2010-20 Ivo Swartjes (UT)
Whose Story Is It Anyway?
How Improv Informs Agency and Authorship of Emergent Narrative
- 2010-21 Harold van Heerde (UT)
Privacy-aware data management by means of data degradation
- 2010-22 Michiel Hildebrand (CWI)
End-user Support for Access to
Heterogeneous Linked Data
- 2010-23 Bas Steunebrink (UU)
The Logical Structure of Emotions
- 2010-24 Dmytro Tykhonov
Designing Generic and Efficient Negotiation Strategies
- 2010-25 Zulfiqar Ali Memon (VU)
Modelling Human-Awareness for Ambient Agents: A Human Mindreading Perspective
- 2010-26 Ying Zhang (CWI)

XRPC: Efficient Distributed Query Processing on Heterogeneous XQuery Engines

- 2010-27 Marten Voulon (UL)
Automatisch contracteren
- 2010-28 Arne Koopman (UU)
Characteristic Relational Patterns
- 2010-29 Stratos Idreos(CWI)
Database Cracking: Towards Auto-tuning Database Kernels
- 2010-30 Marieke van Erp (UvT)
Accessing Natural History - Discoveries in data cleaning, structuring, and retrieval
- 2010-31 Victor de Boer (UVA)
Ontology Enrichment from Heterogeneous Sources on the Web
- 2010-32 Marcel Hiel (UvT)
An Adaptive Service Oriented Architecture: Automatically solving Interoperability Problems
- 2010-33 Robin Aly (UT)
Modeling Representation Uncertainty in Concept-Based Multimedia Retrieval
- 2010-34 Teduh Dirgahayu (UT)
Interaction Design in Service Compositions
- 2010-35 Dolf Trieschnigg (UT)
Proof of Concept: Concept-based Biomedical Information Retrieval
- 2010-36 Jose Janssen (OU)
Paving the Way for Lifelong Learning; Facilitating competence development through a learning path specification
- 2010-37 Niels Lohmann (TUE)
Correctness of services and their composition
- 2010-38 Dirk Fahland (TUE)
From Scenarios to components
- 2010-39 Ghazanfar Farooq Siddiqui (VU)
Integrative modeling of emotions in virtual agents
- 2010-40 Mark van Assem (VU)
Converting and Integrating Vocabularies for the Semantic Web
- 2010-41 Guillaume Chaslot (UM)
Monte-Carlo Tree Search

- 2010-42 Sybren de Kinderen (VU)
Needs-driven service bundling
in a multi-supplier setting - the computational e3-service approach
- 2010-43 Peter van Kranenburg (UU)
A Computational Approach to Content-Based Retrieval of Folk Song Melodies
- 2010-44 Pieter Bellekens (TUE)
An Approach towards Context-sensitive and User-adapted Access to
Heterogeneous Data Sources Illustrated in the Television Domain
- 2010-45 Vasilios Andrikopoulos (UvT)
A theory and model for the evolution of software services
- 2010-46 Vincent Pijpers (VU)
e3alignment: Exploring Inter-Organizational Business-ICT Alignment
- 2010-47 Chen Li (UT)
Mining Process Model Variants: Challenges, Techniques, Examples
- 2010-48 Milan Lovric (EUR)
Behavioral Finance and Agent-Based Artificial Markets
- 2010-49 Jahn-Takeshi Saito (UM)
Solving difficult game positions
- 2010-50 Bouke Huurnink (UVA)
Search in Audiovisual Broadcast Archives
- 2010-51 Alia Khairia Amin (CWI)
Understanding and supporting information seeking tasks in multiple sources
- 2010-52 Peter-Paul van Maanen (VU)
Adaptive Support for Human-Computer Teams:
Exploring the Use of Cognitive Models of Trust and Attention
- 2010-53 Edgar Meij (UVA)
Combining Concepts and Language Models for Information Access

====
2011
====

- 2011-01 Botond Cseke (RUN)
Variational Algorithms for Bayesian Inference in Latent Gaussian Models

- 2011-02 Nick Tinnemeier(UU)
Organizing Agent Organizations. Syntax and Operational Semantics
of an Organization-Oriented Programming Language
- 2011-03
Jan Martijn van der Werf (TUE)
Compositional Design and Verification of Component-Based Information Systems
- 2011-04 Hado van Hasselt (UU)
Insights in Reinforcement Learning; Formal analysis
and empirical evaluation of temporal-difference learning algorithms
- 2011-05 Base van der Raadt (VU)
Enterprise Architecture Coming of
Age - Increasing the Performance of an Emerging Discipline.
- 2011-06 Yiwen Wang (TUE)
Semantically-Enhanced Recommendations in Cultural Heritage
- 2011-07 Yujia Cao (UT)
Multimodal Information Presentation for High Load Human Computer Interaction
- 2011-08 Nieske Vergunst (UU)
BDI-based Generation of Robust Task-Oriented Dialogues
- 2011-09 Tim de Jong (OU)
Contextualised Mobile Media for Learning
- 2011-10 Bart Bogaert (UvT)
Cloud Content Contention
- 2011-11 Dhaval Vyas (UT)
Designing for Awareness: An Experience-focused HCI Perspective
- 2011-12 Carmen Bratosin (TUE)
Grid Architecture for Distributed Process Mining
- 2011-13 Xiaoyu Mao (UvT)
Airport under Control. Multiagent Scheduling for Airport Ground Handling
- 2011-14 Milan Lovric (EUR)
Behavioral Finance and Agent-Based Artificial Markets
- 2011-15 Marijn Koolen (UvA)
The Meaning of Structure: the Value of Link Evidence for Information Retrieval
- 2011-16 Maarten Schadd (UM)
Selective Search in Games of Different Complexity

- 2011-17 Jiyin He (UVA)
Exploring Topic Structure: Coherence, Diversity and Relatedness
- 2011-18 Mark Ponsen (UM)
Strategic Decision-Making in complex games
- 2011-19 Ellen Rusman (OU)
The Mind 's Eye on Personal Profiles
- 2011-20 Qing Gu (VU)
Guiding service-oriented software engineering - A view-based approach
- 2011-21 Linda Terlouw (TUD)
Modularization and Specification of Service-Oriented Systems
- 2011-22 Junte Zhang (UVA)
System Evaluation of Archival Description and Access
- 2011-23 Wouter Weerkamp (UVA)
Finding People and their Utterances in Social Media
- 2011-24 Herwin van Welbergen (UT)
Behavior Generation for Interpersonal Coordination with Virtual Humans
On Specifying Scheduling and Realizing Multimodal Virtual Human Behavior
- 2011-25 Syed Waqar ul Qounain Jaffry (VU)
Analysis and Validation of Models for Trust Dynamics
- 2011-26 Matthijs Aart Pontier (VU)
Virtual Agents for Human Communication - Emotion Regulation and Involvement-
Distance Trade-Offs in Embodied Conversational Agents and Robots
- 2011-27 Aniel Bhulai (VU)
Dynamic website optimization through autonomous management of design patterns
- 2011-28 Rianne Kaptein(UVA)
Effective Focused Retrieval by Exploiting Query Context and Document Structure
- 2011-29 Faisal Kamiran (TUE)
Discrimination-aware Classification
- 2011-30 Egon van den Broek (UT)
Affective Signal Processing (ASP): Unraveling the mystery of emotions
- 2011-31 Ludo Waltman (EUR)
Computational and Game-Theoretic Approaches for Modeling Bounded Rationality

- 2011-32 Nees-Jan van Eck (EUR)
Methodological Advances in Bibliometric Mapping of Science
- 2011-33 Tom van der Weide (UU)
Arguing to Motivate Decisions
- 2011-34 Paolo Turrini (UU)
Strategic Reasoning in Interdependence: Logical and Game-theoretical Investigations
- 2011-35 Maaïke Harbers (UU)
Explaining Agent Behavior in Virtual Training
- 2011-36 Erik van der Spek (UU)
Experiments in serious game design: a cognitive approach
- 2011-37 Adriana Burlutiu (RUN)
Machine Learning for Pairwise Data, Applications for Preference Learning
and Supervised Network Inference
- 2011-38 Nyree Lemmens (UM)
Bee-inspired Distributed Optimization
- 2011-39 Joost Westra (UU)
Organizing Adaptation using Agents in Serious Games
- 2011-40 Viktor Clerc (VU)
Architectural Knowledge Management in Global Software Development
- 2011-41 Luan Ibraimi (UT)
Cryptographically Enforced Distributed Data Access Control
- 2011-42 Michal Sindlar (UU)
Explaining Behavior through Mental State Attribution
- 2011-43 Henk van der Schuur (UU)
Process Improvement through Software Operation Knowledge
- 2011-44 Boris Reuderink (UT)
Robust Brain-Computer Interfaces
- 2011-45 Herman Stehouwer (UvT)
Statistical Language Models for Alternative Sequence Selection
- 2011-46 Beibei Hu (TUD)
Towards Contextualized Information Delivery:
A Rule-based Architecture for the Domain of Mobile Police Work
- 2011-47 Azizi Bin Ab Aziz(VU)

Exploring Computational Models for Intelligent Support of Persons with Depression

2011-48 Mark Ter Maat (UT)
Response Selection and Turn-taking for a Sensitive Artificial Listening Agent

2011-49 Andreea Niculescu (UT)
Conversational interfaces for task-oriented spoken dialogues:
design aspects influencing interaction quality

=====
2012
=====

2012-01 Terry Kakeeto (UvT)
Relationship Marketing for SMEs in Uganda

2012-02 Muhammad Umair(VU)
Adaptivity, emotion, and Rationality in Human and Ambient Agent Models

2012-03 Adam Vanya (VU)
Supporting Architecture Evolution by Mining Software Repositories

2012-04 Jurriaan Souer (UU)
Development of Content Management System-based Web Applications

2012-05 Marijn Plomp (UU)
Maturing Interorganisational Information Systems

2012-06 Wolfgang Reinhardt (OU)
Awareness Support for Knowledge Workers in Research Networks

2012-07 Rianne van Lambalgen (VU)
When the Going Gets Tough: Exploring Agent-based Models
of Human Performance under Demanding Conditions

2012-08 Gerben de Vries (UVA)
Kernel Methods for Vessel Traject

2012-09 Ricardo Neisse (UT)
Trust and Privacy Management Support for Context-Aware Service Platforms

2012-10 David Smits (TUE)
Towards a Generic Distributed Adaptive Hypermedia Environment

2012-11 J.C.B. Rantham Prabhakara (TUE)
Process Mining in the Large: Preprocessing, Discovery, and Diagnostics

- 2012-12 Kees van der Sluijs (TUE)
Model Driven Design and Data Integration in Semantic Web Information Systems
- 2012-13 Suleman Shahid (UvT)
Fun and Face: Exploring non-verbal expressions of emotion during playful interactions
- 2012-14 Evgeny Knutov(TUE)
Generic Adaptation Framework for Unifying Adaptive Web-based Systems
- 2012-15 Natalie van der Wal (VU)
Social Agents. Agent-Based Modelling of Integrated Internal and Social Dynamics of Cognitive and Affective Processes
- 2012-16 Fiemke Both (VU)
Helping people by understanding them
Ambient Agents supporting task execution and depression treatment
- 2012-17 Amal Elgammal (UvT)
Towards a Comprehensive Framework for Business Process Compliance
- 2012-18 Eltjo Poort (VU)
Improving Solution Architecting Practices
- 2012-19 Helen Schonenberg (TUE)
What's Next? Operational Support for Business Process Execution